Technical Report ISTC/MCE/VS/427

ISRO-IISc Space Technology Cell
Indian Institute of Science
Bengaluru

Leak Detection Tapes for Hydrogen Pipelines

(Final Technical Report)

S. Venugopal, ChE, IISc
V. Kavitha, LPSC, ISRO
S. Ingersol (Retd), LPSC, ISRO

STC

April 2022

Technical Report ISTC/MCE/VS/427

ISRO-IISc Space Technology Cell
Indian Institute of Science
Bangalore

Leak Detection Tapes for Hydrogen Pipelines

(Final Technical Report)

S. Venugopal, ChE, IISc
V. Kavitha, LPSC, ISRO
S. Ingersoll (Retd), LPSC, ISRO

April 2022

Data Sheet

<table>
<tr><td>Project Title:

Leak Detection Tapes for Hydrogen Pipelines</td><td>Project Code:

ISTC/MCE/VS/427

Date of Commencement:

01/04/2019

Date of Closure:

31/03/2022</td></tr>
<tr><td colspan="2">Investigator from IISc:

S. Venugopal

Affiliation with email

Department of Chemical Engineering

svgpal@iisc.ac.in</td></tr>
<tr><td colspan="2">Investigator from ISRO

V. Kavitha & S. Ingersol (Retd)

Affiliation

LPSC</td></tr>
<tr><td colspan="2">Type of the project: (Research/Development/etc.</td></tr>
<tr><td colspan="2">Security classification, if any: Open/Restricted</td></tr>
<tr><td colspan="2">Short Abstract (Maximum of 50 words)

This project proposed to build on the results of previous investigations and develop nanostructure-based flexible hydrogen leak detectors using a low-cost fabrication process. We successfully demonstrated the lab-scale hydrogen leak detection of 0.7% hydrogen in air.</td></tr>
<tr><td colspan="2">Keywords

Flexible, Hydrogen, Leak Detection, Palladium Nanostructures</td></tr>
<tr><td colspan="2">Total Budget (in lakh `)

₹ 12.56811</td></tr>
</table>

Products/methodology/algorithms delivered to ISRO/DOS Centre **Palladium nanostructures on flexible Kapton substrate for hydrogen leak detection have been fabricated**
Where it is put into use/embedded in ISRO/DOS activities/programmes ***We hope to see it tested and developed further for field deployment in IPRC/LPSC. A Pvt Company (Envigil Leak Detection Specialists (OPC) Pvt Ltd, Pune) has expressed interest in creating the housing and system around the leak detection tape for deployment along pipelines. In this context, they have written emails on 16/05/2022 to SAO and Director, IPRC requesting guidance to take the development further as per IPRC requirements.***
Number of JRF/students involved (give details of students PhD/MTech) 3 – 2 Staff and 1 PhD **Abhishek Ranade – Research scholar, PhD program, Department of Chemical Engineering, IISc (*Expected to graduate by Dec 2022*)**
Number of papers published (International & National Journals/ Conferences etc.) **To be presented at AICHE Nov' 2022 conference, Two Manuscripts based on these results are in preparation.**
Patents **-None-**
Details of visit(s) to ISRO centre(s). Include centre name, dates, host, nature of interactions (discussions/seminars) **-None-**

Acknowledgements

We acknowledge Dr K. Nandakumar (retd, LPSC-Valiamala) for suggesting the topic of hydrogen gas detection/sensing and for his constant encouragement. We thank Mr S. Ingersol (retd. LPSC- Bangalore) for insightful discussions regarding the nature of the substrate and the mode of detection. We acknowledge Ms Kavitha V for her support in completing the project.

Finally, we thank ISRO for funding and the STC staff for a professional handling of the project implementation.

ABHISHEK RANADE

S. VENUGOPAL

Abstract

Hydrogen (H_2) is emerging as a new energy source to address the need for alternative renewable energy sources amidst concerns about global warming. There are various advantages of using hydrogen as an energy carrier as it undergoes "clean" combustion, and it can be generated in a renewable fashion using water and solar power. However, properties such as its flammability, colourlessness, odourlessness, and tendency to leak through the smallest of gaps make its use a dangerous venture. Such leaks can lead to explosive atmospheres, with the lower explosive limit being 4% v/v in air. It is essential to have a fast and reliable detection system to initiate appropriate action.

ISRO deals with liquid hydrogen-carrying pipelines stretching several hundreds of meters. There is always the possibility of hydrogen leaking through the pipes, joints, bends, or flanges. An economic detection system that can be wrapped around such probable areas of hydrogen leakage and which can respond to leakages in seconds is needed. Presently available technologies are not suitable for this type of application. The available detection systems can be broadly divided into two parts: (i) the detecting element- the active part of the detection system that is sensitive toward hydrogen and (ii) the transducer- which converts the sensor-hydrogen interaction into a signal, preferably electrical. Detection systems available in the market are based on various sensing materials that can transduce hydrogen concentration to an electrical signal.

Palladium is the most studied material in this aspect. When hydrogen is present around palladium, the hydrogen is absorbed into palladium to form palladium hydride. Palladium hydride has a lower bulk density and higher electrical resistance than palladium, leading to changes in volume and electrical properties. These changes can be detected if the palladium-based detecting element is a part of an electrical circuit. The response time can be further reduced if nanostructures are used in the detecting element as they have a higher surface to volume ratio.

Building up on our earlier work (ISTC/MCE/VS/385), and after assessing several processes for *in situ* formation of conductive palladium nanostructures, we developed a simple process based on *in situ* reduction and formation of palladium nanostructures using aluminium as the reducing agent. This involves the adhesion of a narrow strip of aluminium onto alkali-treated Kapton substrates and placing it in contact with a few drops of palladium chloride solution. The aluminium is Galvanically displaced by the palladium to form nanoparticles. By controlling the spread of the solution, the formed nanostructures are deposited along the contours of the aluminium tape and, under appropriate concentrations give rise to percolating structures. After an appropriate time, the sample is washed and the aluminum tape remaining, if any is peeled off. Copper tapes contact the resultant percolating

strips of palladium nanostructures for performance characterization as hydrogen leak detectors. If the precursor metal salt solution is altered to a mixture of palladium and platinum salts, then the deposited nanostructures reflect the bulk composition to form Pd-Pt nanostructures.

Palladium nanostructures are highly sensitive to the presence of hydrogen gas, and upon exposure to a gas containing <2%$_{vol}$ hydrogen in Nitrogen, they rapidly form palladium hydrides that lead to an increase in resistance. The samples can have an initial resistance of 0.1 kΩ to 3 kΩ, depending on the concentration of the precursor salt solution used. The response time, defined as the time taken to reach 90% of the final saturation value, is of the order of 10s of seconds with sensitivities (defined as the ratio of % change in the resistance of the sensing element to the initial resistance) of the order 2-4%. If the hydrogen concentration increases above 2%$_{vol}$, then the resistance drops significantly (sensitivity up to -30%), attributed to the expansion of palladium hydride nanostructures to close the gaps in the percolating network. Upon exposure to air, the resistance, apart from the first run, decreases at all concentrations. This is attributed to the formation of a native oxide film that has to be reduced in the first run.

Pd-Pt nanostructures were also prepared in a similar manner. The Pd-Pt nanostructures in 95:5 ratio do not exhibit an increase in resistance and always show a decrease in resistance upon exposure to hydrogen gas. All the sensors were also able to recover their original resistance values within a minute after the hydrogen flow was stopped and thus can act as leakage detectors in field-based applications.

Overall, we have developed a simple and scalable process to fabricate hydrogen leak detectors on flexible substrates that can be deployed in the field.

Contents

LIST OF FIGURES

1. INTRODUCTION

Hydrogen is the lightest of all elements, with a high diffusion coefficient of 0.16 cm^2/s in air, low ignition energy of 0.018 mJ, high combustion heat (285.18 kJ), and a wide combustion window (4 – 75 vol% in air). Thus, storage, transportation, and usage can be potentially dangerous[1]. Fig 1 shows the percentages of the accidents related to hydrogen reported in the EU since 1985 [2]. From fig 1(b), it becomes clear that the explosiveness of hydrogen was the primary factor responsible for harming onsite workers. Therefore, there is always a need for appropriate safety barriers to be in place to mitigate the risks posed by hydrogen.

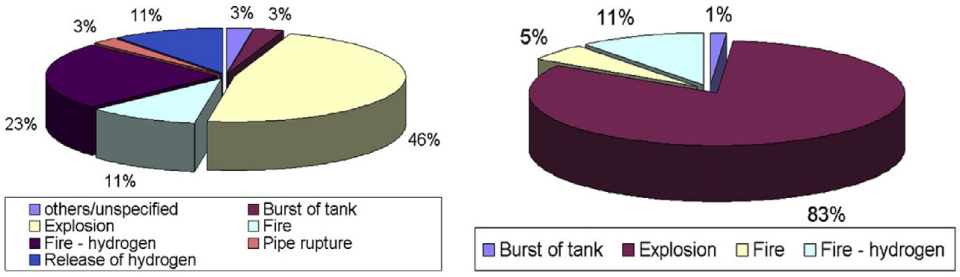

(a) Hydrogen events in EU since 1985: number of events.

(b) Hydrogen events in EU since 1985: number of affected persons onsite

Figure 1: Breakup of hydrogen-related events in the EU since '85

Fig 2 shows a schematic of the various safety barriers required to avert such accidents. Gas sensors are necessary for onsite applications, as they constitute a primary safety barrier against potentially deadly leaks. [3]

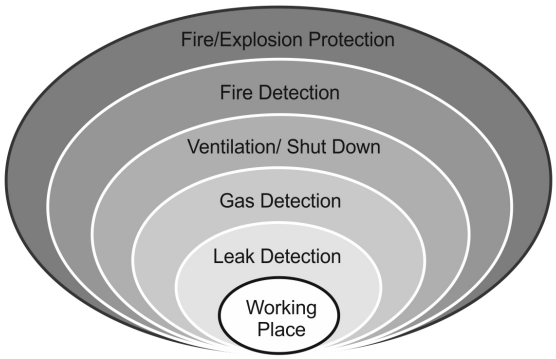

Figure 2: Layers of safety required to prevent hydrogen-related accidents[3]

A sensor is a "device which receives and responds to a stimulus." A sensor comprises several components, as shown in the schematic fig. 3.

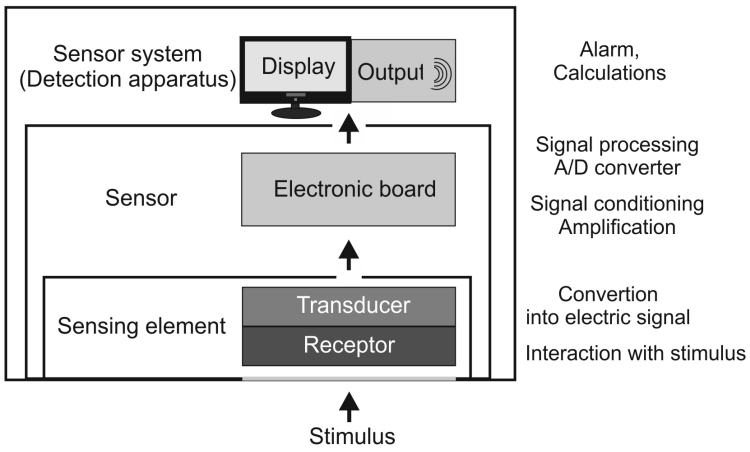

Figure 3: Components of a sensor[3]

The sensing element consists of a receptor and a transducer. The receptor directly interacts with the analyte gas. This interaction is usually converted to an electrical signal by the transducer. The sensor encompasses the electronic components that further amplify the signal from the transducer and convert it to a digital output. The sensor system is the superset, which receives the output from the sensor and sends an alarm accordingly. The focus of this work is primarily related to the development of the sensing element. So, the word "sensor" in this report refers to the "sensing element," as mentioned above.

To determine how "good" any given gas sensor is, one needs information about some parameters specific to that sensor. These parameters are introduced below [3]:

- Measuring range is the range between two extremes, within which a sensor can measure any stimulus with a given accuracy. The lower limit of this range is often known as the limit of quantification (LOQ) or limit of detection (LOD). The upper limit of the measuring range is the point beyond which the sensor fails to yield a proportional change in its output signal.
- Accuracy – It describes the closeness of the sensor measurement with the accepted value of that quantity—e,g. Assume a hydrogen gas sensor exposed to a 100 ppm hydrogen environment responds with a 101 ppm hydrogen concentration. It implies that the sensor's accuracy is within 1% of the reference value.
- Sensitivity – There may be multiple ways to define sensor sensitivity. It can be defined as the ratio of the change in the sensor signal to the stimulus provided. Alternatively, sensitivity is the ratio of the magnitude of the response to the magnitude of the quantity measured [4]. E.g., In this work, the fabricated sensors output a change in their electrical resistance in response to a hydrogen stimulus. The second definition of sensitivity is used in this work, i.e., $((R - R_0)/R_0)*100$, where R is the sensor's resistance at any given instant, and R_0 is the baseline resistance of the sensor in the absence of hydrogen. Thus, the sensitivity for these sensors is the relative change in resistance (signal) to the initial resistance (measured quantity), expressed as a percentage.
- Response time/recovery time – Response time is generally defined as the time taken by the sensor signal to reach 90% of its saturation value in response to a step-change in the stimulus. Similarly, the recovery time is the time the sensor signal takes to get to 10% of its initial value from its saturation value when the stimulus is removed.

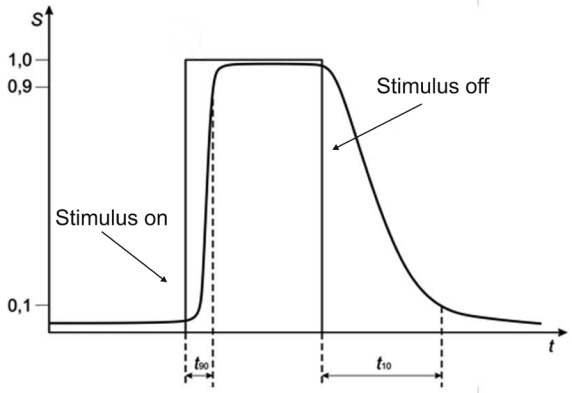

Figure 4: Response time and recovery time[3]

There have been consistent efforts to develop hydrogen sensors over the past couple of decades, as seen by the increasing number of publications addressing this field [5]. Thus, developing hydrogen sensors is currently an active area of research.

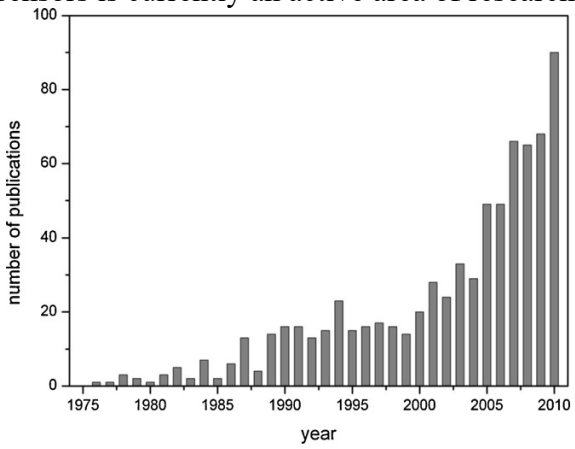

Figure 5: Number of publications addressing hydrogen sensor fabrication since '76[5]

The US Department of Energy (DoE) has set specific criteria that hydrogen sensors must meet, depending upon their end-use [6]. These are depicted in fig. 6.

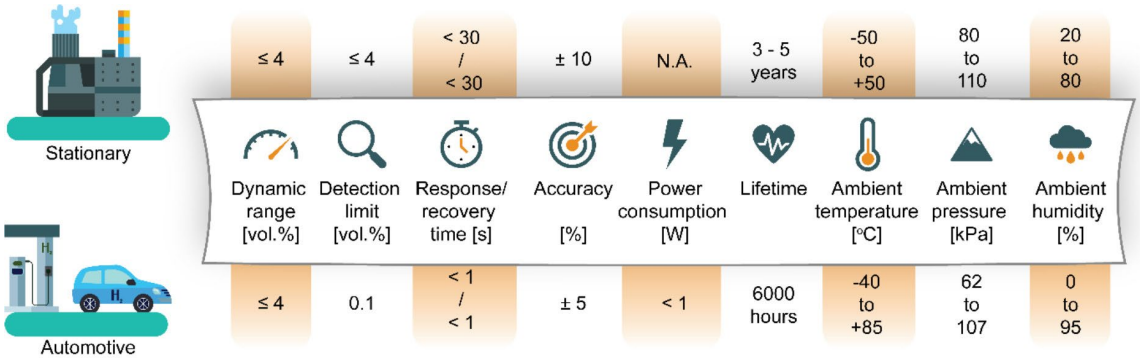

Figure 6: DoE criteria for hydrogen sensors[6]

Fig. 7 is a schematic depicting different aspects of developing a gas sensor. It involves the selection of a "substrate," which provides a support surface for the receptor material. Typically, the substrate is an inert material that doesn't directly participate in the sensing process. In contrast, the receptor material interacts with the target gas through mechanisms depending on the material used or the material property being exploited. E.g., The element palladium can

change its electrical, mechanical, and optical properties when it interacts with hydrogen. Thus, sensor manufacturers can use any property best suited for the purpose. The receptor and the substrate together constitute the sensor. There are various technologies by which the sensor can be fabricated[7]. The upcoming sections/chapters will address these topics in brief.

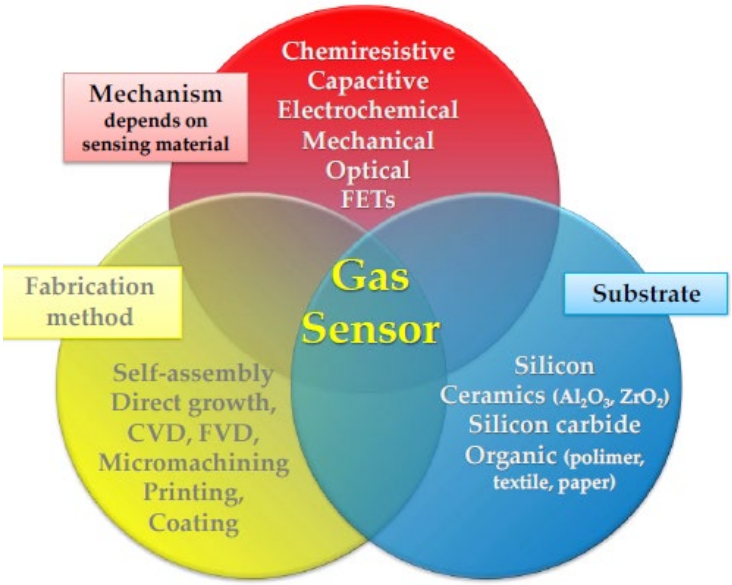

Figure 7: Aspects of gas sensor fabrication[7]

2. HYDROGEN SENSING TECHNOLOGIES

Various technologies are employed for the detection of hydrogen. The sections below describe a few technologies in brief.

2.1 HYDROGEN SENSING TECHNOLOGIES

2.1.1 Metal-oxide based resistive hydrogen sensor

Metal oxide sensors are commonly used due to the low fabrication cost, broad gas detection capability, and reasonable response times (< 20 s). Metal oxides, such as alumina (Al_2O_3), change their electrical properties when exposed to reducing gases. Such sensors use a metal oxide film coated on an insulating substrate material electrically contacted by two electrodes (Fig 8). Typically, the oxide film is deposited on the substrate using screen printing, followed by heat treatment for sintering. Vapour deposition is another method used to deposit thinner films. The sensitive layer consists of an additive layer like Pd or Pt that improves the sensitivity of the oxide. A membrane is used to screen gases such as methane to avoid cross selectivity.

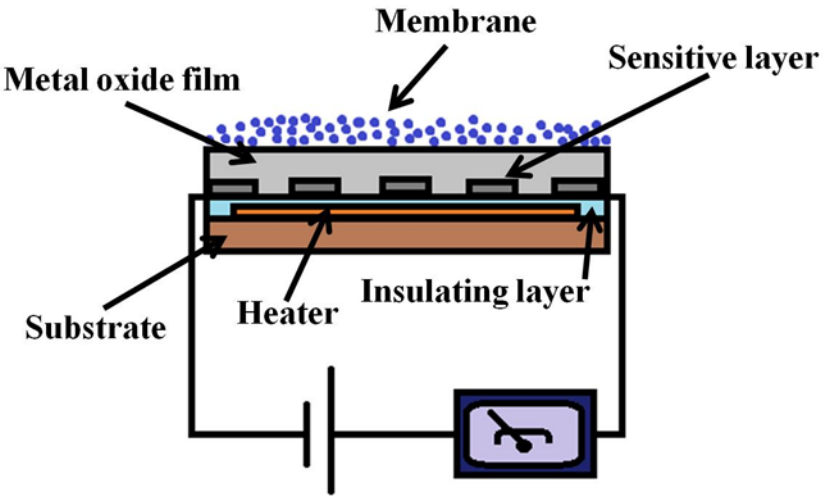

Figure 8: Schematic of a metal oxide sensor[5]

When in operation, this film is heated to a high temperature, which can be anywhere ranging from 180 °C to 450 °C depending upon the metal oxide film. This heating is necessary to promote the reaction with the reducing gas and remove water formed afterward. The measured resistance of the detecting element changes as this reaction happens, which ultimately depends upon the concentration of the reducing gas available in the surrounding environment. A reasonable approximation of this dependence is given by:

$$R(c) = a.cb$$

Here, c is the concentration of the reducing gas, and a and b are sensor-specific constants.

The resistance change is calibrated in terms of the concentration of this gas, which is present in the environment. A commonly available sensor in the market that uses this technology is an MQ-8 hydrogen sensor.

Figure 9: MQ-8 hydrogen sensor module[8]

It uses tin oxide (SnO_2) as the gas-sensitive metal-oxide layer. Reportedly, the reaction involved therein occurs in two steps. The first requires the adsorption of oxygen on its surface, which decreases its surface conductivity. Then in the second step, hydrogen, if any, reacts with the adsorbed oxygen, and the product is water vapour due to the heating of the metal oxide film.

$$O_2 + 2e^- \rightarrow 2O^-_{ads}$$

$$H_2 + 2O^-_{ads} \rightarrow H_2O + e^-$$

Hydrogen reduction releases electrons into the tin oxide's conduction band, making it an n-type semiconductor with increased conductivity. The concomitantly decreased resistance is then correlated in terms of hydrogen concentration. The disadvantages of these sensors are that they are cross-selective to other gases such as CO, CH_4, alcohols, etc. They consume more power owing to the high operating temperature required. They also require the presence of oxygen for their functioning.

2.1.2 Combustible gas sensor

Hydrogen has a standard heat of combustion of 141.9 kJ/g, making its combustion a highly exothermic reaction. If such a reaction is carried out on the surface of a suitable catalyst, then the heat liberated can detect the presence of hydrogen in the environment. The combustible gas sensors target this property for hydrogen sensing. For instance, a pellistor (pellet + resistor) type hydrogen sensor uses two platinum coils embedded in a ceramic bead or “pellet” (usually Al_2O_3).

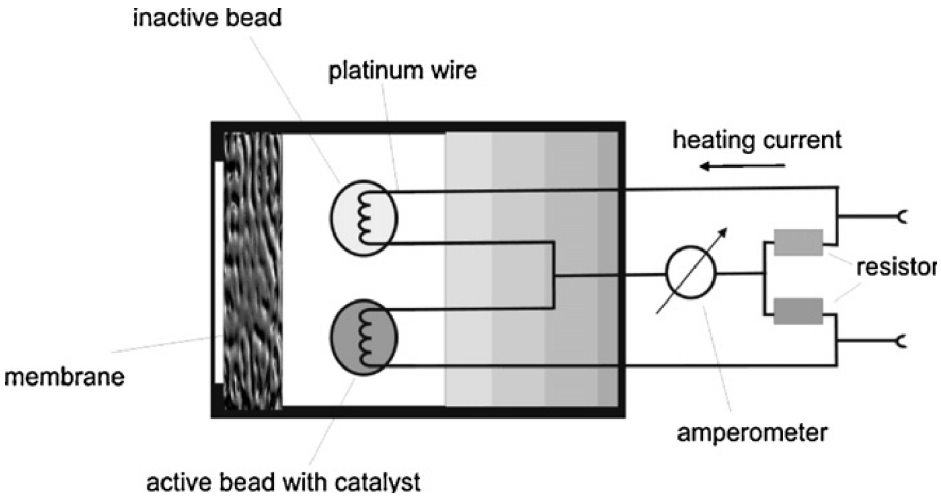

Figure 10: Combustible gas sensor[5]

The metallic coils work as heaters as well as being resistance thermometers. However, the surface of only one of those beads is activated with noble metals like platinum or palladium. The other pellet has no catalyst. Both the beads are a part of a Wheatstone bridge circuit. During operation, an electric current is passed through both the coils, which causes them to heat up to nearly 300°C. In this condition, hydrogen molecules are chemisorbed on the catalyst and become oxidized (in the presence of oxygen) to form water. This reaction leads to the liberation of heat. The heat causes a change in the electrical resistance of the activated coil. It leads to a disturbance in the Wheatstone bridge circuit which constitutes the sensor signal. Being a well-established technology, these types of sensors are widely available. They work until hydrogen concentrations of 4%. They need to be calibrated from time to time to account for their drift. However, their disadvantages are cross selectivity to combustible gases such as hydrocarbons and carbon monoxide. The catalysts are also susceptible to poisoning from inhibitors.

2.1.3 Thermo conductivity sensors

Thermal conductivity detectors measure the concentration of a gas in a binary gas mixture by comparing it to the thermal conductivity of a selected reference gas.

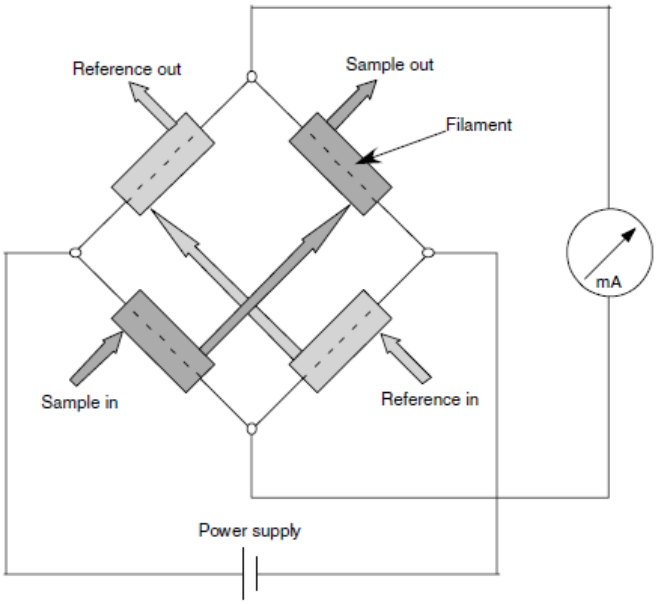

Figure 11: Thermal conductivity-based hydrogen sensor[5]

This sensor (Fig. 11) has four ultra-stable, precision glass-coated thermistors. One pair is in contact with the sample gas, and the other is in contact with the reference gas (like chlorine in a sealed chamber). The thermistors are mounted so that they are in close contact with the walls of the gas chambers. The cell is temperature-controlled, and the thermistors are heated to an elevated temperature in a constant current Wheatstone bridge, similar to the pellets used in the combustible gas sensor. The thermistors lose heat to the walls of the gas chambers at a rate that is proportional to the thermal conductivity of the gas surrounding them. Hence each thermistor will have a different equilibrium temperature. In this way, a disturbance will creep into the Wheatstone bridge, which will then cause the sensor to give a signal. The sensor will detect any gas that will alter the thermal conductivity of the gas chamber.

2.1.4 Chemiresistive sensors

This category of sensors uses pure metals or their alloys for detecting/sensing hydrogen. Palladium is most noted for its ability to selectively absorb hydrogen at ambient conditions, resulting in changes in electrical properties, refractive index, volume, etc. On exposure of palladium to hydrogen, its resistance typically increases due to the formation of palladium

hydride. Palladium hydride has a higher electrical resistance than pure palladium for a given set of conditions.

All the technologies discussed so far have some advantages and some shortcomings. These have been listed in Table 1.

Table 1: Comparison of various hydrogen sensing technologies

Hydrogen detection technologies	**Transduction mechanism**	**Advantages**	**Disadvantages**	**Application**
Combustible gas	Catalytic combustion (ΔR induced by ΔT)	Robust	Cross-sensitivity	Industry-standard; Petroleum industry, infrastructure
Thermo-conductivity	Heat transfer (ΔR induced by ΔT)	Fast response time	Non-selective	Modeling studies; vehicles
Metal oxide	(ΔR) semiconductor doping	Low cost versatile	Reputation for instability requires heating	Containers
Palladium thin film	Selective H_2 absorption	Selectivity	Prone to poisoning	Petroleum industry; specialized applications

2.1.5 Chemochromic Leak Detectors

The issue with the sensor types mentioned above is that as far as leak detection is concerned, they cannot reliably and accurately identify the exact location of the leak. E.g., If hydrogen leaks from a pipeline, the sensors in the vicinity can only detect its presence. But they may not necessarily identify the location of the leak. A hydrogen leak detector was developed to be used at Kennedy Space Center (KSC) launch pad to address this need [9].

Figure 12: Chemochromic hydrogen leak detector tape wrapped around a flange of a pipe carrying H_2 at KSC, Florida[10]

A chemochromic detector can change color upon being exposed to hydrogen. Unlike the aforesaid solid-state sensors, it is flexible and can be wrapped around probable leakage areas. In case of a leak, it changes color, indicating that the leak has occurred very near it, enabling accurate location of the leak. The detecting element consists of PdO and TiO_2, which acts as the pigment and a protective coating. It is incorporated into a base polymer matrix. Such detectors can be injection moulded like plastic parts, fibre spun textiles or extruded tapes.

The tapes are inexpensive, portable, and require no external power source since they are devoid of electronics. However, the tapes rely on human observation to identify the leak event without the accompanying electronics. In contrast, chemiresistive hydrogen detectors can continuously read the detector output and signal an alarm accordingly. They have been widely studied and present ample scope for fabricating viable leak detectors.

2.2 Pd-BASED HYDROGEN SENSING

Chemiresistive sensors offer advantages such as efficient sensing performances, low-cost fabrication, and portable applications. Palladium–based chemiresistive sensors are considered state-of-the-art H_2 sensing systems due to their simplicity, efficient sensing properties, high selectivity, and room temperature operation [11]. Of the various metals that form hydrides shown in fig 13, Pd is the only one that can form a hydride under ambient conditions [12]. Therefore, the use of Pd in fabricating chemiresistive hydrogen sensors has attracted a lot of attention.

Metal	Hydride	wt.% H	P_{eq}, T
Pd	$PdH_{0.6}$	0.56	0.02 bar, 298 K
Mg	MgH_2	7.60	1 bar, 573 K
$LaNi_5$	$LaNi_5H_6$	1.37	2 bar, 298 K
ZrV_2	$ZrV_2H_{5.5}$	3.01	10^{-8} bar, 323 K
FeTi	$FeTiH_2$	1.89	5 bar, 303 K
Mg_2Ni	Mg_2NiH_4	3.59	1 bar, 555 K
TiV_2	TiV_2H_4	2.60	10 bar, 313 K

Figure 13: Hydride forming conditions of various metals[12]

When H_2 molecules approach the surface of the Pd film, they can get absorbed into the Pd. The molecules initially interact with the Pd surface by van der Waals forces. At a distance of approximately one molecular radius from the surface atoms, the potential energy of the H_2 molecules reaches a minimum, causing the molecules to adsorb on the Pd surface. The adsorbed gas molecules get dissociated to H atoms, after which they diffuse inside the Pd lattice [13].

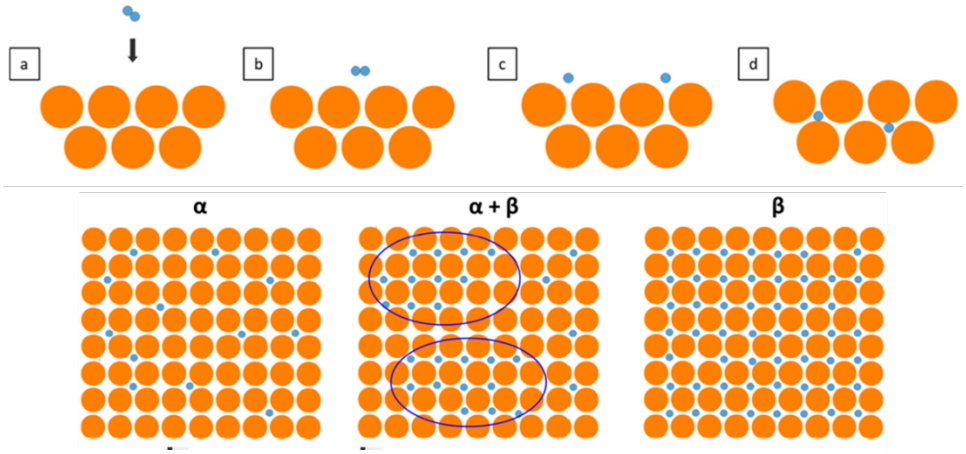

Figure 14: Stages of PdH_x formation[13]

The hydride of Pd can exist in two phases, namely α and β. In the α phase, the distance between the hydrogen atoms is considerable, characterized by weak H-H interaction. As more H atoms get incorporated into the lattice, a new phase called the β phase starts growing. At this stage, both the α phase and the β phase coexist. As more H atoms enter the lattice, the β phase grows at the expense of the α phase. Finally, when the concentration of H atoms in the lattice reaches a threshold value, the hydride manifests itself solely in the β phase. The formation of hydride results in increasing lattice constant (volume expansion) and a change in electrical resistance. [14] e.g., when the atomic ratio of H/Pd reaches 0.02 at room temperature, the lattice parameter increases from 3.889 Å to 3.895 Å. This composition is the last point where the hydride exists in the α phase. Upon increasing H concentration, further lattice expansion forms the β phase, with a lattice constant of 4.025 Å. The two phases coexist until H/Pd = 0.58, after which the α phase disappears completely [15]

A chemiresistive Pd-based sensor consists of metallic Pd as a part of an electrical circuit. Chemiresistive Pd-based hydrogen sensors can exploit two distinct effects to detect hydrogen:

Electronic effect: Metallic palladium can conduct electrons quite freely. However, when the H atoms get incorporated into the Pd lattice, they act as scattering centres for the electrons resulting in increased resistance. Thus, by detecting an increase in resistance, the presence of hydrogen can be confirmed. This phenomenon is called the electronic effect. E.g., Fig 15 shows the response of Pd films to H_2 exposure/recovery cycles. The resistance increases upon the introduction of H_2 in the system as per the electronic effect [16]. The inflection points in fig 15(a) indicate the formation of α + β mixed phases and β phase. Once the β phase takes over the entire lattice, defects such as vacancies and dislocations get introduced into the matrix to maintain the FCC structure of PdH and release the strain produced by volume expansion by the absorbed hydrogen atoms. The deformations are only partially recovered even after the H_2 supply is switched off. Thus, sensors such as these suffer from hydrogen embrittlement and long response times, making them unsuitable for repeated use.

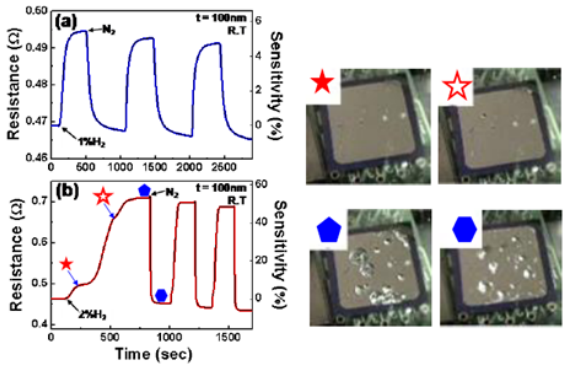

Figure 15:Hydrogen embrittlement in Pd films upon repeated exposure to 2% H_2[16]

Geometric effect/Gap-closure: In discontinuous Pd films, groups of Pd islands are separated by gaps between them. When such a film is exposed to hydrogen, the islands swell due to hydride formation and close the gaps, creating additional percolating pathways (fig 16). Consequently, the resistance of the circuit decreases, in contrast to the electronic effect described above.[17]

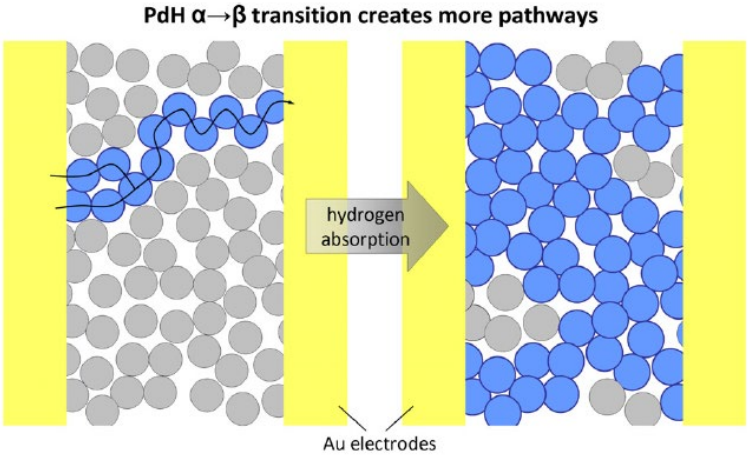

Figure 16: Gap-closure mechanism in discontinuous Pd films[17]

The seminal work by Penner et al. first demonstrated this mechanism in Pd nanoparticles deposited along graphite step-edges. As the hydrogen was introduced into the system, the grains expanded and closed the interparticle gaps, thus decreasing the sample resistance [11].

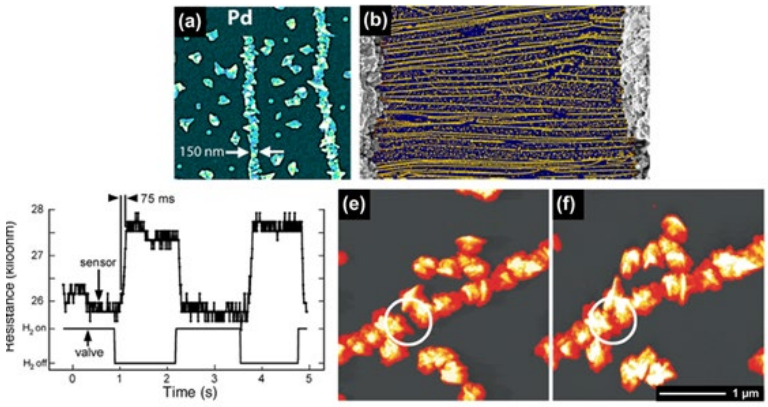

Figure 17: First demonstration of the gap-closure mechanism in Pd NWs[11]

The sensors developed thus demonstrated an exceptionally fast response time of 70 ms. The usage of Pd nanoparticles decreased the distance required for H atoms to diffuse into the Pd lattice, thus leading to a fast response time. Multiple studies since then have demonstrated the use of nano-sized Pd particles as promising candidates for hydrogen sensors [18] - [21]. To summarize this section, nanosized Pd as the sensing element of a chemiresistive hydrogen sensor has shown to be a promising lead. Sensors fabricated thus have the potential to meet the criteria set by DoE in the long run.

3. EXPERIMENTAL METHODS

3.1 INTRODUCTION

A hydrogen sensor typically consists of a sensitive layer that interacts with the gas (Pd-based chemiresistive sensors use Pd as the sensitive layer). The sensitive layer has electrodes meant to provide electrical contacts. Both the electrodes and the sensitive layer are supported on a substrate. Some substrates commonly used are Si, SiC, glass, ceramics such as Al_2O_3, ZrO_2, etc. [22] - [27]. However, these substrates are rigid (or brittle), limiting their application in various new areas, such as portable devices, aerospace science, and civil engineering, requiring flexible, lightweight, and shock-resistive sensors.

In contrast, chemically and electrically inert polymer sheets (such as PET and PEN) provide an ideal class of substrates for hydrogen sensors. e.g., Pipelines can be covered with a large area, lightweight, flexible hydrogen sensors which can detect hydrogen close to the leak-prone areas, thus saving time. Consequently, there has been growing interest in developing flexible sensors over the recent years.

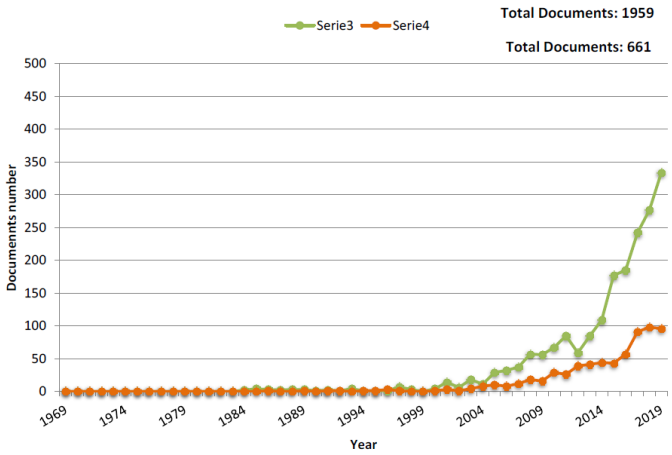

Figure 18: Increasing number of publications on flexible gas sensors[7]

Several methods have fabricated hydrogen sensors on such flexible substrates [28]. This section covers some of these methods in brief. Except for nano-imprinting, these techniques apply to rigid substrates as well.

3.1.1 Sputtering

In sputtering, the target material is bombarded by ions or a plasma resulting in the ejection of sputtered atoms deposited as a thin film on the substrate [3]. The phenomenon is illustrated in fig 19 [29]

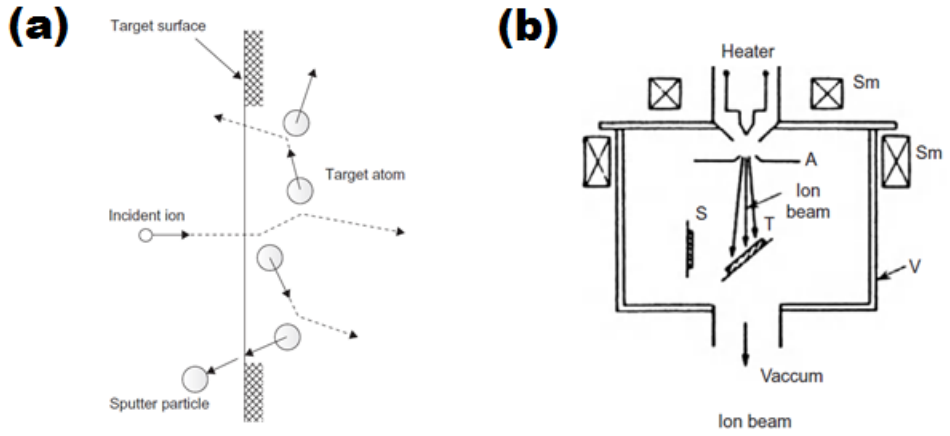

Figure 19: (a) Sputtering mechanism (b)Schematic of a sputtering chamber[29]

The target material needs to be Pd to deposit Pd on any surface. Sputter-deposited thin films of Pd have been used as hydrogen sensors in some studies [30] - [32]

3.1.2 E-beam evaporation [33]

In electron beam evaporation, the source material is evaporated using high-energy electrons in an intense beam. A hot filament causes the thermionic emission of electrons, which after acceleration, provide enough energy for evaporating the target material. The target atoms then travel to the substrate, condense and deposit.

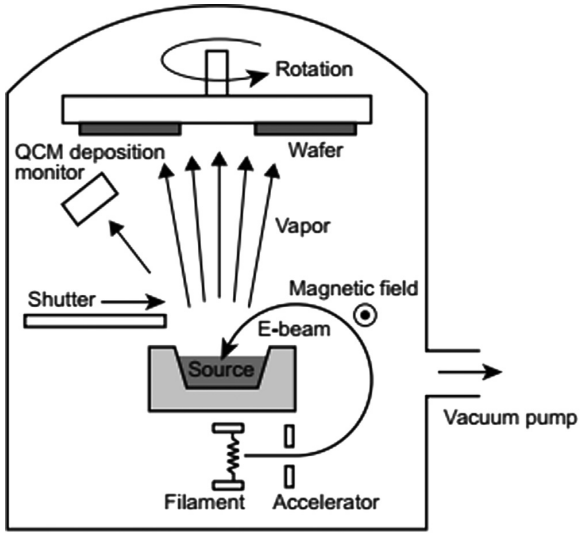

Figure 20: Schematic of an E-beam evaporator[33]

This technique has also been used to deposit Pd to fabricate hydrogen sensors [34][35]

3.1.3 Layer-by-layer self-assembly

LbL is a cyclical process in which a charged material is adsorbed onto a substrate, and after

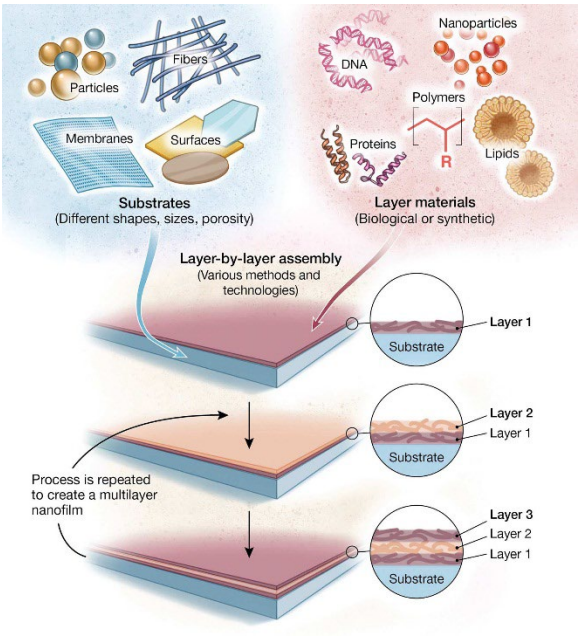

Figure 21: LbL self-assembly procedure[36]

washing, an oppositely charged material is adsorbed on the first layer. Both these oppositely charged layers constitute a single bilayer. The bilayer thickness is of the order of nanometers, and the thickness of the LbL assembly can be increased by repeating the process [36]

As far as fabricating hydrogen sensors is concerned, Su [37] had created bilayers of PSSMA (Poly(4-styrenesulfonic acid-co-maleic acid)) with PAH (poly(allylamine hydrochloride)) on PET substrate. On top of that, an MWCNT-Pd thin film was assembled in situ.

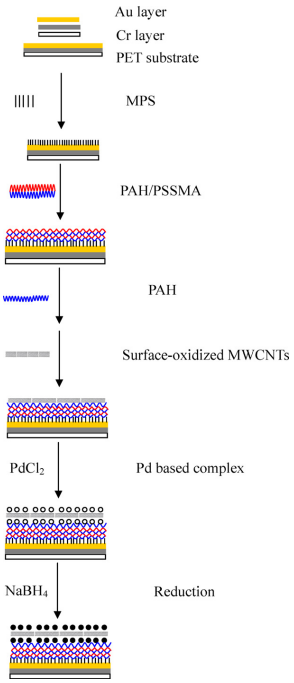

Figure 22: LbL self-assembly used by Su et al. [37]

3.1.4 Nanoimprint Lithography (NIL)[38]

In this method, a mould (stamp) is first constructed with surface relief features on it, and it is then pressed against a polymer material to transfer the pattern. The polymer is typically a sacrificial resist film used as a mask to etch the underlying substrate or film.

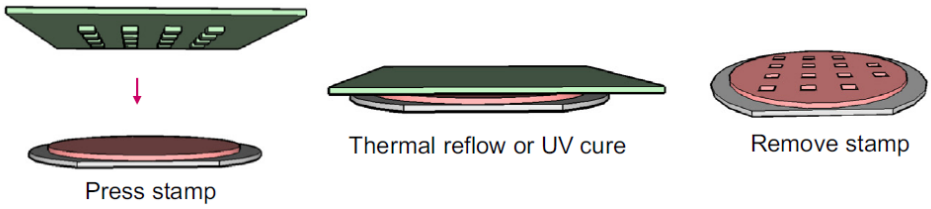

Figure 23: Schematic of the NIL method[38]

NIL technique has been used for fabricating Pd-based hydrogen sensors [39][40]. e.g., nanogaps can be moulded in a polymer material, following which Pd can be deposited on the polymer.

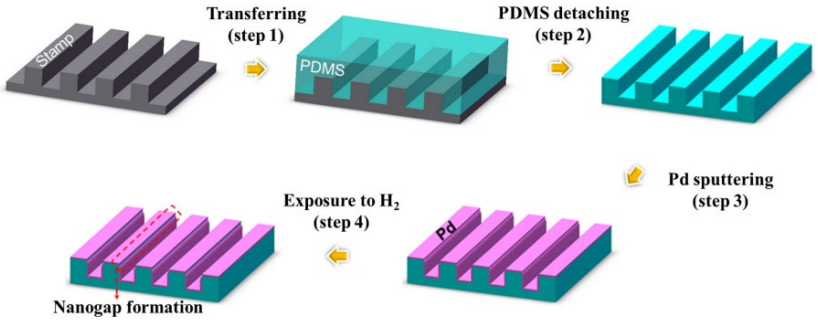

Figure 24: Method used by Jang et al. [39] to create nanogaps using NIL

3.2 GALVANIC DISPLACEMENT

Galvanic displacement is a method to obtain metal nanoparticles by reducing metal ions from solution using a sacrificial metal under ambient conditions[41]. This work first created a "sacrificial" metal layer with a lower reduction potential than palladium on a flexible substrate. The metal-substrate composite would then be exposed to palladium salt solution, depositing palladium on the substrate. For galvanic displacement, metals such as copper and aluminium were chosen as sacrificial metals. Apart from using these metals, a simple process to fabricate conductive silver films on flexible substrates was developed in our group, which also provided an alternate approach. Thus, three sensor fabrication methods were attempted using three different sacrificial metals. These approaches will be discussed in the upcoming sections.

3.2.1 Silver nanostructures

Large-area conductive silver nanostructures could be fabricated on flexible substrates such as paper or plastic, using the 'print-expose-develop' protocol [70]. This process is based on silver halide photography and uses a simple office desktop printer to create silver halide prints. Once ridden of the ink, the printer cartridges could be filled with silver salt and potassium halide solutions separately. The halide film was created by overlaying prints of the silver salt solution with the potassium halide solution on paper. Silver nuclei formed upon photo exposure of the halide film and could be grown further into nanostructures by dipping the prints in a photographic developer solution. These silver nanowires could be functionalized for hydrogen sensing by galvanically depositing palladium. However, this approach lead to a lack of sample repeatability. The conductivity of the samples increased rapidly due to the silver getting

replaced at the expense of the palladium. Therefore, to avoid the galvanic displacement reaction, a modified protocol was used in which the palladium salt precursor was mixed with coffee powder. The coffee could reduce the palladium ions, thereby suppressing the driving force for the galvanic displacement reaction. By dipping the silver prints in the coffee-based precursor, palladium could be deposited on silver with minimal galvanic displacement.

A commercially available inkjet printer, HP 1010, was used for printing aqueous solutions. HP 802, small black cartridges, were broken open and the ink was washed away completely using normal water. MS Powerpoint was used for generating patterns to print. The printer settings were "Photo paper with best quality" and "High-quality grayscale." The average volume per print was found by printing DI water and weighing the cartridge before and after printing, ~1.2 $\mu L/cm^2$. For generating silver nanostructures, two separate cartridges were filled with 0.5 M $AgNO_3$ (99.9%, SD Fine Chemicals Ltd) and 1 M KX. KX was a mixture of KBr (>99%, SD Fine Chemicals Ltd) and KI (>99%, Merck) in a 95:5 weight ratio. The silver nitrate and potassium halide solutions were sonicated in an ultrasonicator for 5 minutes. The solutions were printed alternately, starting from KX, three times (KX – $AgNO_3$ – KX – $AgNO_3$ – KX – $AgNO_3$). The cartridge was filled with roughly 120 µL of the solution, as the area required to be printed was taken as six squares of 16 cm^2 each, with cartridges printing 1.2 µL for every square cm. The silver halide prints were photo-exposed for 15 min using a halogen lamp. D-76 developer was prepared and used for developing the exposed silver halide patterns. 1 L of this developer consists of 100 g sodium sulfite (97%, SD Fine Chemicals Ltd), 2 g metol (99%, SD Fine Chemicals Ltd), 5 g hydroquinone (99.5%, SD Fine Chemicals Ltd), and 2 g borax (98%, Fisher Scientific). The patterns were developed for 15 min. After developing, the patterns were washed in DI water for 10 minutes to rinse off the developer. These printed squares were stored in plastic covers and kept in the dark before future use.
The printed squares were cut into smaller pieces of 1 cm by 1 cm sizes to be used further for deposition.

3.2.1.1 Pd salt solution

The solution was prepared by adding 167.9 mg of citric acid monohydrate (99.5% SD Fine Chemicals Ltd) in 20 mL DI water, followed by 14.1 mg of $PdCl_2$ (99.9%, Sigma Aldrich). The $PdCl_2$ took a couple of hours to dissolve completely.

To prepare the "coffee solution," 15.9 mg of 'Bru Instant' was added per mL of salt solution, mixed well, and allowed to stand for an hour. The coffee solution was then ready to use after the waiting period. After dipping the samples in the coffee solution for the required duration, they were washed with DI water and dried before use.

3.2.1.2 Citric acid pre-treatment

A 20 mL solution having 328 mg of citric acid monohydrate in DI water was prepared, and the paper-based silver prints were immersed inside for an hour. The OHP substrates were dipped in the citric acid bath for 18 hours.

3.2.1.3 Method of resistance measurement

A two-probe multimeter was used for obtaining the data in fig 37. The leads were placed 1 cm apart, and the resistance was measured along the diagonal. A Keithley 6221 – 2182A current source – nanovoltmeter combination was used to avoid disturbance due to contact resistances in a four-terminal configuration.

3.2.1.4 Material Characterization

FESEM imaging: All the samples of detecting elements were washed with DI water, dried, and desiccated for 12 hours before FESEM imaging. All the samples had been sputtered with gold with a sputtering time of 80 s and a sputtering current of 20 mA tofacilitate EDX analysis. The samples were scanned in a few different areas, and the EDS elemental analyses were averaged over four different regions in any given sample

Optical profilometry: Plastic OHP substrates were cleaned with acetone and DI water. They were dried and sputtered with gold for 200 seconds at a sputtering current of 20 mA to form a reflective coating on the surface.

XPS: Samples for XPS were prepared by cutting small pieces of detecting elements and sticking them on a piece of carbon tape, which was then stuck on a larger piece of OHP.

UV-Vis spectrophotometry: Samples were prepared by taking 200 µL of the Pd salt solution in a quartz cuvette and adding 2 mL of DI water. The UV-Vis spectrophotometry of the coffee solution was performed as below:

(i) 9 ml of DI water was added to 1 ml of the coffee solution

(ii) 10 µL of this solution was taken in the cuvette, and a further 3 mL of DI water was added.

3.2.1.5 Gas sensing setups

As per ISO 26142, hydrogen sensors could be tested for their performance, sensitivity, response time, recovery time, etc., in two types of setups.

3.2.1.5.1 Flow-through setup

The sensor/detecting element is placed inside a flange on a pipe carrying the test gas.

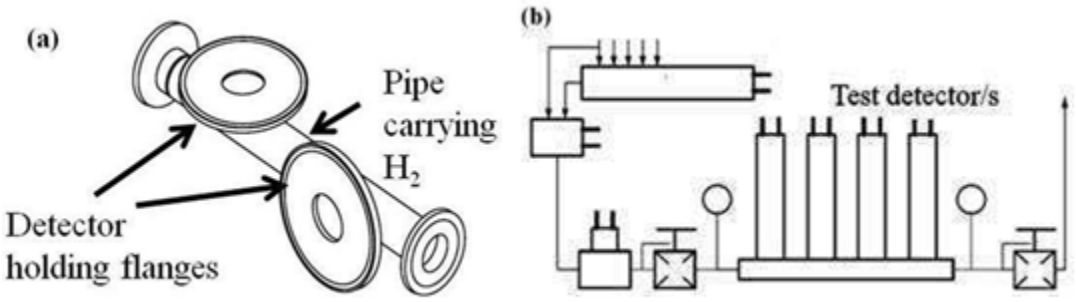

Figure 25: (a) The test manifold consists of a 25 mm ID pipe on which the flanges carrying the sensors/detectors are mounted while gas passes through it (b) The flow-through setup has temperature and humidity meters, test gas selectors, switches as per ISO standard [71]

Figure 26 shows the as-fabricated flow-through setup, consisting of a 1" ID SS pipe with two T-joints. The sensing element was placed inside a flange screwed onto the T-joint.

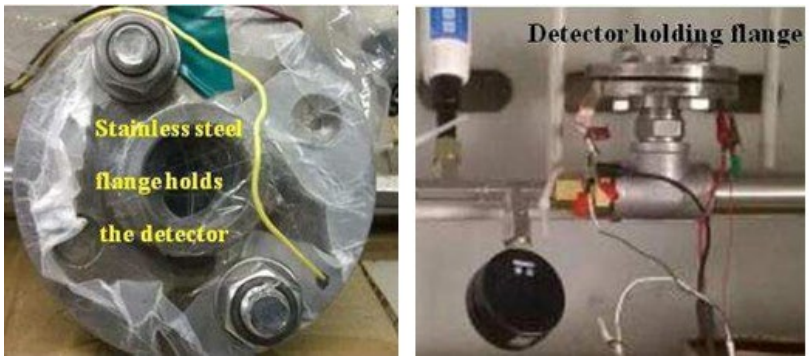

Figure 26: (Left) Detecting element in test manifold. (Right) Sensor housing flange

Figure 27: (Left) O-ring seal used in sensor holding flange. (Right) Keithley 6221-2182A used to measure sensor response

An O-ring sealed the gap between the flanges. An Athena Technology© ATH - 300 H_2 generator was used to produce hydrogen by electrolyzing a lye solution. Hydrogen was diluted by mixing nitrogen before flowing the mixture through the setup. Leaks in the setup were sealed using Ziploc bags as inflatable gaskets.

Figure 28: Ziploc bag used to seal the temperature and humidity meter port

3.2.1.5.2 Diffusion chamber setup

Hydrogen was exposed to detectors in this setup via diffusion through a leak. Acrylic sheets were used to make a box of dimensions 50 cm × 33 cm × 33 cm. A smaller plastic container for housing the detector was kept inside this box. A circulation fan with a flow rate capacity of at least 0.48 m^3/s was recommended [72]. For this purpose, a Havells I-cool 180 mm fan was used, which had a flow rate of 0.66 m^3/s as specified by the manufacturer. Ports were made in the wall of the bigger box for wire connections. Temperature and humidity meters were kept inside the box to monitor the conditions.

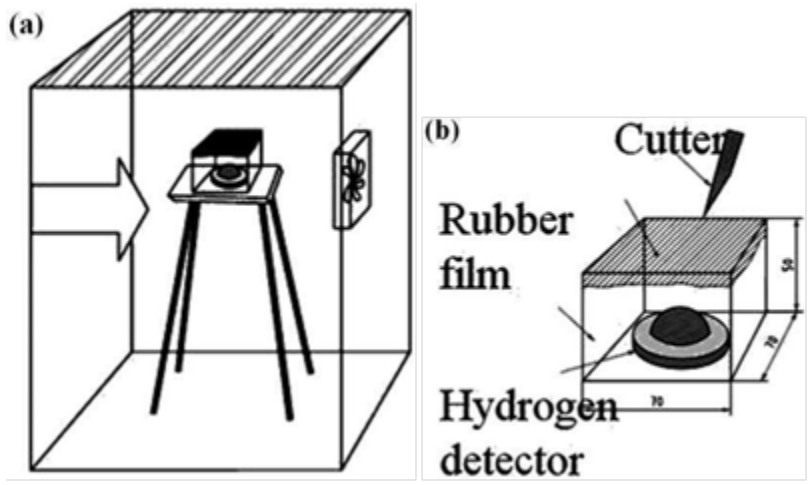

Figure 29: (a) The diffusion chamber setup consists of a box containing a circulatory fan facing the gasinlet (marked with an arrow) and a sensor housing box that holds the sensor. (b) The sensor housing boxhas the sensor which is sealed from the external using a rubber film that can be cut from outside the box [Reproduced from 71]

Figure 30: (Left) Diffusion chamber setup for sensor testing containing circulation fan and sensor holding box. (Right) Wires from Keithley 6221-2182A to measure the signal from the sensor

Hydrogen was filled at 300 ml/min inside the box for 20 minutes, after which the lid covering the detector was removed (image not shown). Thus, the hydrogen entered the detector chamber via diffusion as if through a leak.

3.2.1.6 Using the Keithley 6221-2182A equipment

The Keithley 6221 is a current source that can maintain DC currents from as low as 0.1 pA to 105 mA. It can be combined with a 2182A nanovoltmeter, which can be treated as a single instrument that can supply constant current in various tests and store the corresponding voltage readings.

The reference manual for Keithley 6221 current source [73] was followed to set up the instrument tests. The two instruments were combined using an RS-232 cable and a Trigger

link (8 pin DIN male to the male connector) cable. The power cables were connected to the power outlet. Connecting cables were attached as indicated in the manual [74]. The method to send commands and retrieve the buffer readings is shown in Appendix C. Following was the installed software to communicate with the instruments:

1) Keithley configuration wizard

2) Keithley communicator

3) KI 6220 example software

All the software was downloaded from "www.tek.com."

3.2.1.7 Palladium using photographic deposition recipe

Silver nanowires were obtained on paper as described earlier (see Section 3.2.1). After drying the paper, the silver part was cut into squares 1 cm by 1 cm and dipped into the palladium salt solution kept in plastic bottle caps, as shown in fig 31.

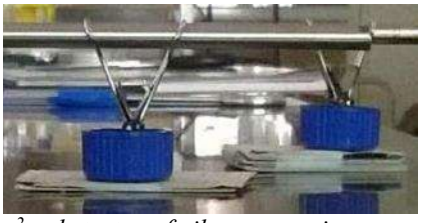

Figure 31: Setup for holding 1x1 cm^2 substrates of silver nanowire on paper for Pd deposition. The blue cup contained the deposition solution, while the clips held the paper substrate

Figure 32 shows silvery flakes floating on the surface of the palladium salt solution after three hours, indicating that this recipe did not suppress galvanic displacement.

Figure 32: Silvery flakes floating on top of the deposition solution after 3 hours of dipping the substrate in a Pd salt solution.

3.2.1.8 Addition of instant coffee powder to suppress galvanic displacement

The coffee powder contains caffeine/polyphenols that can act as reducing and capping agents to form palladium nanoparticles [75]. Caffeine polyphenols can also form complexes with metal ions to suppress Galvanic displacement reactions. Based on preliminary experiments, 159.1 mg of Bru© instant coffee powder was added to 10 mL of the palladium salt solution, mixed well, and kept for 30 minutes. The solution pH did not change significantly upon adding the coffee powder and was estimated to be 2-3 based on pH indicator papers. UV-visible spectroscopy shows that the absorption peak near 412 nm [76], attributed to the presence of Metal-Ligand Charge Transfer (MLCT) in palladium chlorohydroxy complexes (formed by partial hydrolysis of palladium chloride), disappeared after the addition of coffee (Fig.33). The

peak disappeared possibly due to the reduction or the chloride ions complexed with Pd^{2+} had been displaced after adding coffee powder. Gouda et al. [75] have shown TEM images confirming the presence of palladium nanoparticles 30 min after adding the instant coffee powder to the palladium chloride solution.

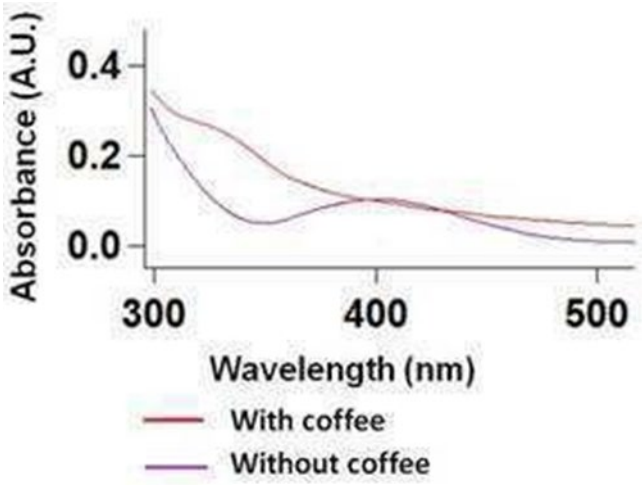

Figure 33: UV-Visible spectra of Pd salt solution and coffee solution.

It is known that citric acid or citrate ions can adsorb on a metal surface via carboxylate groups [77]. The standard palladium salt solution had citric acid to enhance the surface adsorption of palladium by electrostatic interactions with adsorbed carboxylate groups, and this step is a precursor to galvanic exchange. The silver samples were immersed in a 0.16 M solution of citric acid monohydrate for three hours before dipping in a coffee solution. Some silver samples pre-treated with citric acid were also dipped into the palladium salt solution. Figure 34 shows that silvery flakes floated on the top of the standard palladium salt solution, while such fragments were not seen on the coffee solution.

Figure 34: After 3 hours of onto a citrate-activated silver nanowire sample, the Pd salt solution (left) cap shows silvery flakes floating on the surface, while the cap with the coffee solution (right) did not show any fragments.

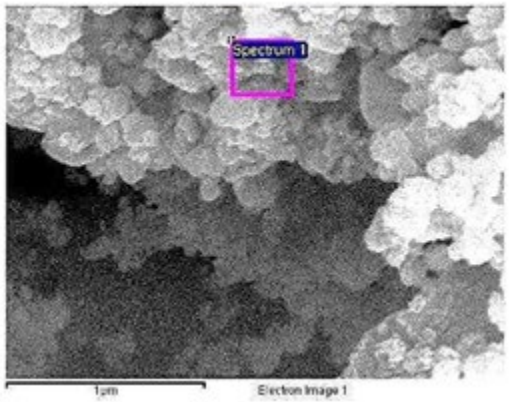

Element	Average Atomic %
Ag	52.65
Pd	19.02
Cl	23.69
Au	4.65

Figure 35: Representative FESEM image of the samples dipped in Pd salt solution for 1 hour with the average elemental analysis for this sample

Figures 35 and 36 show representative FESEM images and averaged elemental analysis of silver nanowire samples dipped for 1 h in Pd salt solution and coffee-modified solutions. Note: these samples were coated with a nominally 8 nm thick layer of gold to eliminate charging during FESEM imaging. The sample's morphology dipped in Pd salt solution was lumpy, unlike silver nanowires. In contrast, the sample's morphology dipped in coffee solution was like that of the as-developed silver nanowires. This differenceis attributed to the effect of galvanic displacement. Galvanic

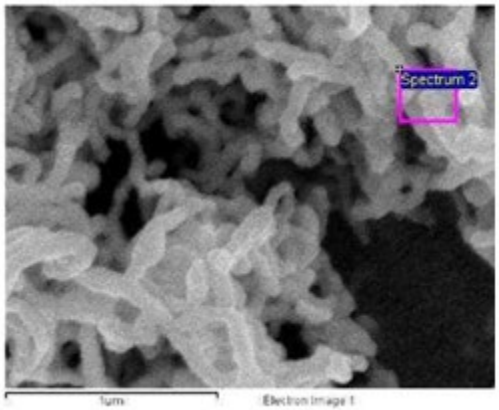

Element	Average Atomic %
Ag	70.65
Pd	23.06
Cl	0
Au	6.28

Figure 36: Representative FESEM image of the samples dipped in coffee solution for 1 hour with the average elemental analysis.

exchange created the lumpy texture owing to the significant free energy difference, resulting in a faster silver displacement rate and truncation of nanowires into more spherical aggregates [78]. The EDX analysis showed the presence of palladium in both types of samples.

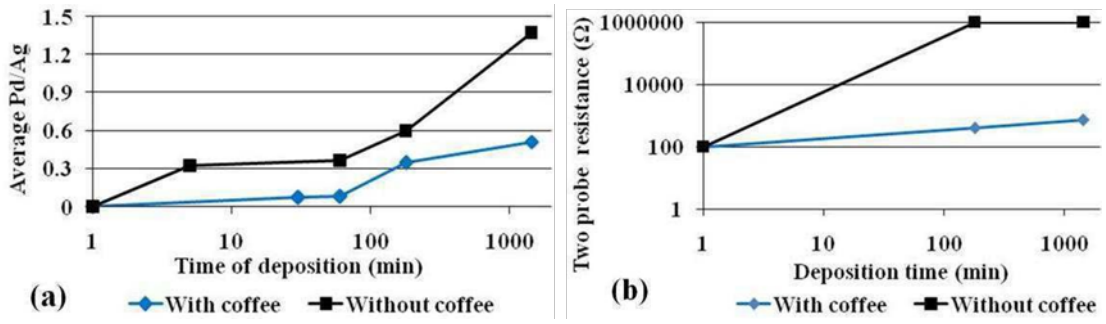

Figure 37: (a) Average Pd/Ag ratios of palladium carried out in the presence and absence of coffee for different deposition times on paper. (b) Two probe resistance of some of these samples.

Palladium deposition was performed by placing the silver prints in the coffee solution for 30, 60, 180, and 1440 minutes. A similar experiment was performed using palladium salt solution for 5, 60, 180, and 1440 minutes. The depositions were done on separate samples of silver on paper, all having the same initial electrical resistance of ~100 Ω. The average Pd/Ag ratios were calculated by EDS. Figure 37a shows a plot of the atomic ratio of palladium to silver as a function of deposition time for samples dipped in Pd salt solution and samples dipped in coffee-modified solution. Figure 37b shows the representative values of resistance measured across the edges of some of these samples. The samples toned using the coffee solution exhibited a slower rate of palladium deposition but maintained their conductivity, indicating that the nanowire morphology was intact. The samples prepared using the Pd salt solution rapidly lost their conductivity, consistent with the rounded nanowire morphology observed using FESEM imaging.

The XPS analysis (figure 38) confirmed that palladium is predominantly present in its reduced form as Pd^0 in the case of coffee-toned Ag nanowires. The peaks observed at 335.5 eV and 340.7 eV correspond to $Pd^0_{3d5/2}$ [79] and $Pd^0_{3d3/2}$ [80] respectively. A bare Ag nanowire substrate was also characterized using XPS analysis and showed peaks at 368.04 eV and 374.04 eV that correspond to $Ag^0_{3d5/2}$and $Ag^0_{3d3/2,}$ respectively [81].

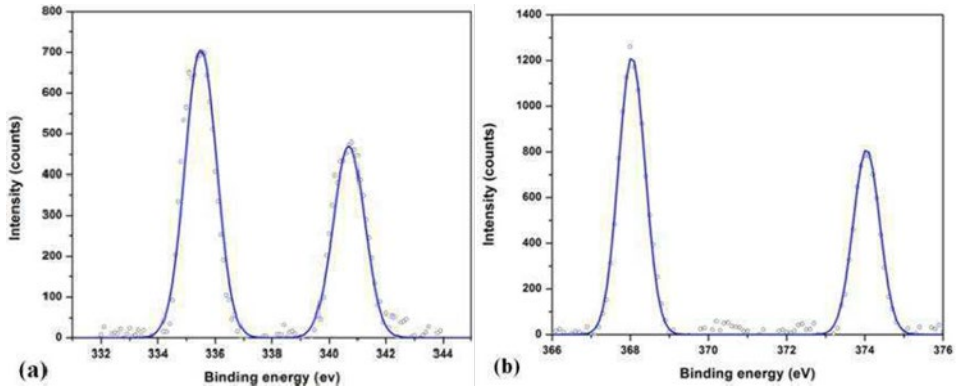

Figure 38: (a) XPS spectra showing palladium-3d signal for samples prepared by dipping in coffee- solution for 1 h. (b) XPS spectra showing silver-3d signal for samples without any Pd deposition

Table 2 summarizes the main characteristics of the samples tested using the flow-through setup for their response to hydrogen.

Table 2: Samples prepared for testing in diffusion chamber and flow through setups

Sample label	**Pd /Ag ratio, (EDX)**	**'Coffee-added'**	**Substrate**	**Base resistance R_0 (Ω)**	**Palladium time (h)**	**$PdCl_2$ concentration used for deposition (mM)**	**Hydrogen Dosage (H_2conc, % /time, s)**
a	0	-	Paper	17	-	-	10.7/ 360
b	0.08	Yes	Paper	29	1	4	100 / 540
c	0.32	No	Paper	248	1/2	4	10.7 / 360

d	0.51	Yes	Paper	717	24	4	10.7 / 360
e	0	-	OHP	60	-	-	10.7 / 360
f	1.06	Yes	OHP	205	24	4	10.7 / 360
g*	1.06	Yes	OHP	205	24	4	10.7 / 120
h	1	Yes	OHP	1054	168	8	10.7 / 120

* g represents a repeat measurement on sample f, for smaller exposure duration

3.2.1.9 Flow-through setup results

The measurement of changes in resistance of the test samples subjected to various gas-phase environments in the flow-through test set-up is summarized as plots of sensitivity ($\Delta R/R_0$) vs. time (Figure 39). The red-colored portion of the curves represents the duration during which hydrogen flow was added onto the base flow of nitrogen to achieve the desired concentration. The temperature during these tests was recorded to be 28 °C. The critical observations based on the results of the flow-through tests are:

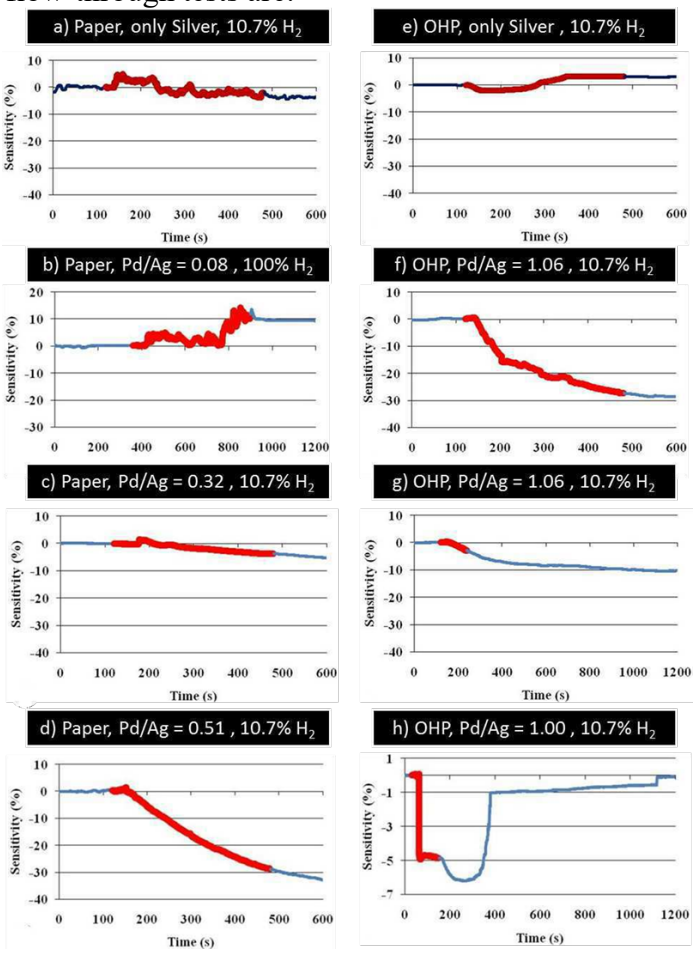

Figure 39: Measured responses of the various samples tested using the flow-through test setup. The red-colored portion of the curves represents the duration during which hydrogen flow was added to the base flow of nitrogen

(i) Role of Palladium

The need for palladium to detect hydrogen is evident in figure 39. With palladium,the sensitivity change upon exposure to hydrogen is more prominent, monotonic, and well above the noise level (root mean square value of sensitivity before hydrogen exposure is 0.24%, in Fig 39 (f)), while the sample without palladium shows random fluctuations (root mean square value of sensitivity during hydrogen exposure is 2.32%, in Fig 39 (e)).

(ii) Effect of palladium content

The Pd/Ag ratio, as measured by EDS, is an indicator of the palladium content of the detector. Pd/Ag ratio $\geq$ 0.32 leads to an appreciable signal upon H_2 exposure. For most samples, the resistance drops upon exposure to hydrogen. The decrease in resistance indicates that the effect of expansion on electrical conductivity is more significant than the formation of palladium hydride. For the sample with a Pd/Ag ratio of 0.08, the sensitivity fluctuated initially for about 400 s and after that showed a clearincreasing trend. We conjecture insufficient palladium in the network to expand the percolation pathway. So the response is slow, and resistance increases after most of the palladium are converted to palladium hydride. Interestingly, even after switching off the hydrogen supply (base flow of N_2 was kept on), the response continues with the same decreasing trend till saturation is reached. We suppose that the plastic sealant bags act as an additional reservoir (capacitance) that limits the ability to change the gas composition. This aspect needs to be investigated more thoroughly in the future.

The samples regained their base resistance value after being exposed to ambient conditions overnight. Thus, the hydrogen desorption from the nanostructured palladium-coated films was reversible but slow.

(iii) Effect of hydrogen dosage

Sample f was re-exposed (after the initial resistance was regained – ca. one day) to the same hydrogen environment but for a shorter duration (sample g). The change in resistance was lower for lower dosage. Thus, the extent of hydrogen absorption into palladium determines the magnitude of the response. The time taken for saturation of signal response is similar for both samples f and g.

(iv) Effect of deposition time

A comparison of the response of samples f and h indicates that the deposition duration significantly affects the response kinetics of the palladium-coated samples. The Pd/Ag ratio measured using EDX was similar for the samples toned for one day and one week, while the base resistance increased from 205 Ω to 1 kΩ. Although the Pd/Ag ratios are representative of the sample, they may need to be verified independently using a bulk technique. Presuming that the averaged EDX ratios are representative of the bulk composition, as the nanostructured films are less than a micron

in thickness, the increase in base resistance with increased deposition duration indicates that some of the silver in percolating paths are etched/displaced by palladium overlayer.

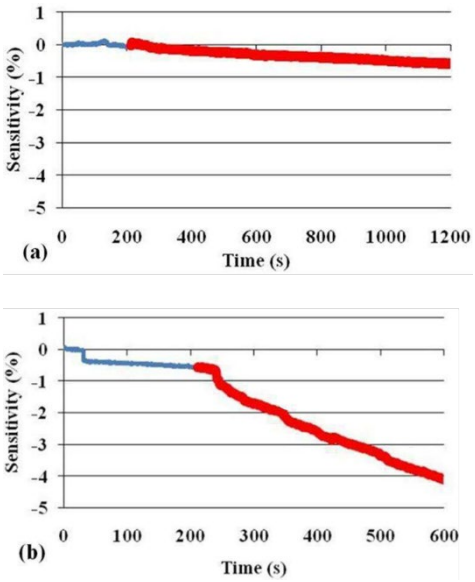

Figure 40: Static leak test– response of samples upon sudden exposure to an atmosphere of 1.62% H_2 (a) sample d – Pd/Ag ratio of 0.51 on paper (b) sample h – Pd/Ag ratio of 1 on OHP.

This sample was also able to recover its baseresistance value more rapidly. Such an architecture, wherein the palladium is present at the junction of percolating pathways, is apt for rapid detection and enables future detector-response optimization studies. Note: The palladium salt concentration was doubled, as a precaution, to account for any loss of activity during the one-week duration of the experiment.

3.2.1.10 Diffusion chamber setup results

Hydrogen was filled for three minutes to keep the test duration short and avoid interference from unknown leaks. After this, the lid was displaced, and the inner chamber opened up to an atmosphere of hydrogen (corresponding to 1.62 % H_2). The response of the sample toned for one week is much faster and more robust than the sample toned for one day. The leak detection response time of sample h was estimated to be 332 s. In calculating the response times, the lowest sensitivity value has been used as a saturation value to get its 90% value. The time taken to reach this value starting from when H_2 was switched on is reported as the response time.

3.2.2 Copper-aided Deposition

Preliminary experiments showed that placing a Cu tape next to a piece of bare OHP in Pd salt solution for a couple of hours yielded electrically conductive Pd – Cu nanoparticles. These deposits adhered well to the OHP sheet. A similar process was done on polyimide as well.

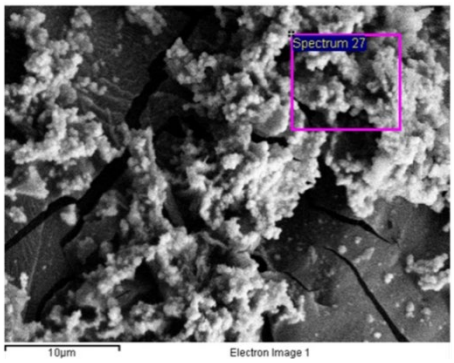

Element	Atom %
Pd	22.14
Cu	34.73
O	42.45
Au	0.69

Figure 41: FESEM image – EDS data of Pd – Cu nanoparticles deposited on polyimide by keeping the polyimide in "close vicinity" of a Cu tape in an 8 mM Pd salt solution for a couple of hours. The FESEM sample was sputtered with 8 nm of Au before imaging

However, there was no control over the amount of palladium deposited. Therefore, a new scheme was devised to confine the palladium to a fixed region. A copper tape would be placed on a polyimide substrate, and a "slot" would be cut. By restricting the Pd salt solution to the slot, the resulting deposits would only be formed in the slot. Thus, excess Pd, which could act as a reservoir for hydrogen molecules, could be avoided, enabling faster recovery.

A piece of Cu tape (½" width) was cut and stuck on polyimide. A cutter was used to make a slot between the Cu tape (schematic below).

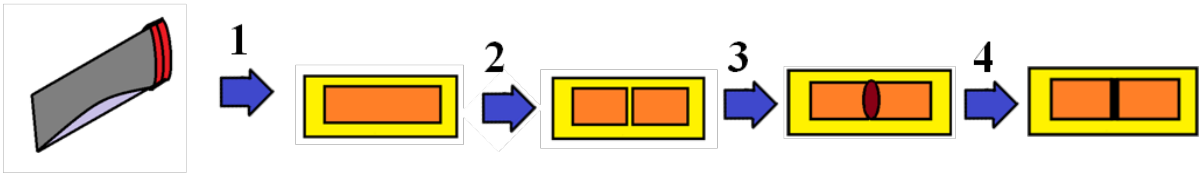

Figure 42: Schematic showing the sequence of steps in preparing a gap bridged by Pd – Cu nanoparticles

A 10 µL drop of Pd salt solution was placed on the slot (t = 0). After the first 10 minutes, another 10 µL drop was added and kept for two hours. The sample was then washed with DI water and dried. It was tested for its gas sensing performance.

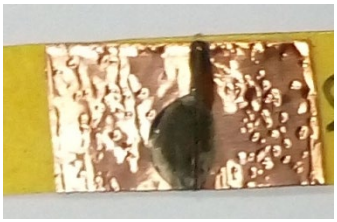

Figure 43: A slot bridged using 20 µL of Pd salt solution to lessen the reaction between Pd and surrounding Cu

However, the drop couldn't be confined to the slot, creating unwanted deposits on the surrounding tapes. Thus, the process wasn't repeatable. Therefore, a method to confine the solution drop to the slot was needed.

3.2.2.1 Slotted copper tape on polyimide

The sample shown in Fig. 43 was examined under an SEM. The SEM-EDS analysis showed that several Pd – Cu nanoparticle clusters bridged the slot gap between the Cu tapes. Fig. 44(4) is a magnified image of such nano-particles.

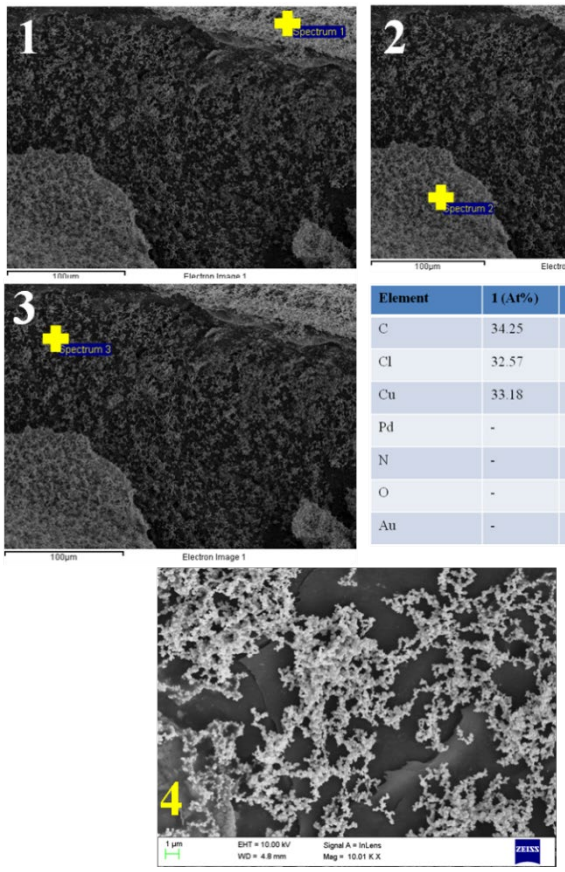

Element	1 (At%)	2 (At%)	3 (At%)
C	34.25	22.79	64.31
Cl	32.57	13.41	-
Cu	33.18	51.97	1.98
Pd	-	11.83	0.84
N	-	-	15.24
O	-	-	17.42
Au	-	-	0.21

Figure 44: (1) & (2) FESEM images of a bridged slot, with EDS spectra taken on Cu tape on either side of the slot. (3) FESEM of bridged slot, with EDS spectra taken. (4) Magnified image of Pd – Cu nano-particles inside the slot

. The base resistance was 72.04 Ω. The N_2 flow rate was 7 LPM, whereas the H_2 was 200 ml/min (2.85% H_2). The response plot is given below.

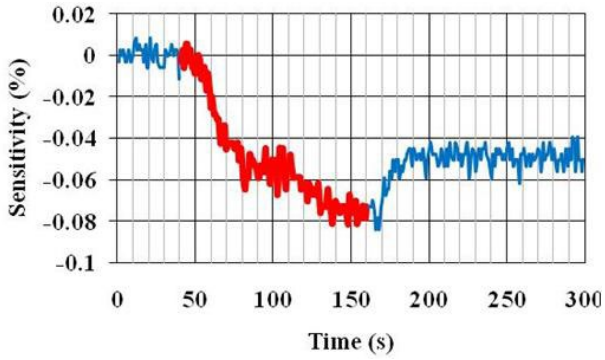

Figure 45: Response graph of the sample in Fig. 43 upon exposure to 2.85% H_2 during 40 – 160 s of the test

As Fig.46 shows, the sensitivity of the response was ~0.08 % at its lowest. It could recover partially at the end of the 300 s test.

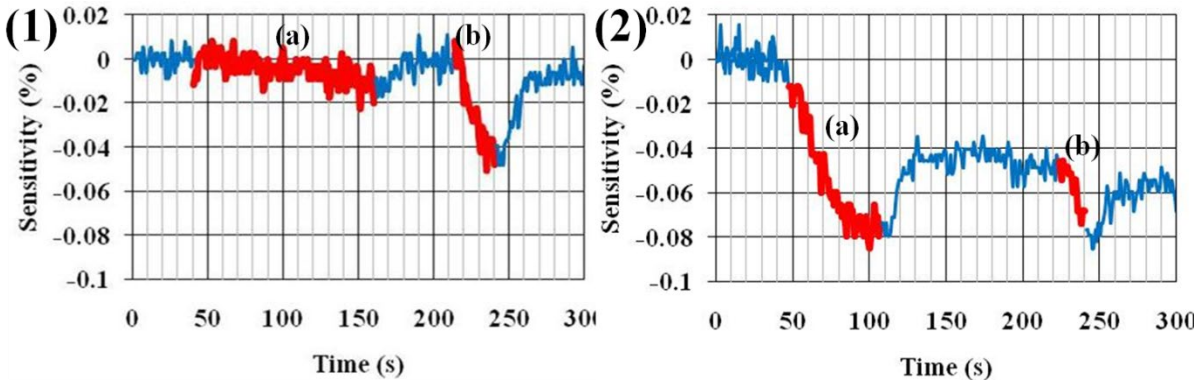

Figure 46: (1) Response graph of the sample in Fig 43. upon exposure to (a) 1.07% H_2 during 40 – 160 s & (b) 2.85% H_2 during 213 – 240 s. (2) Response graph of the same sample upon exposure to 2.85% H2 during (a) 47 – 107 s & (b) 223 – 240 s

Another test was carried out where the concentration of H_2 was varied. From 40 s to 160 s, the N_2 flow rate was 7 LPM, and the H_2 flow rate was 75 ml/min (1.07% H_2). Then, from 213 s to 240 s, the H_2 flow rate was 200 ml/min (2.85 % H_2).

In another test, the concentration of H_2 was kept the same, but the exposure time was varied. The concentration was fixed at 2.85% H_2. H_2 was passed from 47 s till 107 s (duration: 60 s) and from 223 s till 240 s (duration: 17 s). The sensor recorded a drop of 0.08% for the first pulse of H_2. It didn't recover to its original baseline but instead to a lower, shifted one. The second pulse recorded a drop of 0.03% from the lower baseline. Thus, the Cu-Pd deposits were able to respond to the hydrogen stimuli. However, the repeatability of the sample preparation was poor. The sensitivity was also less, even at relatively high hydrogen concentrations of >1%. Thus, it was necessary to confine the Pd deposits to the slot itself.

3.2.2.1.1 Two-drop method

The solution drop was placed at the edge of the slot (see schematic below). It was expected that the drop would flow in the slot by capillary action.

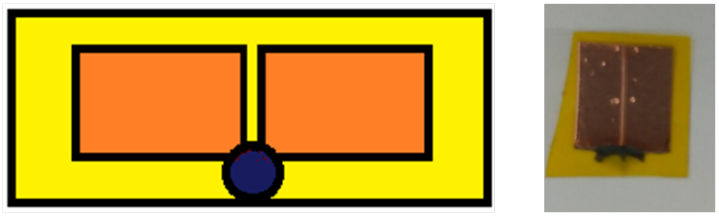

Figure 47: (Left) A Pd salt solution drop (misrepresented in blue, for the sake of clarity) kept at the edge of the slot, presuming that it would flow in by capillary action (Right) Actual sample showed that the drop did not wick into the slot

However, the drop didn't flow in the slot, as it didn't wet the polyimide. A different scheme was devised to make the drop flow in the slot.

A drop of aqueous Pd salt solution was placed at one end of the slot. Scotch tape masks protected the edges of the Cu tape so that the Pd didn't contact the Cu. Then, a drop of ethanol was kept at the other end of the slot. The ethanol drop flowed through the slot and reached the other end, where the aqueous $PdCl_2$ drop was situated. When the ethanol drop reached the other end, it could mix

with the Pd salt solution drop. Thus a continuous and stable film of aqueous $PdCl_2$ was able to form across the length of the channel. The slot was bridged with minimal wastage of $PdCl_2$ owing to the drop confinement to the slot only.

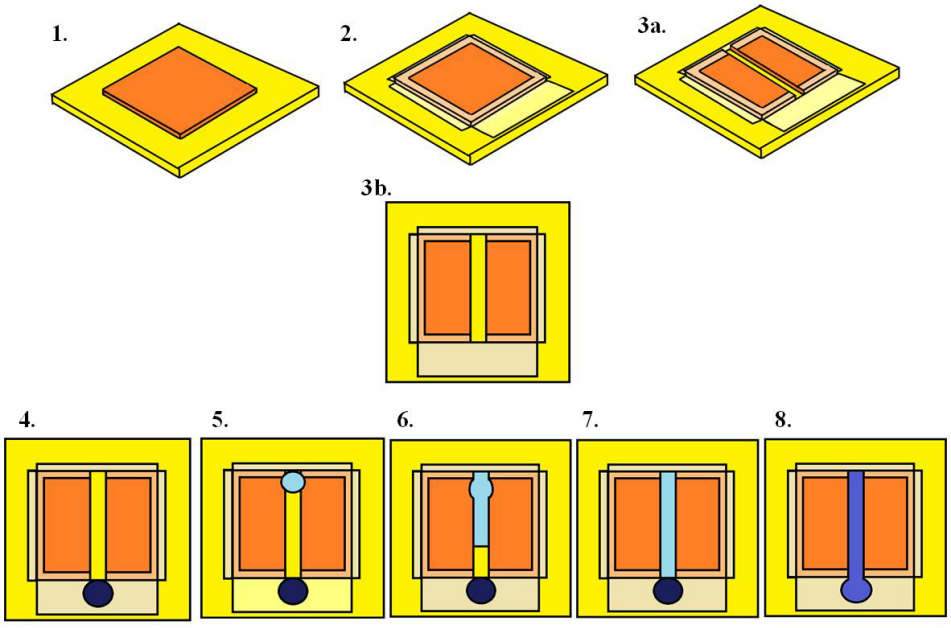

Figure 48: Schematic of the process that can flow the Pd salt solution through the slot (1) Cu tape on polyimide (2) Cu tape edges protected by scotch tape masks (3a) Slot made by precision knife (3b) Top view of the slot (4)Aqueous Pd salt solution drop (misrepresented by dark blue, for clarity) at one end of the slot (5) A smaller ethanol drop at the other end of the slot (misrepresented by light blue, for clarity) (6) The ethanol drop moves through the slot, (7) reaches the other end and (8) mixes with the Pd salt solution drop to form a continuous film (misrepresented by medium blue) spanning the entire length of the slot

Figure 49: A sample made by the process shown in Fig. 48

This experiment was performed by making the slot on a Cu tape. 10 µL of 20 mM Pd salt solution (in HCl) was kept at one end, while 4 µL of ethanol drop was kept at the other end, as shown in the schematic above. This arrangement was maintained for 1 hour. The sample was washed and dried after that.

The two-drop method was able to confine the Cu-Pd to the slot itself. The base electrical resistance (R_0) of the sample prepared thus was 12.03 Ω. The slot had Cu-rich particles that were a few hundred nanometers in diameter. We hypothesized that there was not enough palladium entering the slot to be reduced by reacting with the copper.

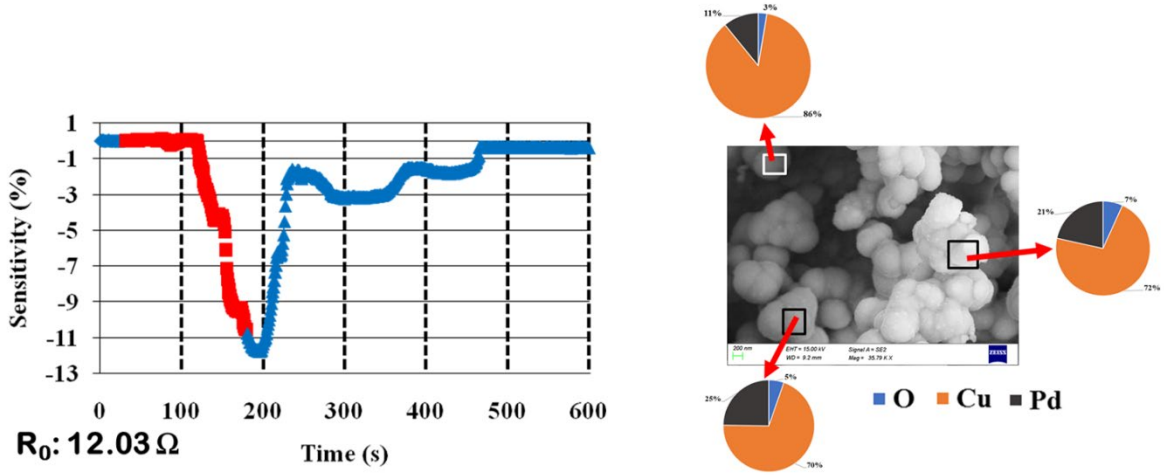

Figure 50: (Left) First response of the sample prepared by the two-drop method to 3.6% H_2 in N_2 (Right) SEM-EDS analysis of the slot showing Cu-Pd nanoparticles

The corresponding sensitivity vs. time response curve is shown in Fig. 50. The detector was exposed to 3.6% H_2 in N_2 background. The detector was able to respond with better sensitivity than the one shown in fig. 45, 46. However, a long lag was observed between switching the hydrogen flow to the instant the detector started responding. The reference sensor showed a lower lag time in an identical test when tested in the same flange.

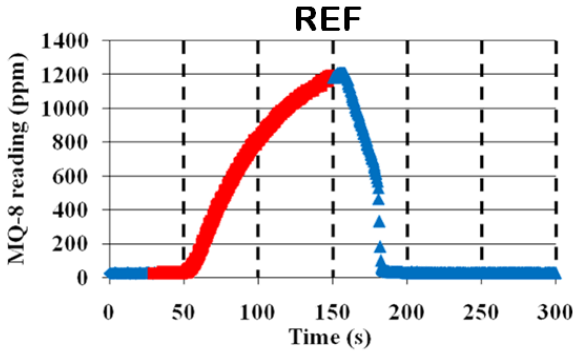

Figure 51: Response of the reference sensor to 3.6% H_2 in N_2, placed in the same flange as the detector

Although housed in a similar flange, the reference sensor protruded into the T-section, unlike the detector. Therefore, it would have been possible that the reference sensor would have experienced a different environment than the sample, resulting in a faster response. COMSOL 5.1 was used to simulate the flow to verify the flow inside the T-section. A T-section with similar dimensions was created, and nitrogen was passed in a laminar flow condition. The pipe exhibited a parabolic velocity profile as expected. However, going higher up inside the T – section, the fluid velocity gradually decreased. Thus, unlike the reference sensor, the sample would have experienced

stagnant flow conditions leading to delayed response. After removing the flanges, the detector and the reference sensor were placed inside the pipe to eliminate this disparity. The detector was placed on a stage at the same height inside the pipe as the reference sensor.

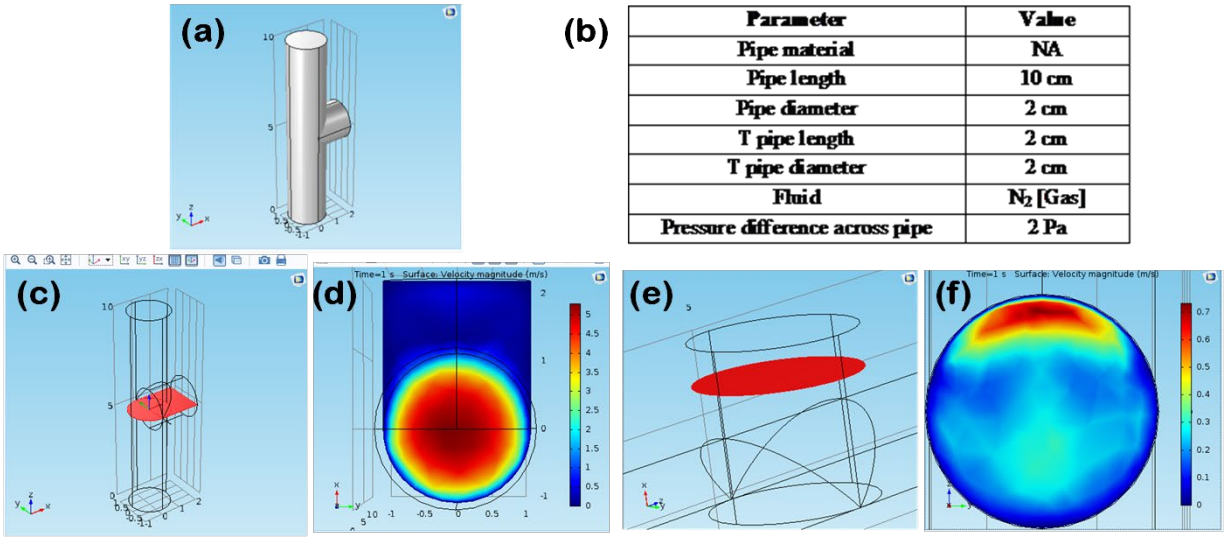

Parameter	Value
Pipe material	NA
Pipe length	10 cm
Pipe diameter	2 cm
T pipe length	2 cm
T pipe diameter	2 cm
Fluid	N_2 [Gas]
Pressure difference across pipe	2 Pa

Figure 52: (a) T in pipe (b) Parameters used (c) Cut plane 1 (d) Velocity profile in cut plane 1 (e) Cut plane 2 (f) Velocity profile in cut plane 2

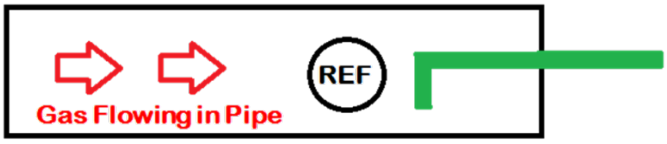

Figure 53: Schematic of the flow-through setup for gas sensing characterization. The circled "REF" represents the reference sensor, while the green rod represents the stage

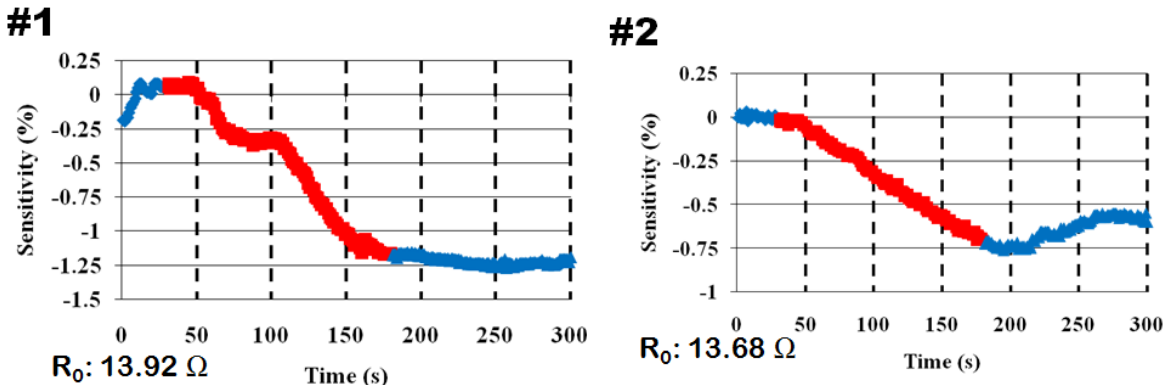

Figure 54: Back-to-back responses of the detector to 3.6% H_2 in N_2, placed inside the pipe

When the same detector was placed as per the arrangement shown in fig 53 and tested under the same conditions, the response began simultaneously as the reference sensor. However, the recovery wasn't observed. We hypothesized that higher Pd content would give rise to reproducible responses. The upcoming sections highlight the efforts to increase the Pd content in the slot.

3.2.2.1.2 One drop method

The low levels of Pd seen in the previous case could be due to the highly aqueous nature of the film formed in the slot. The higher ethanol content in the film would ensure that the Pd solution flowed well in the slot due to higher wettability. Ethanol was mixed with Pd salt solution in the desired proportion, unlike the previous two-drop method, to make the drop directly flow into the slot. Higher ethanol content was preferred to make the drop flow spontaneously into the slot. For this purpose, an experiment was performed to see what vol% of ethanol could best serve this purpose. Alternatively, masked samples were made, where a layer of tape was stuck on the slot where the drop was to be placed to avoid contact between the Pd salt solution drop and the copper tape underneath.

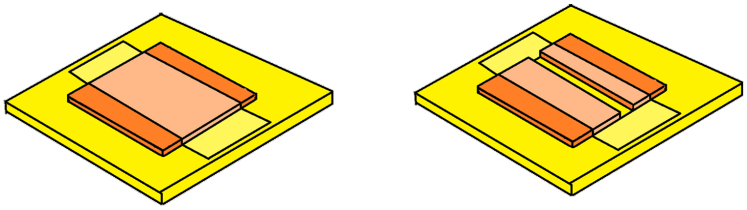

Figure 55: Methodology showing preparation of a centrally masked sample. A central tape on a copper contact pad was cut through to make the slot

3.2.2.1.2.1 Malachite green experiment

A pure ethanol drop would volatilize rapidly in ambient conditions, leaving little time for particles to form. Hence optimizing the ethanol content in the drop was the first step. The ethanol was mixed with an aqueous solution of malachite green dye in various proportions to visualize the drop flowing in the slot.

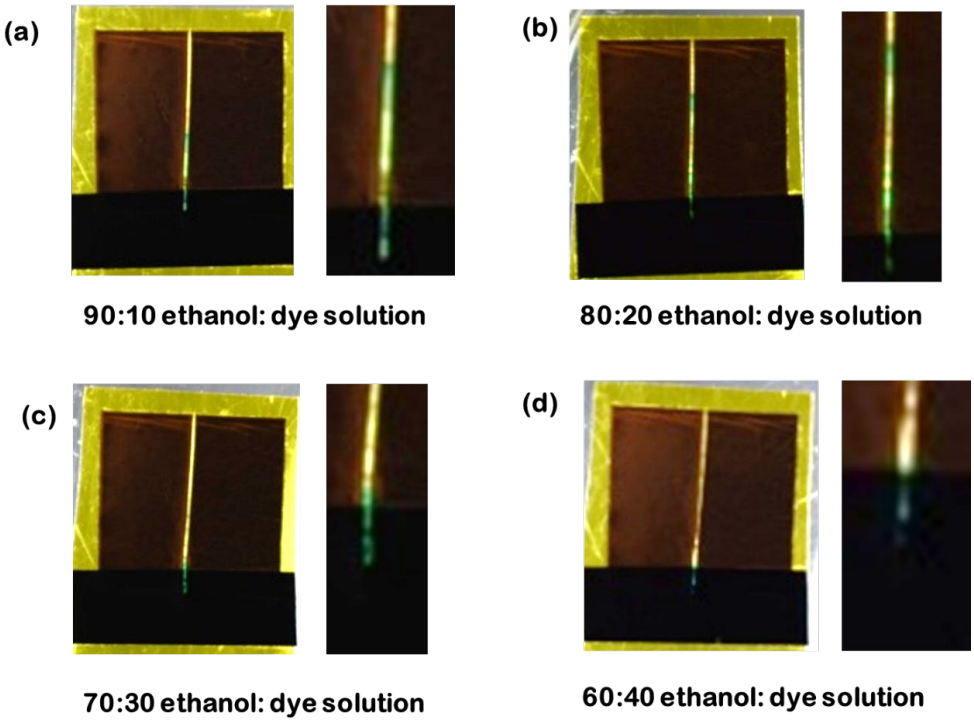

Figure 56: Dye solution visualized in the slot for various ethanol concentrations

The fig. 56 above shows 1 µL drops of four different ethanol: dye mixtures attempting to flow into similar slots. The 90:10 and 80:20 solution drops could flow partially into the slot. Both types of drops were contained in the slots. The 90:10 drop volatilized within 1 minute, whereas the 80:20 drop volatilized between 3-4 minutes. Since the 80:20 drop could stay longer, it was decided to use this proportion for future experiments.

3.2.2.1.2.2 80:20 experiments

An unmasked sample was prepared by placing a 200 mM (80:20) drop of 5 µL at one end of the slot for 20 minutes under ambient conditions. The sample image is shown in fig. 57. As can be seen, there was some spillover from the slot onto the copper tape. Despite that, particles partially bridged the slot, resulting in a base resistance of 2.30 Ω.

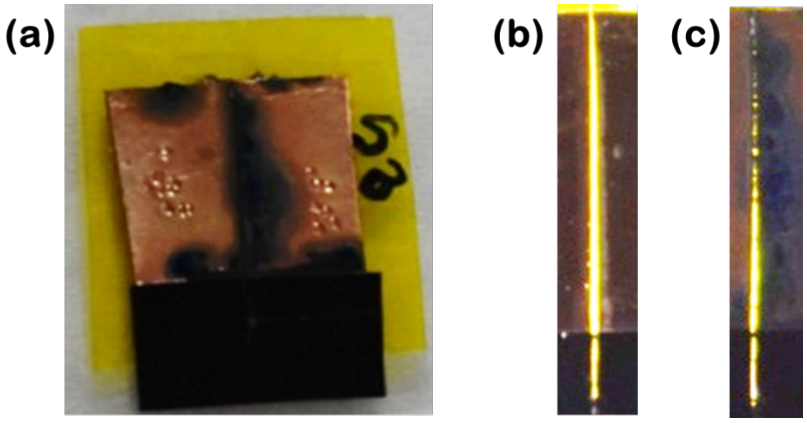

Figure 57: The unmasked sample had extraneous deposits (black stains on copper) on the contact pads (a), (b) slot with no mask, (c) slot seen after deposition

The SEM-EDS analysis of these samples is shown in fig. 58. The particle sizes were also quite like that observed in fig. 50. It might have been possible that the drop spillover from the slot could have depleted the amount present in the slot itself.

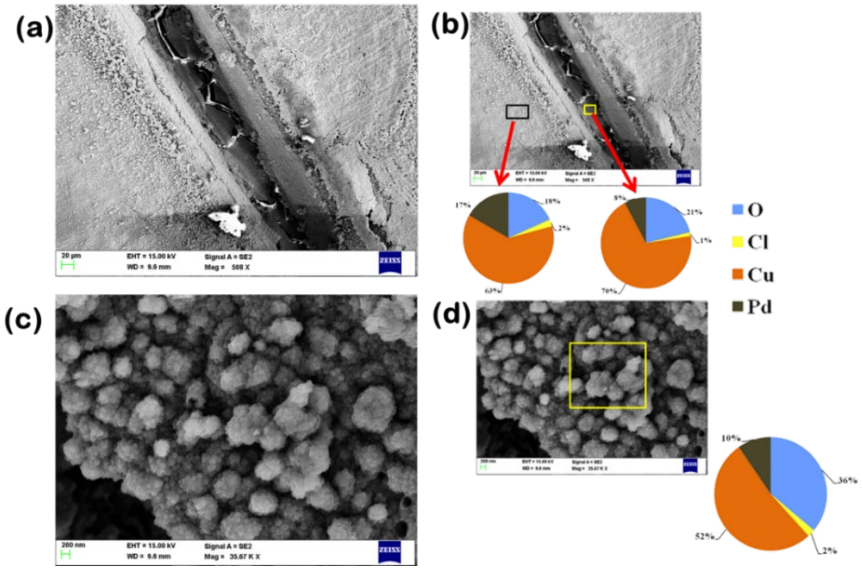

Figure 58: (a), (b): SEM-EDS characterization of the slot of the unmasked sample. (c), (d) The Cu-Pd particles deposited in the slot were copper-rich

The gas sensing of the sample was carried out in a pipe configuration. Fig. 59 shows the corresponding response obtained upon pure hydrogen flow at 300 ml/min in the pipe. As can be seen, the sensor showed a drop in resistance owing to the nanogap closing mechanism. Partial recovery was also seen upon stopping the hydrogen flow.

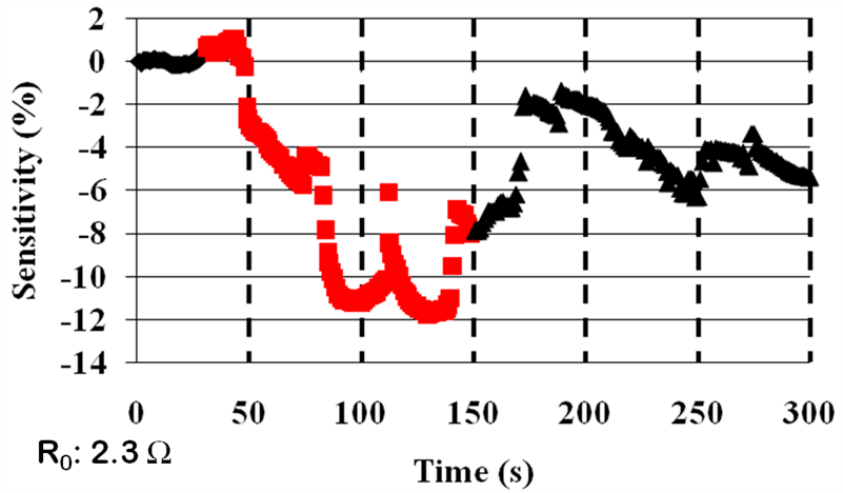

Figure 59: Response of the unmasked sensor to pure hydrogen

However, the sensor wasn't responsive to dilute hydrogen, as the Pd content observed in the EDS analysis was low.

The samples were masked before the drop placement to prevent the drop from contacting the copper tapes. The mask was an electrical tape stuck on the copper tape. After masking the sample, a slot was cut through it. A 5 µL (80:20) aliquot of 200 mM $PdCl_2$ drop was placed for 20 minutes at ambient conditions, just like the unmasked sample.

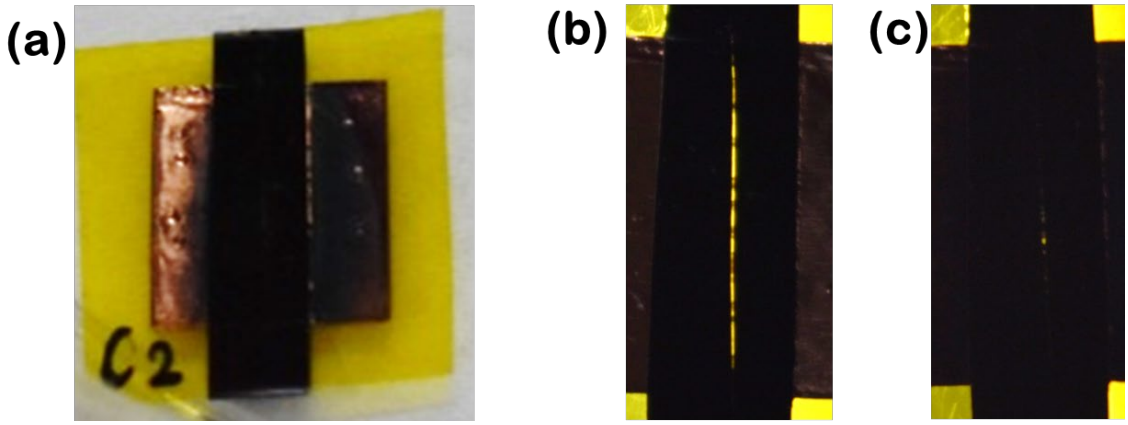

Figure 60: Centrally masked sample after deposition (b) Image of the slot before deposition (c) Image of the slot after deposition

Figure 60(c) above shows that the slot showed deposition. It had a base electrical resistance of 13.60 Ω.

Fig. 61 below shows the SEM images along with the EDS spectra. The Pd content was significantly higher than in previous samples. The particles (fig. 61(c)) were also smaller than those of the unmasked and the two-drop method samples.

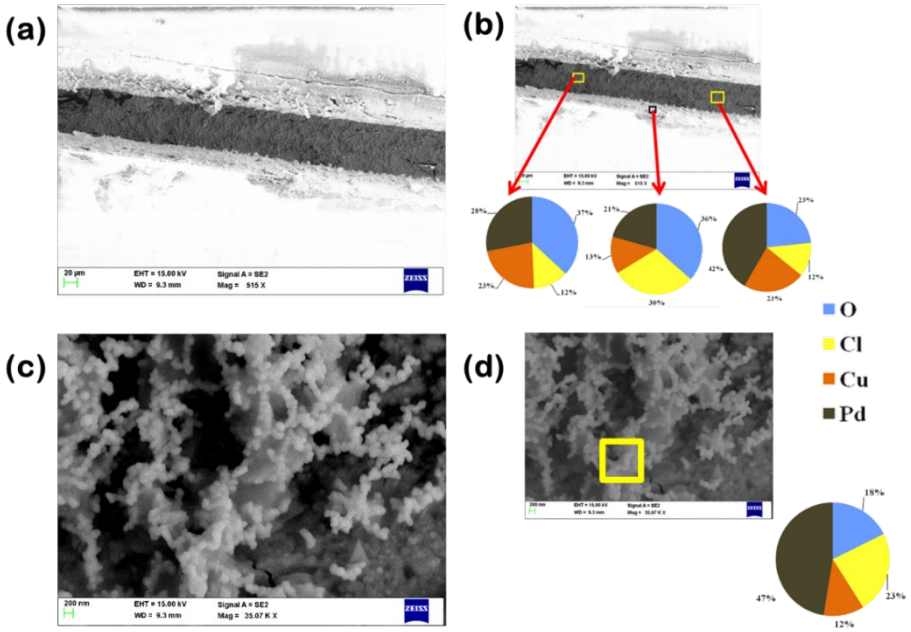

Figure 61: (a), (b) FESEM image of the slot of the centrally masked sample and its EDS analysis (c), (d) The Cu-Pd slot particles showed a higher Pd content than the unmasked sample

The sample was mounted as per the schematic in fig 53 and exposed to pure hydrogen, flowing at 300 ml/min in the pipe. The corresponding response is shown in fig—62 (a). The sample exhibited a drop in resistance upon exposure to pure hydrogen. The drop in sensitivity was more than that observed in the case of the unmasked sample. It showed a partial recovery when hydrogen flow was stopped like the unmasked sample. The sample was also exposed to 3.6% H_2, to which it responded less sensitively (fig 62(b)), as opposed to pure hydrogen.

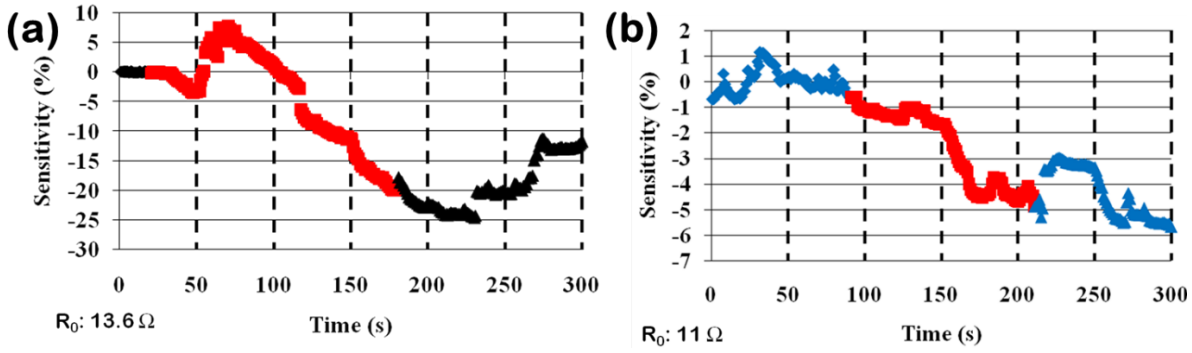

Figure 62: (a) Response of the unmasked sample to pure hydrogen (b) Response to dilute hydrogen

These tests showed that a higher Pd content in the slot was desirable. However, the Pd content in the nanostructures wasn't enough to ensure recoverable responses. Therefore, the Pd content needed to be increased further. It might have been possible that the small slot volume would have

limited the extent of Pd-rich nanostructures. Based on this hypothesis, the slot gap was increased to accommodate greater drop volume.

3.2.2.1.3 Increased slot spacing

A wider slot was made by removing copper tape from between. Since the slot spacing was more than before, it would require more deposits to bridge the gap. A larger volume of Pd salt solution would be required to achieve that. So the samples were immersed in a 2 ml pool of Pd salt solution. Three different values of concentration (5 mM, 20 mM, and 100 mM) were used for deposition times of 20 minutes, 1 hour, and 2 hours. All samples were made in triplicate, except for the 100 mM, 20-minute experiment, which was only repeated twice.

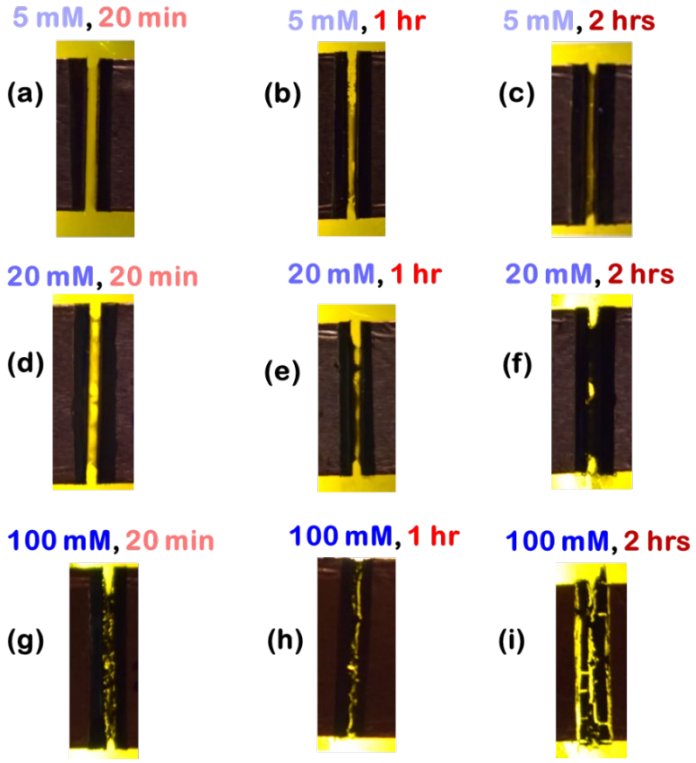

Figure 63: Slot images of samples exposed to various points on the C, t plane

Fig. 63 shows the images of the slots on polyimide, with Cu tapes on either side after deposition for the nine points on the C, t plane. For the 5 mM and 20 mM samples, the density of particles increased as the time was increased. For the 100 mM row, the 2-hour sample appears sparser than the others. That was because the high concentration's duration was such that bulk galvanic displacement of the copper from the Cu tape started. That leads to lessening contact between the Cu tape and the slot particles. It manifested in higher electrical resistance across the two copper tapes. The sample kept for 20 minutes in 5 mM Pd salt solution yielded no visible deposits and was non-conductive. Hence it wasn't analyzed for SEM-EDS characterization or gas sensing experiments. The electrical resistance of all the samples is given in the below table. All values, unless specified, are in ohms. "NC" stands for non-conducting.

Table 3: Resistance repeatability of triplicate samples for various points on the C, t plane

C, t	20 min	1 hr	2 hrs
5 mM	NC	59.91, NC, 12.93 kΩ	23.00, 36.90, 47.25
20 mM	524.95, 116.01, 1.21 kΩ	74.00, 36.44, 239.47	93.77, 50.63, 16.80
100 mM	448.26, 33.33	80.63, 86.30, 3.49 kΩ	16.30 kΩ, 138.56 kΩ, 304.12 kΩ

The resistances have sample to sample variation for the same experiment, so they can't be compared. However, as the time became longer, the average resistances reduced. It is also evident by looking at the density of particles in fig. 63. The particle density increased as time went by. The drop in resistance was prominent in the case of 20-minute and 1-hour experiments. The 100 mM experiment saw a bulk attack on the Cu tape due to the high Pd salt solution concentration, leading to increasing average resistances.

The SEM images of the Cu-Pd particles in the slot are shown in fig. 64. The scale bar for all the images is the same. As can be seen, the particle size increased as the Pd salt solution concentration and the deposition time increased. The EDS analysis shows the elemental breakup of the slot particles. The EDS showed carbon as well, which was due to the underlying polyimide.

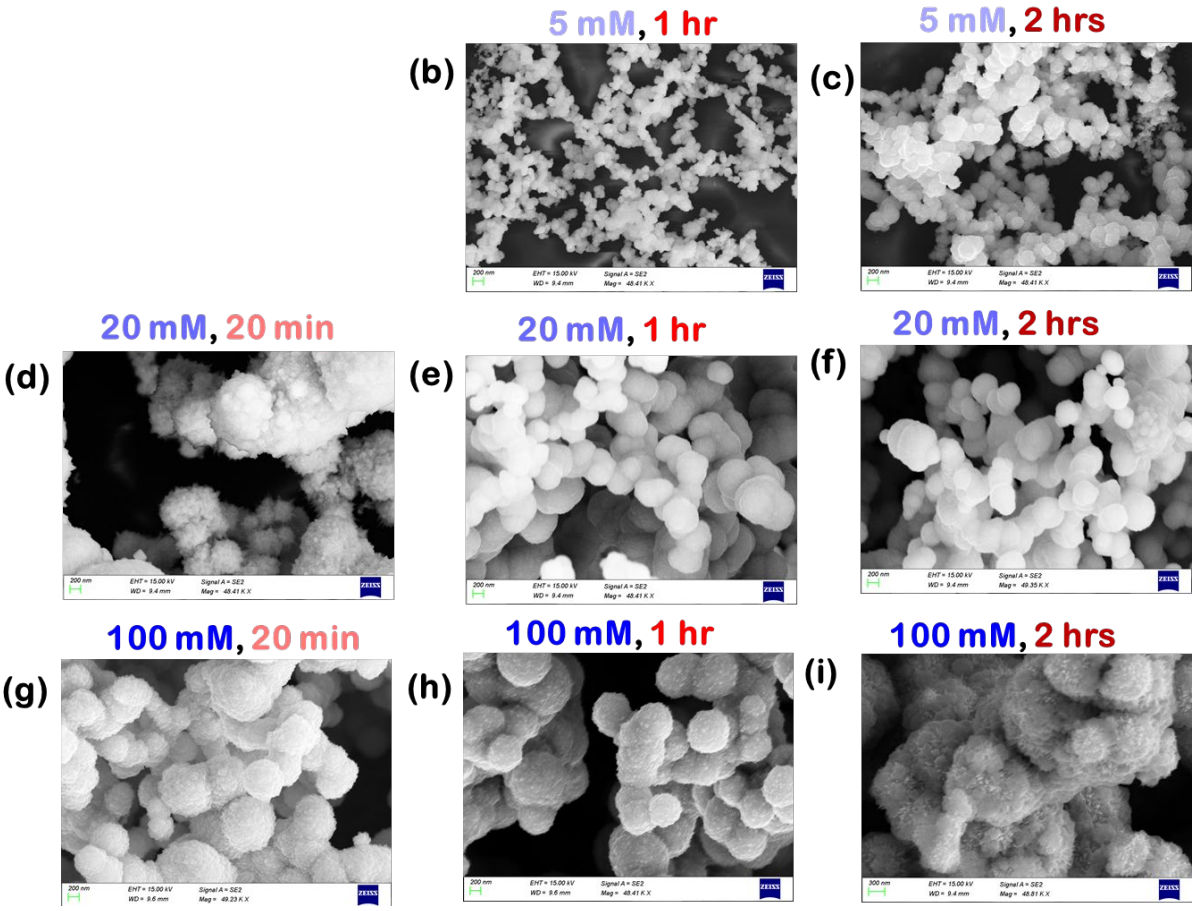

Figure 64: FESEM images of slot particles of samples on various points of the C, t plane

Fig. 65 shows the EDS spectra of the slot particles. As can be seen, the Pd content was similar in all the samples on average. The Pd content was slightly higher than the one seen with the one-drop method. But the range of concentration and time over which the experiment was carried out was quite extensive. Even then, any clear trend of Pd content among these images wasn't evident. It possibly meant that the particle's content was not as strongly affected by the Pd salt solution concentration and the time. The same material was deposited in the slot, regardless of the Pd salt solution concentration. Nevertheless, as the samples were conductive, they were tested for hydrogen sensing experiments.

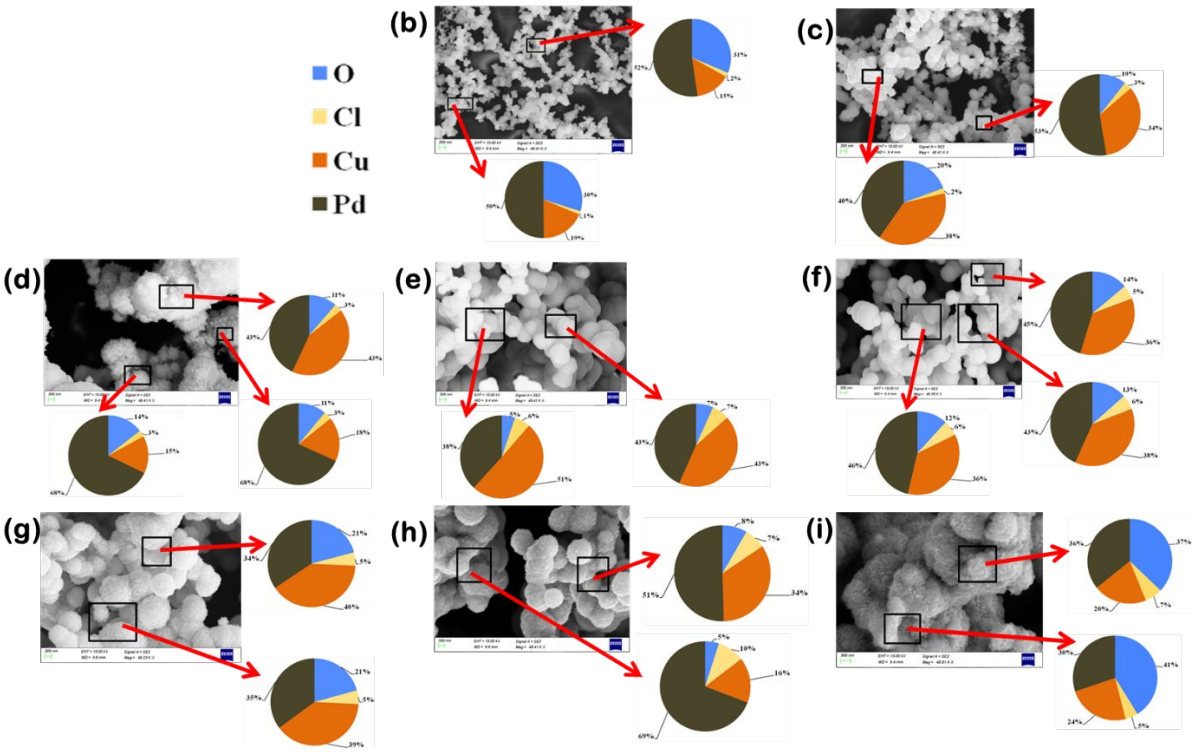

Figure 65: EDS analysis of slot particles of samples on various points of the C, t plane

Fig. 66 shows the responses of all the samples when exposed to 2.4% H_2 in N_2 (red part of the curves). The graph labeled "REF" shows the response of the reference sensor, kept in front of the sensor. The lag faced by the reference sensor was the same as seen in most sensors in fig. 66. It showed that the lag was extrinsic. The responses were alike; all resistances dropped upon exposure to hydrogen and didn't recover. The sensor in fig 66(b) showed sluggish recovery, probably due to smaller particle sizes [5].

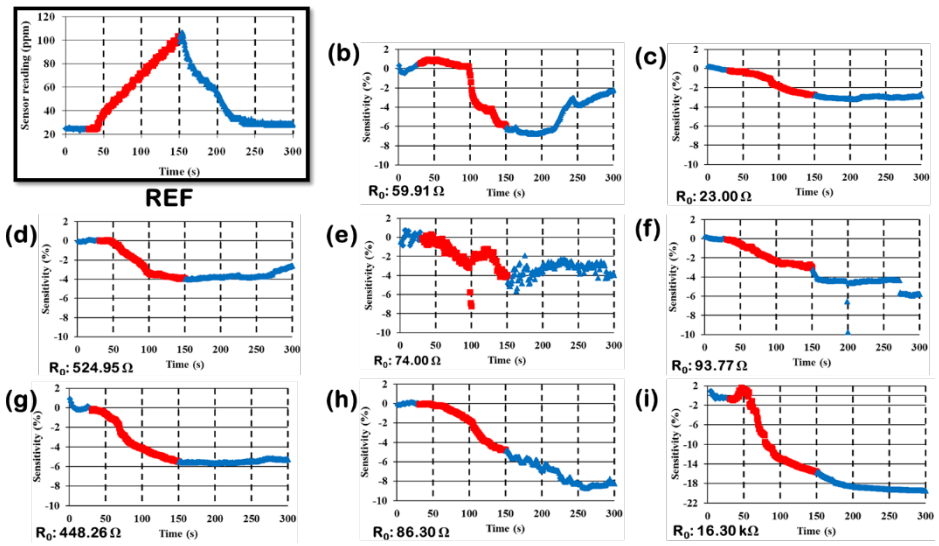

Figure 66: Gas sensing results of samples on various points of the C, t plane

The sensors developed in this experiment didn't have any intrinsic lag. However, they didn't have any recovery in the 5-minute tests. More Pd content in the nanostructures was required to get faster recovery. However, the Pd content was probably driven by the copper metal itself, as discussed earlier. It wasn't strongly affected by the Pd salt solution concentration and the time as was expected before.

3.2.3 Aluminum-aided

Aluminum (Al) has a low reduction potential (E^0 = -1.662 V), which means it can act as a reducing agent for a variety of metal ions, including Pd^{2+} as well [42]. However, the surface of metallic aluminum is naturally passivated by an oxide layer, limiting its use as a practical reducing agent [43]. Despite this limitation, anions such as F-, Cl-, Br- etc., have penetrated the oxide layer and generated H atoms. These H atoms could travel to the surface of the aluminum and reduce any metal ions present in the solution[44].

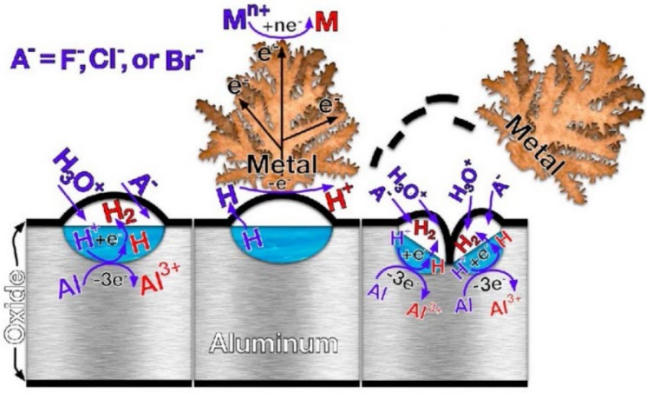

Figure 67: Al-aided metal used by Manthiram et al. [44]

This method was adapted for depositing metals such as Pd and Pt on plastic substrates in this work. The preliminary experiments were conducted by immersing samples covered with aluminum in

Pd salt solutions. The Pd^{2+} ions from the solution would then get reduced and deposit on the. However, this method required an excessive Pd in the salt solution. Therefore, the process was modified to obtain samples using a significantly less Pd. The modified method was used throughout this work for depositing both Pd and Pt on substrates, with minor variations. The following sections describe the fabrication method using both approaches.

3.2.3.1 Pd via immersion

3.2.3.1.1 Pd salt solution

450 mg of $PdCl_2$ (99.9%, Sigma) was added to 10 ml DI water to prepare a 250 mM stock solution. 10 drops of conc. HCl (SD Fine Chemicals Ltd., 35 – 38%) was added to the solution so that $PdCl_2$ could dissolve faster [45]. The solution was kept overnight at ambient conditions for the complete dissolution of the Pd salt. 200 mM of Pt salt solution was prepared by adding 83 mg of K_2PtCl_4 to 1 ml DI water. No acid was added, as the Pt salt readily dissolved in an aqueous solution.

3.2.3.1.2 Sample preparation

A tape was stuck on a PET sheet and cut into 1 cm × 1cm pieces. A piece of aluminum tape (Pinball 608) was stuck on the surface (Fig..68 (1)). It was covered using a plastic tape (Wonder Achem, Made in Taiwan) (Fig 68(2)). The sacrificial aluminum was added by sticking another aluminum tape on top of the plastic tape (Fig 68(3)). A trench was made by cutting through all the three layers of sacrificial tape, plastic tape, and the bottom aluminum tape (Fig 68(4)). It was expected that after immersion in the Pd salt solution, the sacrificial aluminum would reduce the Pd^{2+} ions and yield Pd deposits inside the trench (Fig.68 (5)). Since these deposits would be composed of Pd^0, they would have to be electrically conductive. Assuming the trench Pd deposits would contact the bottommost aluminum (Fig 68(6)), the latter would serve as electrical contact pads situated on either side of the deposit. This approach was based on a similar experiment involving copper as the sacrificial metal.

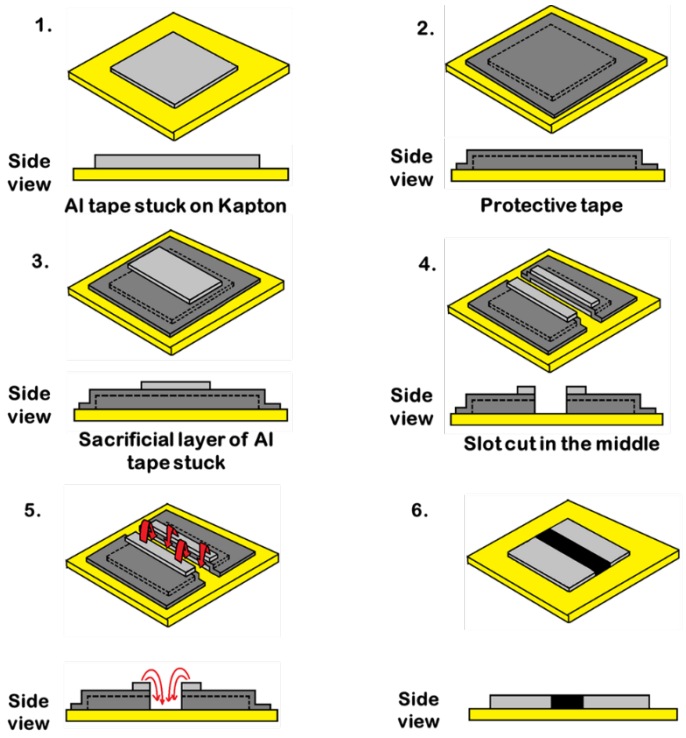

Figure 68: Schematic of the sample preparation for the immersion approach

The Pd salt solution was prepared by taking 1 ml of the stock and diluting it to 2 ml by adding DI water in a glass vial. The sample was immersed in the diluted solution and stored for one hour, after which it was taken out and washed thoroughly with deionized water. The protective tape was removed.

3.2.3.2 Pd by drop-casting

The process described in the previous section was modified to decrease the amount of Pd required per sample. It was done using the following modifications:

i. Less aluminum: Since reduction via aluminum was the driving factor for the Pd, by decreasing the amount of aluminum contacting the salt solution, one could principally decrease the amount of deposited Pd, thereby requiring less Pd in the salt solution
ii. Drop casting the salt solution: Sample immersion required a large volume of salt solution (2 ml) per sample, as seen in the previous section. Drop casting could allow significantly fewer volumes (10 – 100 µL) per sample.
iii. Avoiding the usage of contact pads: The "contact pads" were eventually found not to be in electrical contact with the trench deposits, which rendered them unnecessary

An additional issue encountered with using bare Al tapes directly for depositing Pd was that the ensuing deposits used to be "loosely" adhered to the surface. The scratch resistance of such samples used to be poor (experiment not shown). It had been demonstrated previously that the treatment of Kapton with KOH is a ring-opening reaction, which could implant the K+ ions into the top sublayer. The K+ ions could then be replaced with the desired metal ions and form a layer. This metal interlayer was found to improve the adhesion strength of the depositing metal on Kapton [46]

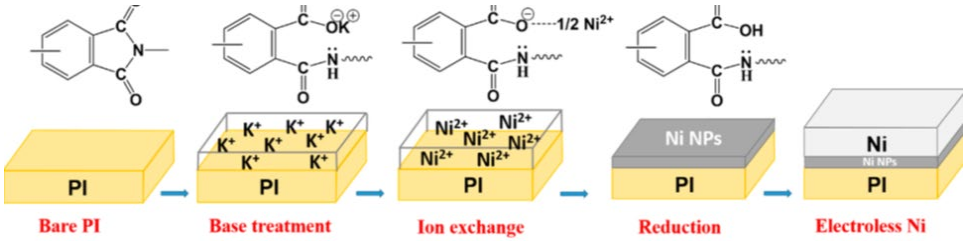

Figure 69: Schematic of the process to improve adhesion strength of metals on [46]

The following methodology was used to fabricate samples, considering the above points.

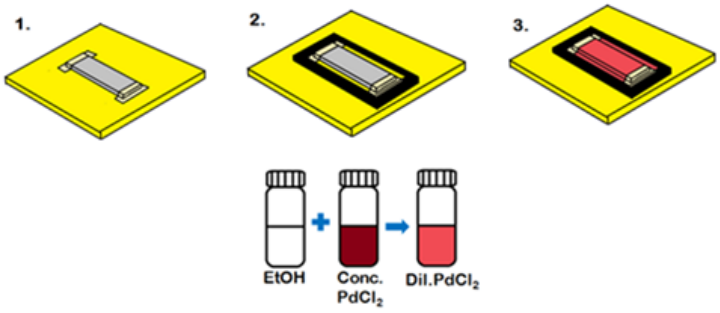

Figure 70: Schematic of the drop-casting method using diluted Pd salt solution as the precursor

Firstly, aluminum foil was stuck on Kapton using adhesive tapes. A rectangular frame (1.25 cm × 0.7 cm) was carved out of electrical tape and stuck around the foil. The stock $PdCl_2$ solution was diluted using ethanol, and 20 µL of the dilute solution was drop cast inside the frame. The solution was contacted with the foil for 5-6 minutes, after which the frame and the foil were removed. The sample was washed thoroughly with deionized water.

The purpose of diluting the salt solution using ethanol was that the ethanol-rich solution could easily spread on the hydrophobic substrate, unlike the aqueous stock. Thus, it enabled the usage of lower volumes of the salt solution. The plastic frame acted as a container for the drop.

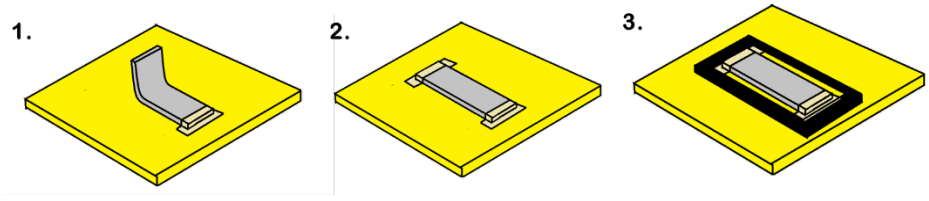

Figure 71: Steps involved in sticking the Al foil on

It was essential to stick the foil uniformly on the substrate, which was done by the following steps:

- The foil was first cut into the desired size mentioned above
- A piece of cello tape was stuck at one end of the foil
- The foil was then placed on the desired region, and the tape was pressed down uniformly (Fig 71(1))
- 5-10 µL ethanol was drop cast on the foil, and the foil was flattened by using a roller

- Another piece of cello tape was stuck at the other end of the foil (Fig 71(2))
- The electrical tape frame was stuck such that it surrounded the foil entirely

A similar method was followed for depositing Pt, except that the stock solution was used without dilution. For obtaining the bimetallic Pd-Pt, the stock solution of Pd and Pt were mixed in various proportions, followed by dilution with ethanol as mentioned below:

1. 79:21 Pd:Pt – 30 µL of 250 mM $PdCl_2$ + 10 µL of 200 mM K_2PtCl_4 + 40 µL ethanol
2. 30:70 Pd:Pt – 30 µL of 200 mM K_2PtCl_4 + 10 µL of 250 mM $PdCl_2$ + 40 µL ethanol + 40 µL deionized water
3. 95:5 Pd:Pt – 85 µL of 250 mM $PdCl_2$ + 5 µL of 200 mM K_2PtCl_4 + 90 µL ethanol + 90 µL deionized water

These different solutions were prepared to investigate whether it would be possible to control the Pd: Pt content of the resulting s by varying the Pd: Pt content of the solution. 30 µL of these solutions were used per sample, while the deposition time was 5-6 minutes. The frames were removed, and the samples were thoroughly washed with deionized water.

4. Pd-BASED SENSORS

4.1 Pd BY IMMERSION

The figs 72 below are digital photographs of the sample after obtaining the Pd deposits in the trench.

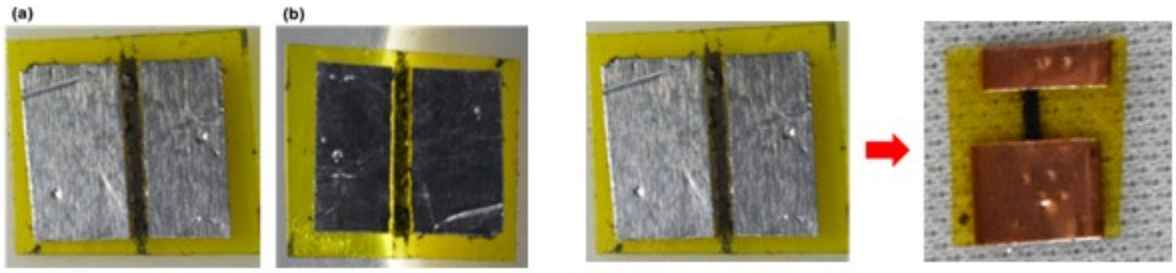

Figure 72: (a) Pd obtained in the trench was not in contact with the contact pads (b). So, the contact pads were eventually removed, and double-sided copper tapes were used as contact pads to fabricate the sensor

Fig 72(a) on the left is the top view of the sample, showing the bottommost aluminum tape on either side of the Pd deposits (black). There was no contact between the aluminum and the deposits. The outer edge of the aluminum was exposed to the salt solution, which would have led to its dissolution in the galvanic exchange reaction. Fig 72(b) is the digital photograph of the sample when illuminated from below. It highlights the gap existing between the aluminum and the trench deposits. As a result, the bottommost aluminum could not be used as a contact pad. Since the aluminum could not be used, it was removed, and two pieces of copper tapes were stuck on either side to act as contact pads. These tapes were conducted on their adhesive and non-adhesive sides, enabling their use as contact pads. These pads avoided direct contact between the sensing probes of the instrument and the nanostructures. Thus, the deposit was physically protected and used for hydrogen sensing experiments. Samples prepared using the other method had better adhesion to the Kapton, thereby not requiring contact pads.

A part of the sample shown above was analyzed under a scanning electron microscope. Fig 73 shows the micrographs at both low and high magnification. The elemental composition was analyzed via EDS, and pie charts depict the corresponding compositions.

At low magnification, fig 73(a) shows the trench deposit between aluminum tapes on either side. The gap between the deposits and the aluminum is also visible in this image. The trench deposits have an uneven landscape, with concentrated patches in some regions. At high magnification, the trench deposits are comprised of nano-sized Pd particles.

The sample shown in fig 74 was tested for gas sensing experiments. The sample was mounted on the stage, kept inside a pipe, and exposed to 2.4% H_2 in an N_2 background. The test results are shown as sensitivity vs. time plots in fig 74. The sensitivity $((R - R_0)/R_0 * 100)$ is the percent relative change in resistance compared to a baseline resistance R_0. This baseline resistance is the resistance of the sample in background N_2. Typically in all the gas

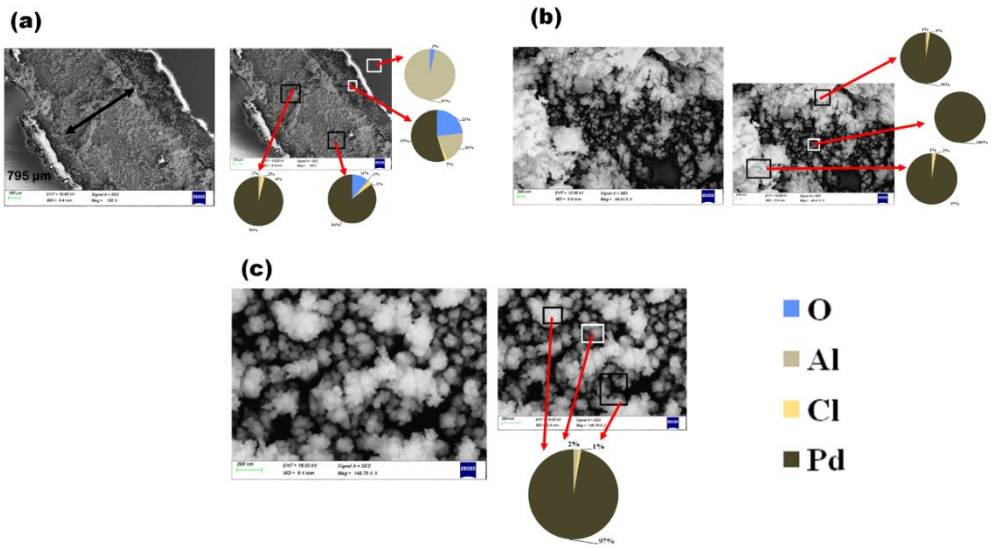

Figure 73: SEM micrographs of the trench deposits

tests described in this work. The first thirty seconds of any test involved exposure to the background N_2 only. The R_0 was computed as the average of all the resistances sampled during the first thirty seconds. The corresponding response of the MQ-8 reference sensor is also shown below every test. The response is shown in the context of investigating any lag in response/recovery of the fabricated sensor. The y-axis of the reference sensor is labeled as "Sensor reading," which are the values displayed by the sensor. These values do not indicate the actual hydrogen concentration of the test gas in the pipe. Therefore, the interpretation of the responses of the reference sensor is purely qualitative.

Upon the first exposure of the sample to hydrogen, the sample exhibited a drop in resistance (Fig 74(1)). The sensitivity dropped further before leveling to a lower baseline resistance when switched off the hydrogen flow. The second H_2 exposure showed an increase in sensitivity which recovered to the baseline after the H_2 was switched off. Subsequent exposures (not shown) exhibited a similar increase in resistance. A possible explanation for this type of behavior is the presence of palladium oxide (PdO) on the surface. It has been reported that oxygen can adsorb on Pd surfaces [47] [48]. When PdO is exposed to hydrogen, it gets reduced to Pd, lowering the resistance. [49]. The PdO, having been converted to Pd in the first test, showed the expected hydride formation in the second test. The hydride formation is typically characterized by increased resistance due to increased electron scattering in the hydride phase [16]. However, the presence of the oxide is yet to be confirmed by XPS analysis.

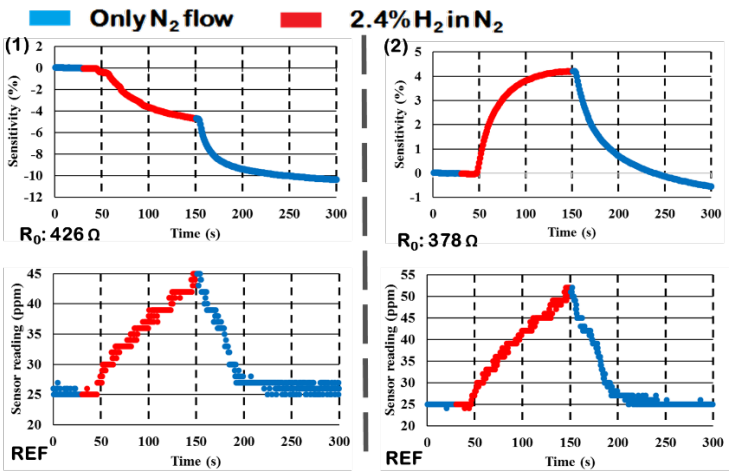

Figure 74: Responses of the sample to 2.4% H_2

The same sample was later exposed to 3.8% H_2 in N_2. The response of both the fabricated and reference sensors is shown below. The base resistance had increased several orders of magnitude. It was due to accidentally mishandling the sample, causing the removal of some deposits from the surface. Nevertheless, the sample still had a stable baseline, which enabled its testing. By increasing the H_2 concentration, the sample showed an inverted response, i.e., the resistance decreased. After an initial rise in resistance like the one observed in the previous test, there was a sudden drop in resistance. This drop-in resistance was attributed to the closure of nano-sized gaps between Pd nanoparticles. At sufficiently high H_2 concentrations, the β phase of palladium hydride gets formed, which has a higher lattice constant than its α counterpart. It leads to the volume expansion of the nanoparticles, which can close any gaps between them. It leads to the formation of alternative conducting pathways in the circuit [50]. Multiple such gaps could have closed upon exposure to H_2, causing an overall drop in the resistance. Once the hydrogen was switched off, the initial baseline resistance was recovered. However, there was a lag observed between the formation of the two phases. This lag could have been possible because the interparticle gaps were "large," requiring larger volumes of H2 to diffuse in the nanoparticles, resulting in the delay observed. The ~70% change in sensitivity was also significant, implying that many gaps would have been closed to achieve the drop.

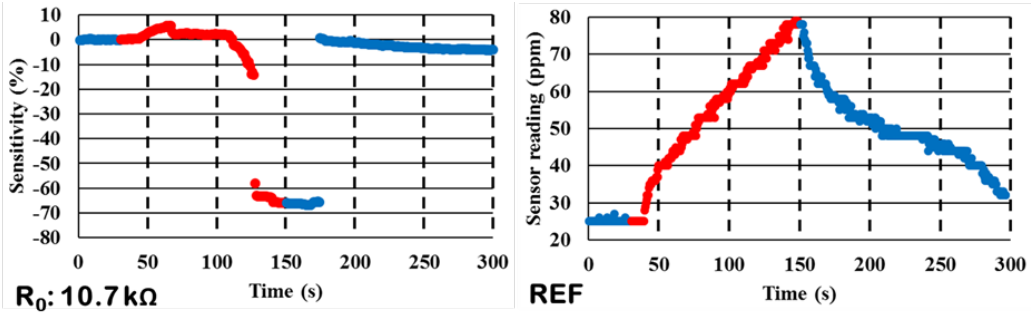

Figure 75: Gap-closure mechanism (left) at 3.8% H_2

4.2 Pd BY DROP CASTING

This approach also required less time per sample than the immersion method. The samples made by this approach required significantly less Pd in the solution than the immersion method. The substrate used in these experiments was also pre-treated with 0.5 M KOH solution. The treatment was done to improve the adhesion strength, as explained in the "experimental methods" section 3.2.3.2. A schematic of the process timeline is shown in fig 34 below. In figure 34(1), a top view of the flattened aluminum foil is held in place using two cello tapes at either end. The containment frame (black rectangle), which is supposed to restrict the solution in the vicinity of the foil, is stuck. In fig 76(2a), the solution (pink) dropped cast inside the frame. After 5-6 minutes, the solution is washed away, and the foil, frame, and tapes are removed. The sample is again washed thoroughly with deionized water. Fig 76(3a) depicts the Pd obtained on the surface. The Pd deposition occurs along the edges of the aluminum foil. A possible reason for this type of pattern could be that it requires space to deposit, which is only initially available close to the edges. If the concentration of Pd in the drop cast is sufficient to react with the entire foil (fig 76(2b)), a fully covered aluminum strip can be obtained (fig 76(3b)). In this case, the space for Pd is created by the dissolution of the aluminum foil. The patterns were electrically conductive. The samples with unbroken patterns could be tested as chemiresistive gas sensors.

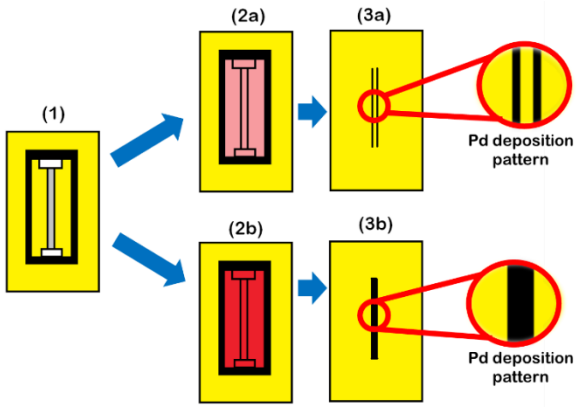

Figure 76: Stages of Pd on

By altering the mass of Pd in the drop cast (concentration of Pd in the solution), it was possible to alter the mass of Pd deposited. Fig 77 shows the Pd nanostructures obtained on Kapton for different concentrations of Pd in the drop cast.

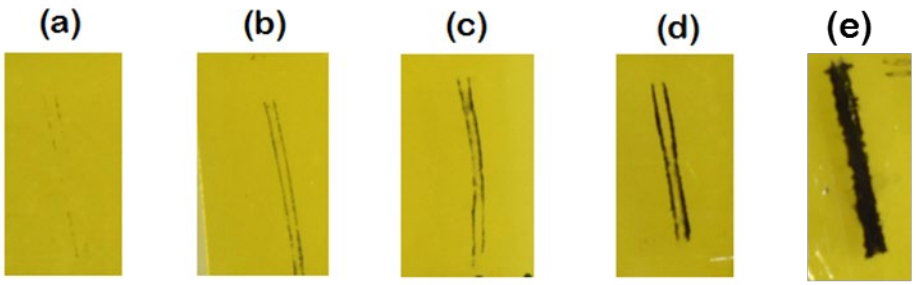

Figure 77: Pd patterns obtained using increasing Pd concentration, (a) being the lowest and (e) being the highest

As the Pd concentration increased, the nanostructures became progressively prominent. Fig 77 (a), (b), (c), (d) and (e) were prepared by solutions having Pd concentrations 3 mM, 9 mM, 12 mM, 14 mM and 160 mM respectively. However, of all the samples shown above, only (d) and (e) could be used for gas sensing, as their deposits were continuous from end to end.

The SEM-EDS analysis of all the above samples is shown below, except (a). The images in the top row are the SEM micrographs at low magnification. The width is indicated in each of the top row images. Although the width increased as the Pd concentration increased, it could also be due to differing aluminum foil widths. As mentioned earlier, the foil pieces were cut manually, implying there could certainly be variations in foil widths. Therefore, it could be possible that the increasing widths are merely coincidental with the increasing Pd concentration. The bottom row images are the corresponding micrographs for the top row images at higher magnification. There is particle morphology in all the samples observed, with the particles being composed primarily of Pd. The particles were of different sizes as well. The deposition at low magnification appeared to be more even than that observed for the immersion sample (fig 78).

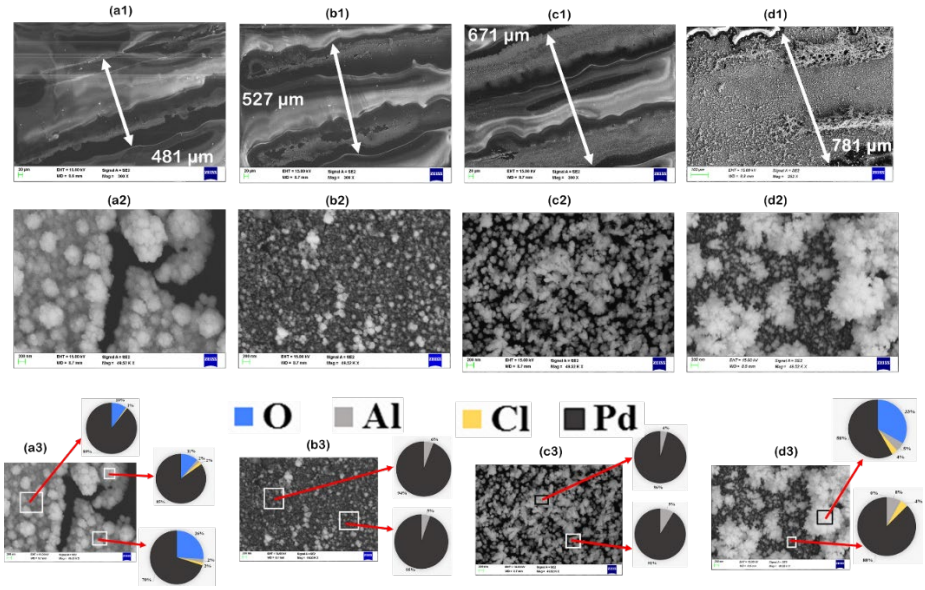

Figure 78: SEM micrographs of the samples shown in Fig 77, except (a)

The gas sensing experiments were conducted on sample (d) from fig. 77 at 3.8% H_2 and 0.7% H_2 in N_2, repetitively. The corresponding responses of the reference sensor are shown below that of each test. The sample exhibited a drop in sensitivity at 3.8% H_2 instead of at 0.7% H_2 (fig 79 and fig 80, respectively). This negative response could be attributed to the different hydride phases driving each behavior. At higher H_2 concentration, the β phase of PdH is the dominant phase, which has a higher lattice constant. If the interparticle gaps are small enough, the lattice expansion will close them, resulting in new conducting pathways and lowering the resistance. At lower H_2 concentration, there is no β phase formation; only the α phase exists. Since the lattice expansion in the α phase is much less than its β counterpart, new conducting pathways are not created by the gap-closure mechanism. The resistance of the already existing pathways increases due to the hydride phase's higher resistance. Therefore, the resistance increase mechanism was observed in this case. The hydride in the α phase exists at room temperature when $x < 0.015$ in PdH_x. Due to

such a low hydrogen concentration in the Pd lattice, the sensitivity change is also less than observed in the gap-closure mechanism.

Tests #3, #4, and #5 exhibited an initial rise in resistance before the eventual drop. It could indicate the α phase as hydrogen begins diffusing inside the Pd matrix. Once sufficient hydrogen gets incorporated into the matrix, the β phase formation manifests as the dropping resistance. This behavior has been observed previously [51] - [53]. However, the first two tests didn't exhibit a prior increase in resistance. The reason could be due to the existence of the PdO in the conducting pathways, as discussed previously. After the first two exposures to hydrogen, the oxide would have been entirely reduced to Pd. Once the reduction to Pd was complete, the hydride sensing mechanism was observable in tests #3, #4, and #5.

A comparison between these responses to those shown in fig 75 indicates that the lag observed in the formation of the β phase was not observed here; the drop ensued immediately after the initial rise in resistance. A possible reason for this difference could be smaller interparticle gaps. The sensitivity drop is also smaller than the immersion sample, which could imply that the expanding particles, in this case, would have bridged a smaller % of empty volume. Hence, the smaller sensitivity drop also points to the possibility that a smaller % of voids existed in this sample, i.e., smaller interparticle gaps. However, additional characterization (such as TEM analysis) might confirm this hypothesis.

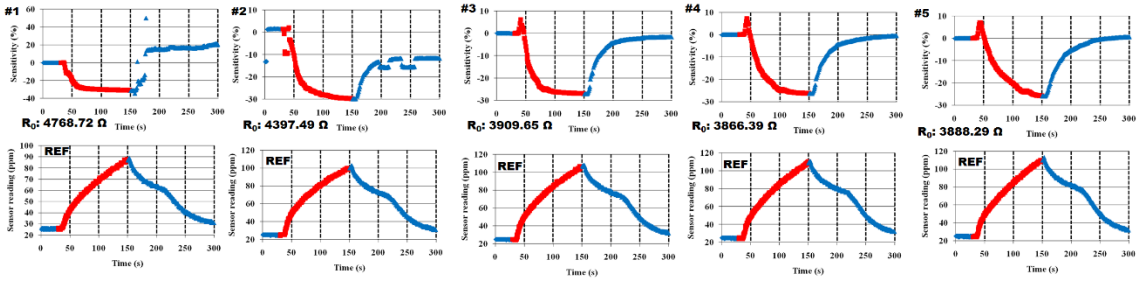

Figure 79: Gas sensing responses of the 14 mM sample to 3.8% H_2 (top row) with the corresponding reference sensor responses (bottom row)

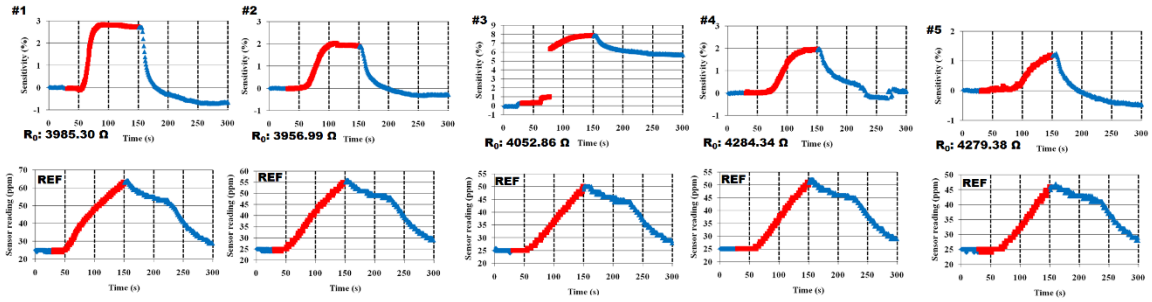

Figure 80: Gas sensing responses of the 14 mM sample to 0.7% H_2 (top row) with the corresponding reference sensor responses (bottom row)

The α → β phase transition has been reported to take place between 1 - 2% H_2 at room temperature [18][54][55]. A similar sample was exposed to different concentrations of H_2 to confirm this observation. The top row of fig 81 shows the observed gas sensing responses of the fabricated sample to different hydrogen concentrations, namely (a), (b), (c), and (d) being exposed to 3.8%, 2.3%, 1.3% and 0.7% H_2 in N_2 respectively. The gap-closure mechanism was the dominant

mechanism in the first two instances, while the electron scattering mechanism was the only sensing mechanism in the latter two. So the transition would have occurred somewhere between 1.3% - 2.3%, which is close to the expected range. The α phase preceded the gap-closure mechanism in both (a) and (b), as previously observed in different samples as well (the inset in (a) shows a zoomed image of the α phase formation). The corresponding responses of the reference sensor are shown in the row below. Since the reference sensor maintained its qualitative response at all hydrogen concentrations, it can be concluded that the α → β phase transition was indeed occurring, signifying that the sensor was responding via a hydride formation mechanism.

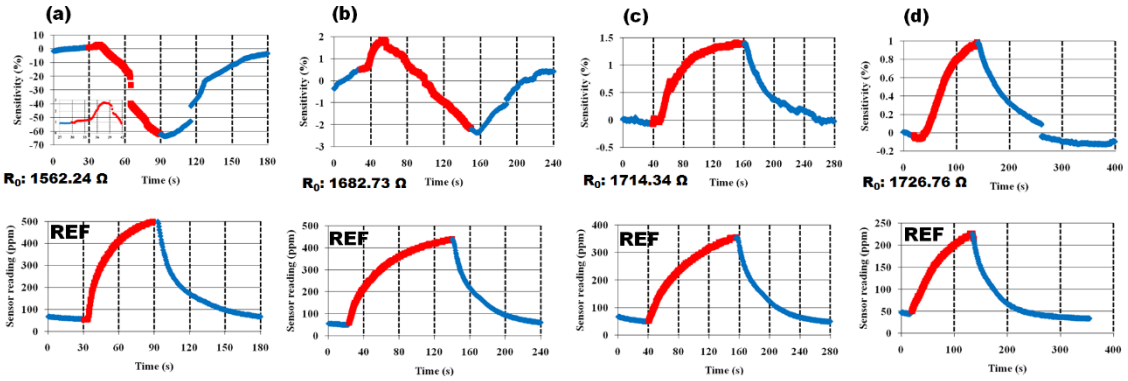

Figure 81: Gas sensing responses (top row) to (a) 3.8% H_2 (b) 2.3% H_2 (c) 1.3% H_2 and (d)0.7% H_2 with the corresponding reference sensor responses (bottom row)

A commercially available Pd "varakh" was tested for gas sensing responses under similar conditions (fig 82). The first exposure to 3.8% H_2 showed the irreversible reduction of PdO to Pd, which manifested as a drop in resistance. Once the oxide was reduced, the subsequent tests exhibited the hydride sensing mechanism. Since the baseline resistance was relatively low, there would have been considerably fewer interparticle gaps than in the fabricated samples. As a result, the gap-closure mechanism wasn't observed in this case. The increase in resistance would have occurred due to the hydride phase formation. At lower hydrogen concentrations (fig 83), the sensor resistance didn't change significantly from its baseline during the hydrogen exposure. However, the resistance dropped significantly after the hydrogen was switched off.

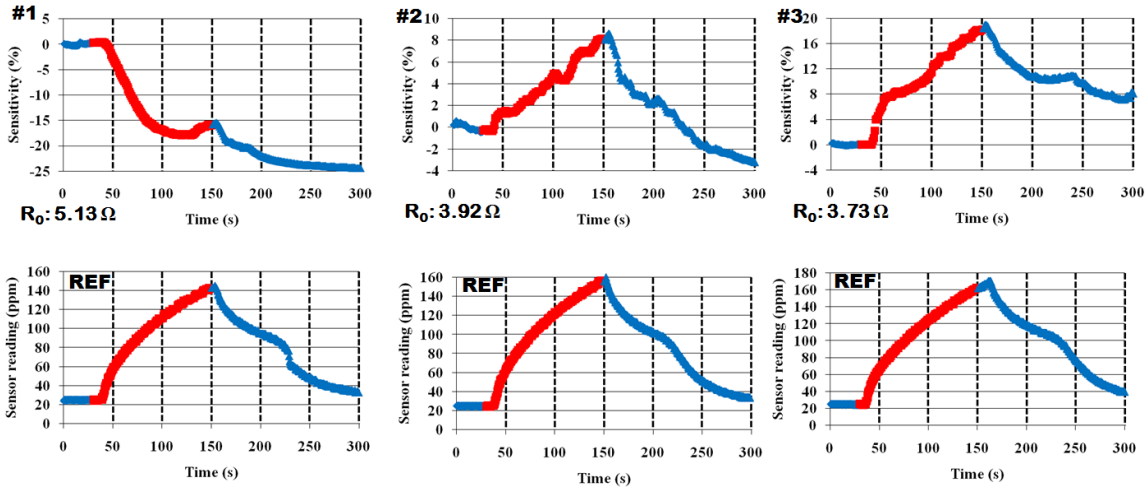

Figure 82: (Top row) Back-to-back responses of a commercially available Pd "varakh" to 3.8% H_2 with the corresponding responses of the reference sensor (bottom row)

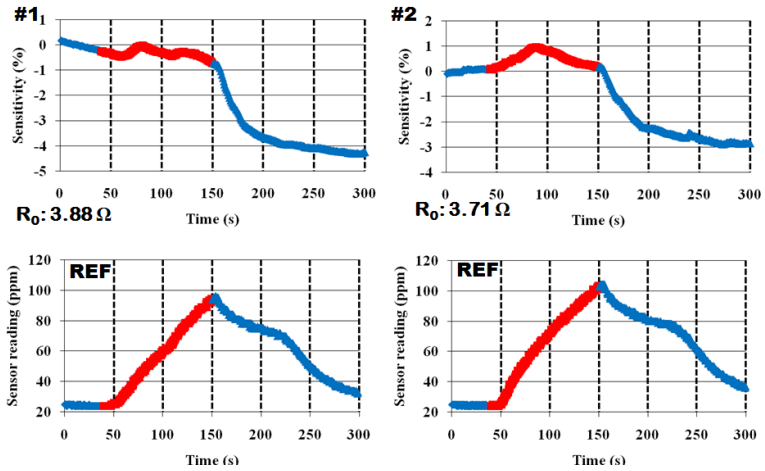

Figure 83: (Top row) Back-to-back responses of a commercially available Pd "varakh" to 0.7% H_2 with the corresponding responses of the reference sensor (bottom row)

Thus, the oxide reduction phenomenon was also observed in the "varakh" sensor. Since it comprised of bulk Pd, the gap-closure mechanism wasn't observed here [56]

A different sample prepared using 14 mM solution was also tested in an air background. It was previously reported that the oxygen in air could act as a competing species for adsorption sites on palladium surfaces. This effect causes Pd sensors' delayed response/recovery kinetics in an air background [57]. Therefore, similar samples were tested in an air background to see the effect. The samples were exposed to 3.8% H_2 (fig 84(a)) and 0.7% H_2 (fig 84(b)) in air background. The sensor responded by decreasing resistance in both cases. A possible explanation for this behavior could be that the phenomenon observed here was PdO reduction in hydrogen, which could have reversibly reconverted to PdO in the air background. Since hydrogen can react with adsorbed oxygen, its reaction with palladium to form hydride gets suppressed in air, as reported by Noh et al. [58]. However, contrary to our findings, Noh's work also reports decreasing sensor resistance in the N_2 background. A plausible explanation could be that the nature of response might depend on the amount of PdO and porosity of the nanoparticle matrix. The higher the content of PdO

relative to Pd in the sensor, the more likely it will be not to observe the increasing resistance effect. Additionally, the higher the porosity, the more resistance is suppressed due to a lack of percolating pathways. Nevertheless, the responses in our case were not saturating, unlike those in nitrogen background, indicating delayed response/recovery kinetics as expected.

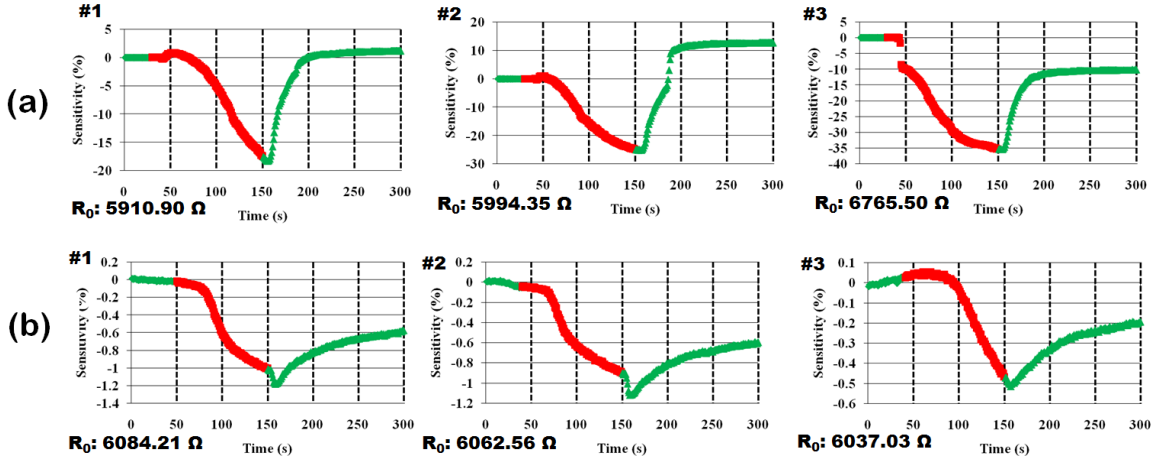

Figure 84: (a) Back to back tests at 3.8% H_2 in air and 0.7% H_2 in the air (b)

Thus, the response characteristics of the Pd sensor were observed in the air as well.

Since the sensors comprised conductive Pd nanostructures on a flexible substrate, they could conduct the gas sensing experiments on bent sensors. One could visualize a scenario where the sensor could be wrapped outside a pipe flange to detect leaks. The first question is whether the fabricated samples could function in a bent position. Therefore, it was decided to place the bent sensor inside the pipe simply. However, the samples fabricated using 14 mM solution couldn't be contacted with the copper contacts, as the lines were too thin. The copper contacts couldn't form an electrical contact with the sample. As a result, the area of the deposits had to be increased. For this purpose, the sample shown in fig(77 (e)) was used as it had enough area to contact the copper pads. Once the sample was mounted, as shown in fig 53, the sample was exposed to four response/recovery cycles at 3.8% H_2 in N_2. Then, it was exposed to four response/recovery cycles at 0.7% H_2 in N_2. The larger area of the sample manifested as a lower base resistance (R_0: 321.08 Ω) than the previously tested samples prepared using the 14 mM solution (R_0: 1.56 kΩ, 5.91 kΩ, 4.77 kΩ)

The first exposure to 3.8% H_2 exhibited a non-recovering response, indicating the reduction of oxide species to Pd. Unlike the experiments performed in an air background, these oxide species couldn't have re-formed due to a lack of oxygen molecules in the nitrogen background. Cycle #2, #3, and #4 exhibited an increasing resistance upon exposure to hydrogen, which recovered to their original baselines. This mechanism was unexpected since the "flat" samples were used to show the decreasing resistance mechanism at this concentration. The cycles at 0.7% H_2 exhibited the expected electron scattering mechanism. The responses of the reference sensor (labeled as "REF") indicate that the responses of the flexible sensor were qualitatively matching with its response.

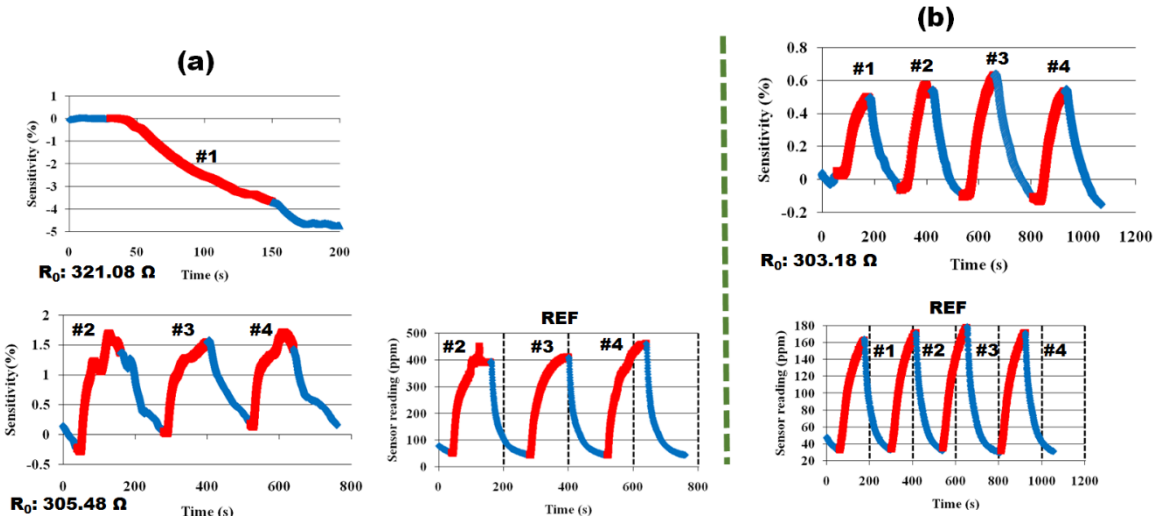

Figure 85: (a) Flexible sensor responses at 3.8% H_2, and (b) at 0.7% H_2

The gap-closure mechanism was observed when the hydrogen concentration was increased to 7.9% by lowering the N2 flow rate (fig 86) during the three response/recovery cycles. It meant that there indeed existed interparticle gaps within the sample matrix. The sensitivity change was also considerably less (`~10%) as compared to those observed in previous samples (>30 %), even though the H_2 concentration was higher for the former.

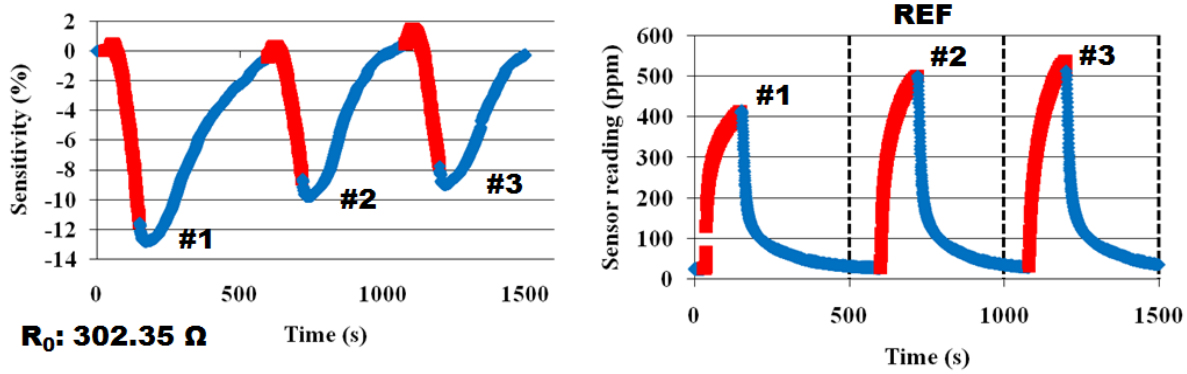

Figure 86 Flexible sensor responses at 7.9% H_2

After a couple of hours, the sample was removed from its bent state and tested as a flat sensor placed at the pipe centerline. It was exposed to 2.6% H_2 twice (fig 87 (a1), (a2)). In the first exposure, the sample exhibited the irreversible oxide-reduction phenomenon. It implies that the oxide species had re-formed during the interval. Further tests need to be conducted to study the kinetics of the formation of this oxidation phenomenon. However, in the second cycle, the gap-closure mechanism was seen. Its sensitivity change at 2.6 % H_2 in the flat state was similar to its sensitivity change at 7.9% H_2 in the bent state.

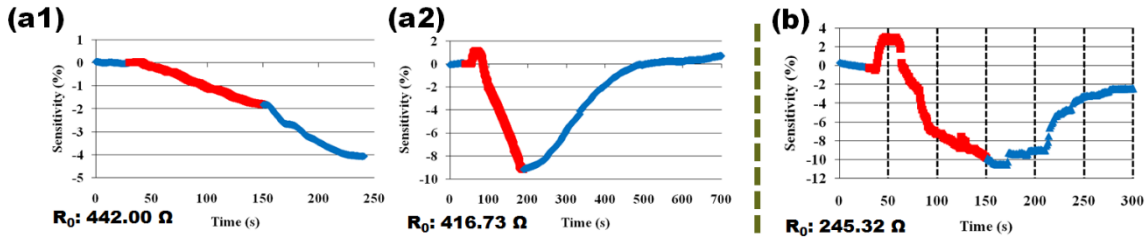

Figure 87: (a1), (a2) Exposure of the "flexible" sensor tested as a flat sensor to 2.6% H_2 (b) replicate sample response

A replicate sample prepared using a similar Pd concentration of the displacement solution was also tested as a flat sensor. This sample hadn't been tested in the bent state previously. It exhibited a similar gap-closure mechanism as well (fig 87(b)), while the sensitivity change was similar to its predecessor (~10 %). The following points could be inferred from these flexible sensor experiments:

i. Bent vs. flat (same sample): The sample in a flat position showed a nanogap-closure mechanism that didn't in the bent state.
    i. It could mean that the interparticle gaps would have changed from their flat state by bending the sample. Although the β phase would also have formed in the bent state, the interparticle gaps would have been too large to have been bridged by the hydride expansion.
    ii. Another possibility is that the hydrogen concentration near the pipe wall could be less than that at the centerline. This case implies that only the α phase would have formed in the bent sample. The β phase formation was observed only when the hydrogen concentration was increased to 7.9%. The increase would have been sufficient to increase the hydrogen concentration near the pipe wall to be >2% to facilitate the β phase formation. The sample was tested as a flat sensor that exhibited the β phase formation like previously tested flat samples. Even the sample that hadn't been tested as a bent sensor (fig 87(b)) showed a similar response as a flat sensor (fig 87(a2)). This test confirmed the β phase formation in sensors when placed at the pipe centerline as a flat sensor.

ii. R_0 as a possible indicator of interparticle gap volume: The sensitivity change observed due to the gap-closure mechanism was ~10% in the samples with lower R_0. The samples with higher R_0 exhibited a higher sensitivity change (at least 30%) due to the same mechanism. Even the "varakh" sample, which had the lowest base resistance, didn't exhibit any gap-closure mechanism at the same hydrogen concentrations, falling in line with this observation. Thus, it could be possible to use higher base resistances to have higher sensitivities. However, not all interparticle gaps may be the same size. Consequently, it may not be helpful to increase the R_0 of samples beyond a specific limit without controlling the gap size. E.g., The R_0 of the sample shown in fig 81(a) is 1.56 kΩ, while the R_0 of the sample shown in fig 79(a) is 4.77 kΩ). Yet the former sample showed a higher drop in resistance (~60%) than the latter (~30%) despite having a lower R_0 at the same hydrogen concentration. It could have been possible due to the majority of the interparticle gap sizes of the 1.56 kΩ sample being in a "bridgeable" range in contrast to the other sample. Thus, the process of fabricating sensors in this work could be further optimised to control the interparticle gap sizes.

5 ALUMINUM AIDED BIMETALLIC Pd-Pt

5.1 INTRODUCTION

Pure Pd undergoes structural deformation upon repeated exposure to H_2 due to the lattice strain experienced during the $\alpha \rightarrow \beta$ phase transition. One way to mitigate this effect is to expand the lattice of Pd before exposure to H_2. The expanded lattice thus leaves larger space for H atoms to diffuse into the Pd matrix. It can be achieved by alloying Pd with other metal(s). Pd – Pt bimetallic hydrogen sensors have responded faster than pure Pd-based sensors [59].

5.2 Pd – Pt

Like the aluminum-aided Pd, it was found that even conductive Pt patterns could be deposited using aluminum and aq. Pt salt solution as precursors. Fig 88 shows the SEM-EDS characterization of the as-deposited Pt films. The morphology was composed of a bulk Pt film situated beneath clusters of Pt nanoparticles (fig 88(b1)). The EDS spectra revealed that the particles and the film were primarily composed of Pt, followed by oxygen.

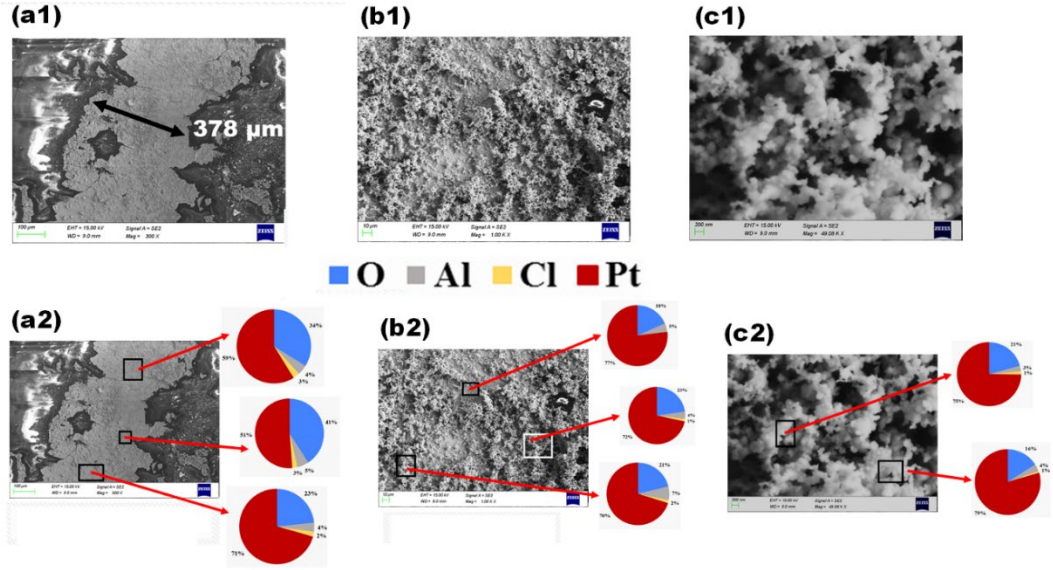

Figure 88: SEM micrographs of the Pt

Since aluminum aided deposition was applied to both Pd and Pt, the salt solutions of both these metals were mixed in one solution. This solution was used for depositing bimetallic Pd-Pt conductive patterns on Kapton. Different molar ratios of Pd: Pt were used to see whether the Pd: Pt content of the resulting deposits could be thus influenced or not. E.g., Three different stock solutions of Pd and Pt salts were prepared such that their Pd: Pt molar ratios were 19:1 (Pd rich), 3.75:1 (intermediate), and 0.42:1 (Pt rich). The SEM-EDS analyses for the "19", "3.75," and "0.42" samples are shown in fig 89, 90, and 91, respectively. The "19" sample contained mostly oxygen, as per EDS analysis. It is unclear whether the oxygen signal arose primarily from the deposits or the polyimide substrate. EDS analysis of a "control" in conjunction with XPS analysis of the sample is needed to understand this.

Nevertheless, the atomic ratio of Pd: Pt could be computed, as both these elements were detectable despite Pt being outnumbered 19:1 by Pd. The ratios indicated next to the element distributions

(dark grey indicates "Pd," red indicates "Pt") seemingly varied largely from location to location. However, the % of Pd (or Pt) relative to the total atomic % of Pd and Pt was consistent, E.g., The highest and the lowest Pd: Pt ratios observed were 32:1 and 18:1, respectively. Although these ratios appear to be vastly different, they correspond to a Pd content of 97% and 95%, respectively. The expected content (95% Pd) lies approximately in this range.

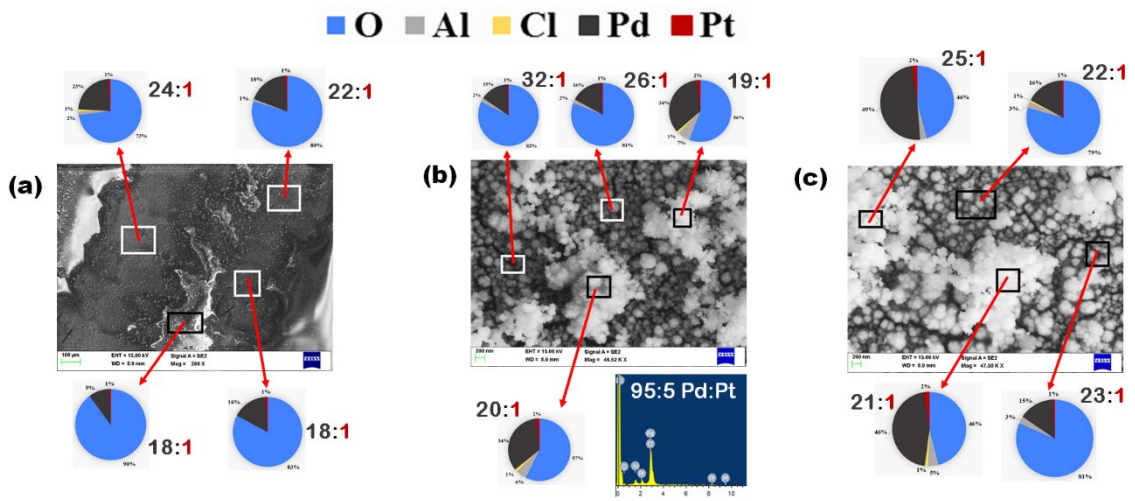

Figure 89: SEM micrographs of the 95-5 Pd-Pt sample

The SEM-EDS analyses for other samples were done similarly. As the Pt content of the sample increased, the morphology became closer to that of Pt samples (Pt nanoparticle clusters on top of a film).

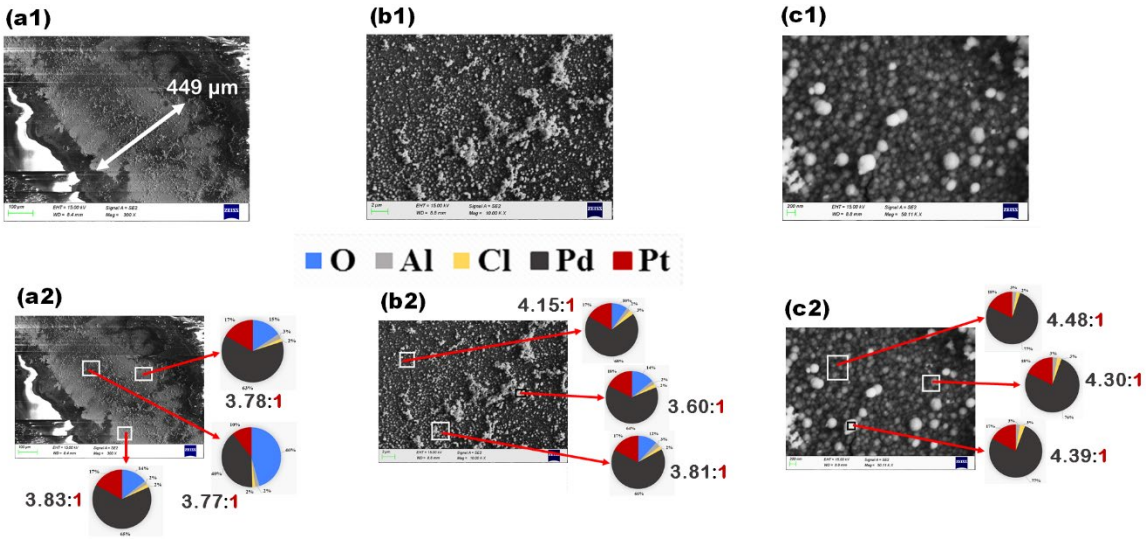

Figure 90: SEM micrographs of the "75 – 25" Pd – Pt sample

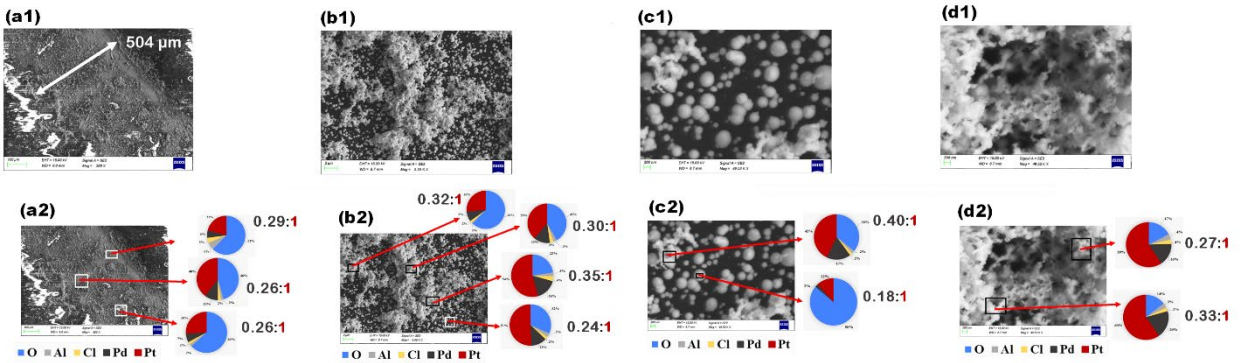

Figure 91: SEM micrographs of the "30 - 70" Pd – Pt sample

E.g., the nanoparticle clusters which are seen in fig 91(b1) and 91(d1) of the sample "0.42" were not visible in the "19" and "3.78" samples but only in the Pt sample (fig 88(b1) and 88(c1)). The Pd: Pt ratio also decreased when the Pt concentration was increased. However, the electrical conductivity of the "0.42" sample was poor owing to insufficient percolation. Therefore, it could not be tested for gas sensing experiments. Nevertheless, the Pd: Pt ratio of the deposits could be controlled by the Pd: Pt ratio of the solution.

5.3 GAS SENSING

5.3.1 Pt-BASED SENSOR

All three Pd-Pt and Pt samples were tested for their gas sensing responses. The Pt sample exhibited a dropping resistance upon exposures to both 3.8% H_2 fig 92(a) and 0.7% H_2 fig 92(b).

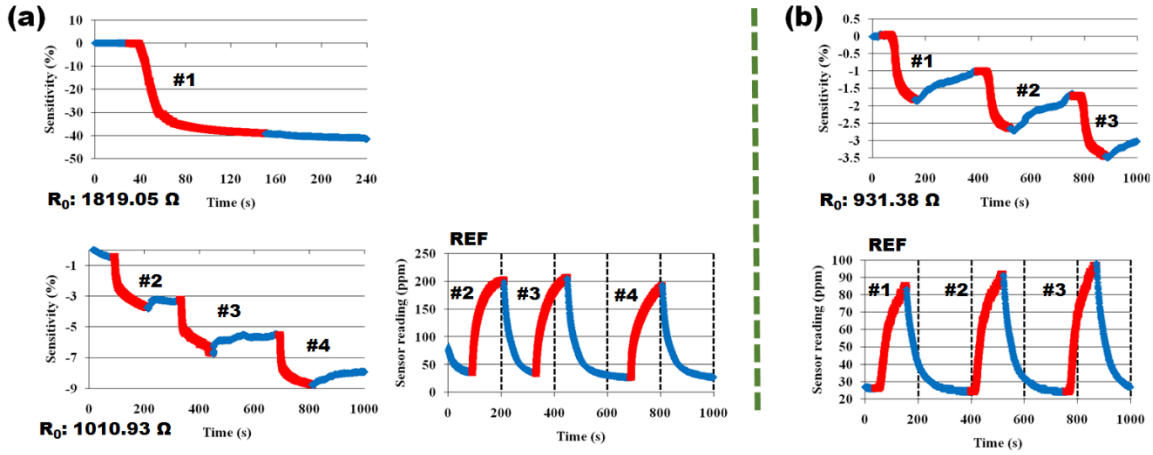

Figure 92: (a) Responses of the "Pt" sample to 3.8% H_2 and (b) 0.7% H_2

The sensitivity dropped irreversibly upon the first cycle of exposure to hydrogen. Pt, just like Pd, also has surface oxide species at room temperature[60]. The first exposure to hydrogen would have reduced the surface oxide species, causing the drop in resistance. The subsequent exposure/recovery cycles also exhibited a drop in resistance. However, unlike Pd, Pt doesn't absorb hydrogen in its lattice. This behavior is instead explained due to decreased electron scattering of Pt-H compared to the oxygen terminated Pt-O surface [61]. The adsorbed hydrogen doesn't react with the inert nitrogen, resulting in a sluggish recovery [62]

5.3.2 Pd-Pt BIMETALLIC SENSORS

5.3.2.1 "Less" Pd

This sample consisted primarily of Pt (fig 91). However, the pattern wasn't electrically conductive, due to which this sample couldn't be tested. The sample prepared using only Pt salt solution (100 mM) wasn't electrically conducting either. On the other hand, a 100 mM of Pd salt concentration was enough to yield conductive patterns. The difference in this behavior between Pd and Pt needs to be understood further before using diluted Pt salt solutions.

5.3.2.2 "Intermediate" Pd

This sample consisted of ~80 at% Pd, the rest being Pt. It was subjected to identical hydrogen response/recovery cycles as the "Less" Pd sample. The initial oxide reduction phenomenon was observed in this case as well. Subsequent exposures to 2.6% H_2 (fig 93(a)) and 0.7% H_2 (fig 93(b)) exhibited a similar dropping resistance behavior. There would have been some alloying between Pd and Pt, as a result of which no hydride phase transition was observed, unlike previously tested Pd samples (fig 91).

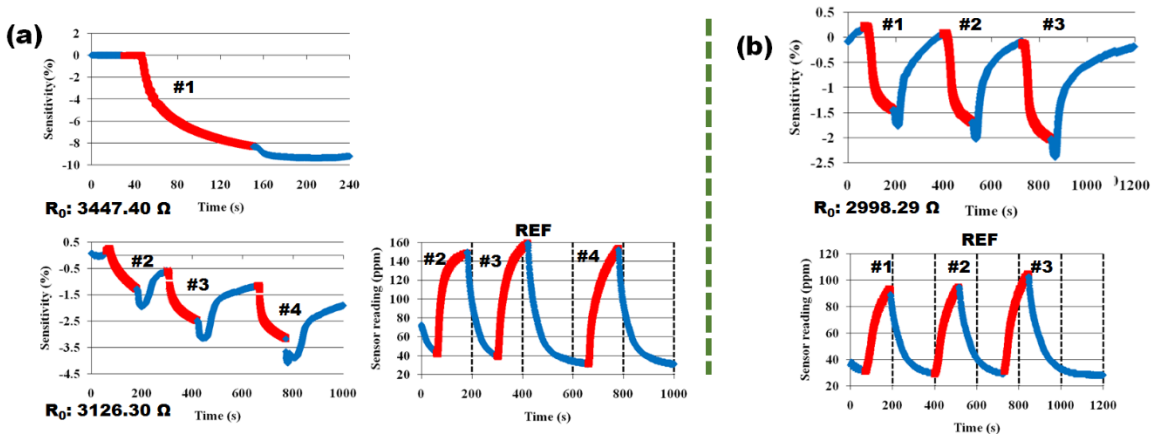

Figure 93: (a) Responses of the "75-25" Pd-Pt sample to 3.8% H_2 and (b) 0.7% H_2

The sample recovered faster than the Pt sample at the same hydrogen concentrations. This change could have been due to the higher Pd content, which shows fast recovery even in a nitrogen background. However, the sample baseline drifted to lower values after each test, signifying that the recovery was still incomplete in the test duration.

5.3.2.3 "Rich" Pd

This sample consisted of ~95 at% Pd, as per the EDS analysis. The sample was exposed to four cycles of 2.6% H_2 (fig 94(a)) followed by four cycles of 0.7% H_2 (fig 94(b)) ("REF" data not shown here). The initial exposure exhibited the oxide reduction phenomenon here as well. However, subsequent exposures exhibited an increasing resistance at both concentrations, in stark contrast to the responses shown by previous samples. In addition, the responses saturated rapidly, implying that the sample's response time would have been much faster. The sample resistance drifted beyond its initial baseline upon recovery, indicating a faster recovery time. Just like previous Pt and Pd-Pt samples, this sample was also exhibiting no phase transition at hydrogen concentrations on either side of the miscibility gap, unlike the Pd samples (Refer to Appendix A)

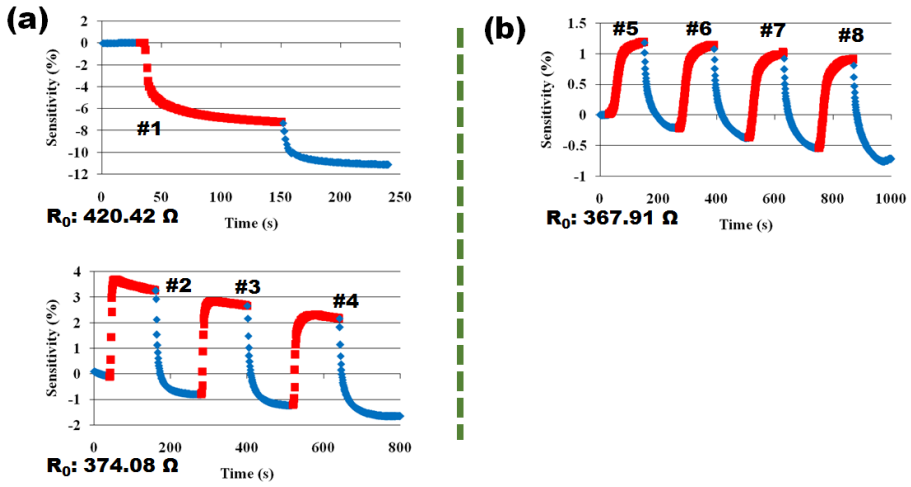

Figure 94: (a) Responses of the "95 - 5" Pd-Pt sample to 3.8% H_2 and (b) 0.7% H_2

Since this sample exhibited fast response and recovery, its kinetics were compared with those of previous Pt, Pt-Pd, and Pd samples to ascertain this observation. The plots shown in fig 95 are those of normalized resistances of four samples: "Rich" Pd, "Less Pd," Pt, and Pd (14 mM). The "95 - 5" Pd sample showed the fastest response and recovery at the higher hydrogen concentration. The Pd (14 mM) sample was slightly faster at the lower hydrogen concentration. On the other hand, the "less" Pd and the Pt samples were the slowest.

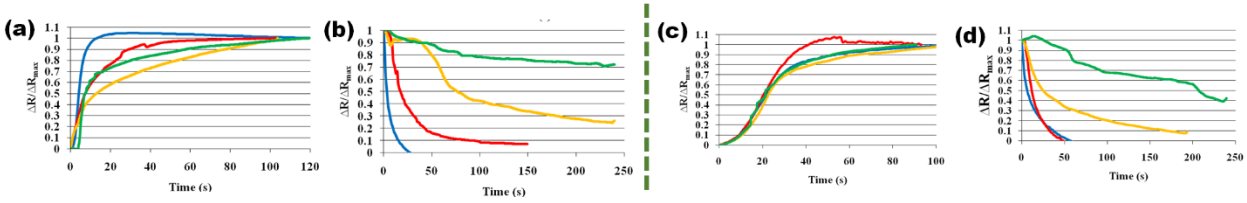

Figure 95: Normalized responses/recoveries of the "Pt" (green), "Pd" (red), "75 – 25" (yellow) and "95 – 5" (blue) to (a), (b)3.8% H_2 and (c),(d) 0.7% H_2

The "95 - 5" sample showed the following distinct features:

- No phase transition: As all the responses increased resistances, it can be developed into a sensor instead of a leak detector. The Pd-based samples suffer a phase transition between 1 – 2% H_2 miscibility gap, limiting their use as a sensor. In contrast to the "75 – 25" Pd-Pt sample, this sample exhibited an increasing resistance upon exposure to the same hydrogen concentration. It can be explained that increasing Pt content in the bimetallic Pd-Pt nanostructures has decreased the amount of hydrogen absorbed in the lattice [63]. As a result, the sensor would show more characteristics of a Pt sensor as the Pt content were to be increased because Pt doesn't absorb H_2. It might explain the decreasing resistance of the 75 – 25 sample, similar to that of Pt. However, the 95 – 5 sample could absorb hydrogen but not expand since the Pt atoms would have expanded the lattice even before the H_2 exposure. Thus, the gap-closure mechanism wouldn't have been observed, but only the increased scattering, manifesting as the increasing resistance.
- Fast response and recovery: Since the ultimate objective would be to make the fastest sensor possible, this sample would be a better foundation to work upon

- Drift in baseline: the resistance used to recover beyond its baseline after every cycle, indicating drifting baseline
- Decreased sensitivity: The "95 - 5" sample was less sensitive for the same hydrogen concentration than the Pd samples.

Despite the observed drift and decreased sensitivity, the "95 – 25" sample was a promising candidate for development.

It was important to understand the nature of the drift before correcting it. The sensor drift was observed to decrease progressively during the test (Refer to Appendix A). Could it be possible to eliminate sensor drift by successive cyclic hydrogen exposure? To investigate this observation, a freshly prepared "95 - 5" sample was subjected to 6 cycles of exposure/recovery @ 3.6% H_2 (fig. 96 (b)) and 4 cycles of exposure/recovery at 0.6% H_2 (fig 96(c)). The initial exposure to 3.6% H_2 resulted in the oxide reduction phenomenon (fig 96(a)), as observed in the previous "95 – 25" sample as well.

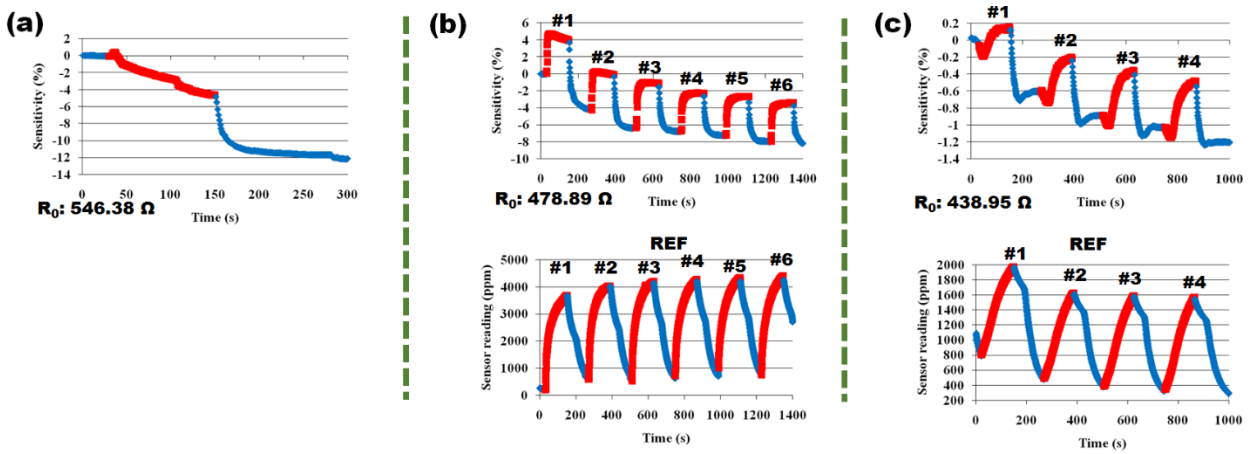

Figure 96: (a)First exposure to 3.6% H_2 (b) Subsequent exposures to 3.6% H_2 (c) Exposures to 0.6% H_2 on "day zero"

The drift of the sensor baseline resistance decreased with the passage of exposure cycles. E.g., in fig 96(b), the net baseline drift between the first three cycles was ~7%. For the last three cycles, the net drift had decreased to ~1%. A parameter called "drift ratio" was defined as the ratio between the change in baseline sensitivity for one cycle and the change in sensitivity upon hydrogen exposure for the same cycle. A perfect sensor response would have zero change in baseline, no matter what change was observed in its signal sensitivity. Thus, the drift ratio would be zero for a perfect sensor response.

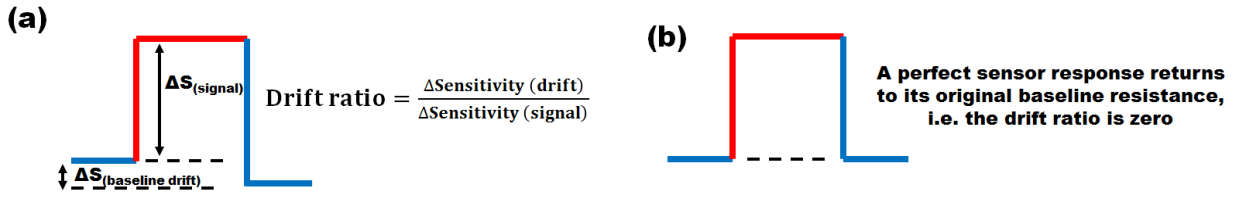

Figure 97: Drift ratio

It made sense to express the drift as a ratio relative to its signal. As such, there may be some baseline fluctuations in all sensors. However, their significance can only be understood if the signal-to-noise ratio (SNR) is considered. Therefore, the signal was included in the denominator of the drift ratio. When the drift ratio was plotted for each exposure/recovery cycle, it was found that the drift decreased as the cycles went by (fig 98).

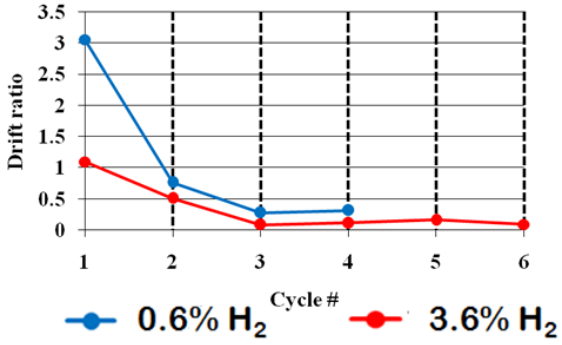

Figure 98: Drift ratio for each cycle at 3.6% H_2 and 0.6% H_2 on "day zero"

The closer the drift ratio is to zero, the closer the response is to ideality in terms of baseline drift. In practicality, a drift ratio close to one or more would be useless, as it would be difficult to decipher the signal from the baseline drift in such a case. Fig 98 indicates that the sensor responses at 0.6% H_2 were closer to the ideal than those at 3.6% H_2. Nevertheless, the decreasing drift ratio indicated that the sample was getting closer to a stable baseline. Thus, repeated hydrogen exposure seemed to solve the drift problem. However, what if this phenomenon was temporary? If the drift ratio were to increase again after a few days of sensor inactivity, another strategy to eliminate drift would have to be devised. Therefore, the same drift experiment was conducted two days later to investigate whether the drift ratio had increased after a period of inactivity or not.

The exact sequence of tests was run on the sample after two days of inactivity. The baseline resistance had dropped to 409 Ω in this duration. The initial exposure to 3.6% H_2 revealed the presence of oxide in the sample (fig 99(a)). The sensitivity change (%) was ~6% this time compared to the ~12% change experienced two days before. It could imply that the surface oxidation had diminished significantly during this period. The sample was then exposed to 6 response/recovery cycles of 3.6% H_2 (fig 99(b)), followed by four response/recovery cycles of 0.6% H_2 (fig 99(c)), just like the test two days before. The baseline drift seemed to have lessened at both concentrations. E.g., At 3.6 % H_2, the six cycles showed ~2% drift on day two compared to ~8% drift on day zero. Similarly, at 0.6% H_2, the four cycles showed ~0.8% drift on day two compared to ~1.2% drift on day zero.

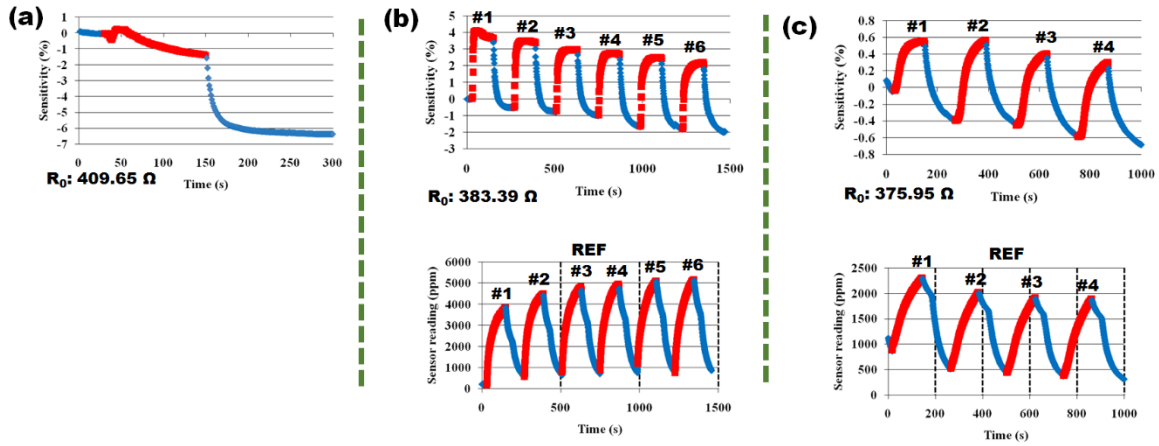

Figure 99: : (a) First exposure to 3.6% H_2 (b) Subsequent exposures to 3.6% H_2 (c) Exposures to 0.6% H_2 on "day 2"

The sensor responses had maintained their sensitivity for both concentrations. The source of drift for the first response at 0.6% H_2 was present here, which coincided with a drift in the reference sensor.

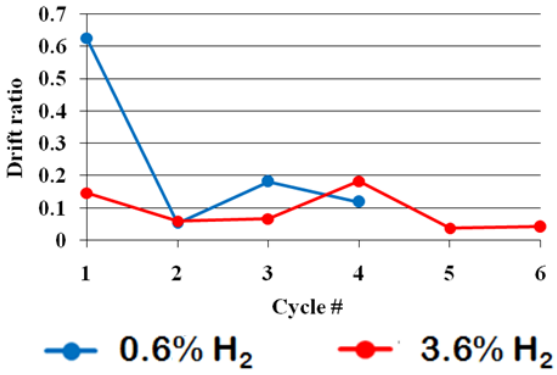

Figure 100: Drift ratio for each cycle at 3.6% H_2 and 0.6% H_2 on "day 2"

The drift ratios for the day two exposure/recovery cycles had significantly decreased from those on day zero. Thus, the observation that baseline drift could be reduced by repeated exposure to hydrogen was confirmed. However, to investigate whether the drift could be further decreased, the same test was conducted two days later, i.e., four days after the first test. The baseline resistance had slightly increased to 387 Ω during the two days of inactivity. The first exposure showed the presence of an oxide layer once again (fig 101(a)). The subsequent tests exhibited negligible drift at 3.6% (fig 101(b)) H_2. At 0.6% H_2, the drift was visible in the first exposure, whereas #2, #3, and #4 exposures didn't show much drift (fig 101(c)). The plot of drift ratios for each cycle confirmed that the drift was decreasing consistently, just like the trend observed in the past four days of experiments. Thus, these tests confirmed that the baseline drift could be eliminated significantly by repeated exposure/recovery cycles to H_2.

It was intriguing how adding 5 mol% of Pt salt to the sample could vastly differ the observed gas sensing responses. A "control" experiment was performed where the sample was prepared with the same solution, sans Pt. The "control" Pd sample was subjected to the same sequence of gas sensing tests as the "95 – 5" Pd sample.

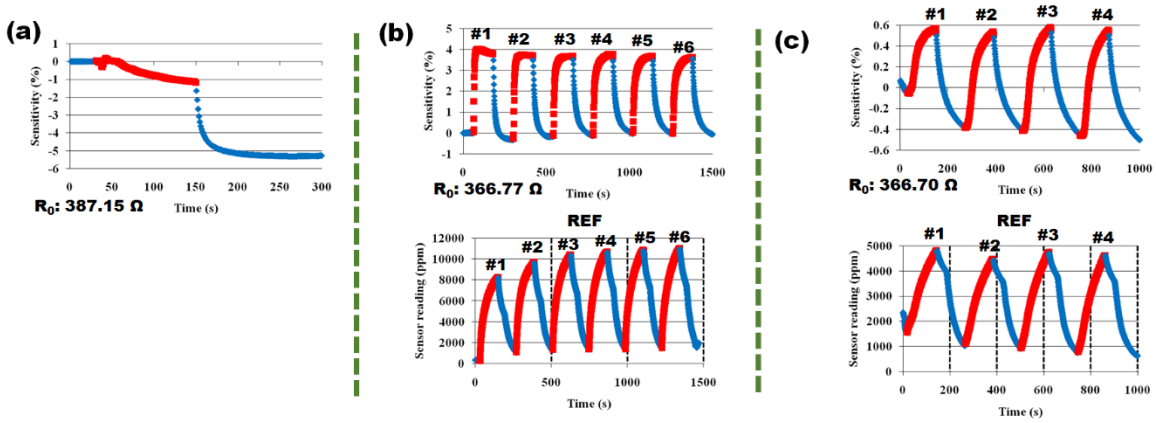

Figure 101: (a) First exposure to 3.6% H_2 (b) Subsequent exposures to 3.6% H_2 (c) Exposures to 0.6% H_2 on "day four"

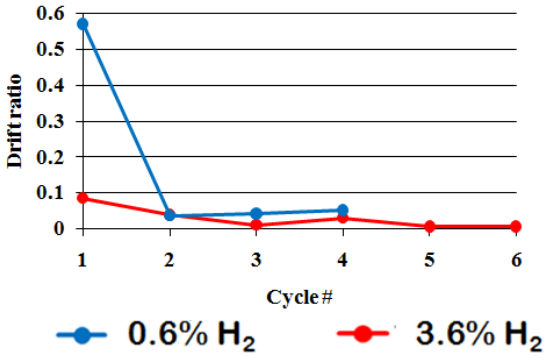

Figure 102: Drift ratio for each cycle at 3.6% H_2 and 0.6% H_2 on "day four"

Fig 103 shows the raw gas sensing responses of the "control" Pd sample on day zero, day two, and day four of testing. Each day, the sample was subjected to 6 cycles of 3.6% H_2 and four cycles of 0.6% H_2. The first cycle of 0.6% H_2 exposure hasn't been shown in fig 103, so the three "REF" response/recovery cycles appear to be without drift in contrast to those of the "95 – 5" sample.

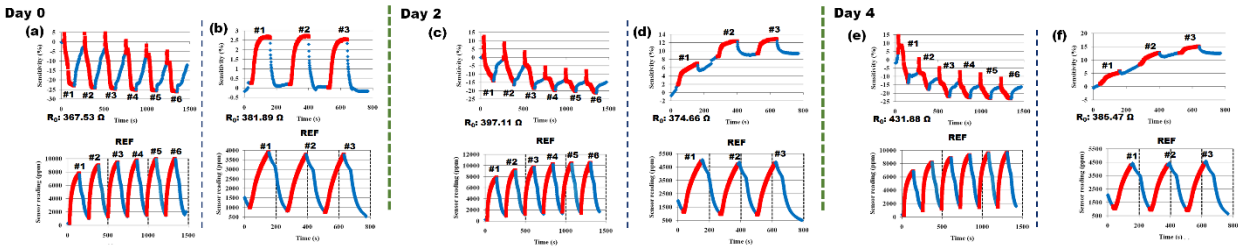

Figure 103: Responses of the "control" Pd sample on "day zero", "day 2" and "day four" at 3.6% H_2 (a), (c), (e) and at 0.6% H_2 (b), (d) and (f)

As observed in previous Pd samples, this sample too exhibited the gap-closure mechanism at 3.6% H_2. At 0.6% H_2, the electron scattering mechanism was the only observable effect leading to increased resistance. Fig 104 compares various sensor metrics such as maximum sensitivity, drift ratio, etc., for both the "95 - 5" Pd sample and the "control" Pd sample for a more straightforward interpretation of the raw gas sensing responses.

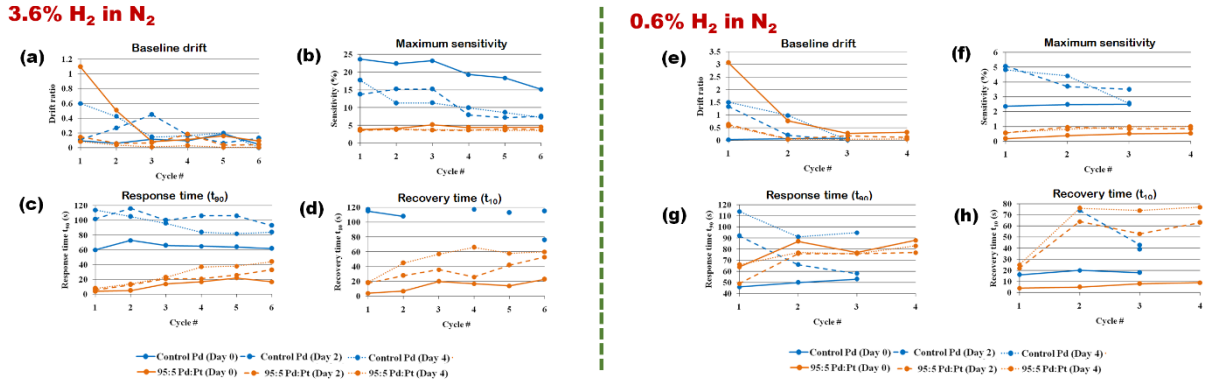

Figure 104: Comparison between the sensor metrics of the "95 – 5" sample vs. the "Control" Pd sample

These sensor metrics need to be interpreted in the drift ratio, i.e., only cycles with a "low" drift ratio should be considered meaningful data. E.g., Consider the maximum sensitivity of the first cycle of the "control" Pd sample on day two or day four (fig 104(f)). The sample had a very high sensitivity of ~5%. But a closer look would reveal that the corresponding drift ratio for those points was ~1.5 (fig 104(e)), implying that the drift was more significant than the signal itself. It can be verified by looking at the raw gas sensing responses of the "control" Pd sample (fig 104(d), 104(f)). Indeed, the sensor hadn't attained a stable baseline for the above cycles. Therefore, any interpretation of such data points must be avoided. Following observations can be made from the above fig 104, assuming a drift ratio of 0.5 as the qualifying criteria for any meaningful interpretation:

Drift ratio

- The drift ratio for the "95 – 5" sample consistently decreased throughout testing at both H_2 concentrations; the drift ratio was less at the higher concentration
- The drift ratio for the "control" Pd sample was considerably less than the Pd-Pt sample on day zero but increased on day two and day four (for both concentrations).

Maximum sensitivity

- For the Pd-Pt sample, it remained consistent on all four days of testing at both the H_2 concentrations; higher H_2 concentration resulted in higher sensitivity and vice versa
- Pd-Pt sample was always less sensitive than the "control" Pd sample
- For the "control" sample, the sensitivity decreased as the exposure/recovery cycles progressed (testing at 3.6 % H_2). At 0.6% H_2, the sensitivity remained consistent in the third cycle (the first two cycles had a high drift ratio)

Response time and recovery time ("faster and "slower" refer to both response and recovery times)

- The Pd-Pt sample was always faster than the "control" Pd sample at 3.6% H_2. The "control" Pd sample started faster on day zero but slowed on day two and day four, at 0.6% H_2
- Both the "control" Pd and the Pd-Pt sample became slower with increasing exposure/recovery cycles on all days

Thus, the following conclusions can be drawn from the above observations:

1. The drift ratio exhibited a decreasing trend as the Pd-Pt sample was gradually eliminated due to more response/recovery cycles. E.g., For the first cycle on day zero, 2, and 4, the drift ratio became progressively lower at both H_2 concentrations (fig 104(a) and (e)). In contrast, for the "control" Pd sample, this "drift elimination" phenomenon wasn't observed
2. The addition of Pt caused the resulting sensor to be faster and yield more consistent performance throughout testing compared to the "control" Pd sample
3. The addition of Pt also results in diminished sensitivity to the same hydrogen concentrations
4. Repetition of exposure/recovery cycles throughout testing slowed down both the samples

5.4 PERFORMANCE COMPARISON

Table 4 compares the response time and recovery time of some of the flexible Pd-based chemiresistive hydrogen sensors with those developed in this study. The response time and recovery times have been reported for the "control" Pd and the 95 – 5 sample, as observed on the fourth day of the gas sensing. For the 95 – 5 sample, the response/recovery times have been averaged for the last three cycles at both 3.6% H_2 and 0.6% H_2. For the "control" Pd sample, the response time-averaged for the last three cycles at 3.6 % H_2. Since only the last cycle recovered, it has been reported as the recovery time. At 0.6% H_2, the response/recovery time for the last cycle has been reported, as the drift ratio was less than 0.5 only for that cycle.

Table 4: Comparison of response recovery times of various sensors to hydrogen at room temperature

Sr. no.	Active element	Method used	Substrate	t_{90}(s)	t_{10} (s)	Test gas	Year
1.	Pd-WS2/Si thin film	DC sputtering	Ultrathin Si	44.7	35.1	4% H_2 in N_2	2019[64]
2.	Pd thin films	RF sputtering	PI	750	~750	1% H_2 in N_2	2016[30]
3.	Pd strip@Si NM	E beam evaporation	PET	22 (10-90%)	-	0.5% H_2 in air	2018[65]
4.	AuPd alloy	Sputter of $Au_{0.5}Pd_{0.5}$	PI	6	400	1% H_2 in N_2	2016[66]
5.	Pd NP@ZnO NR	RF magnetron sputtering	PI	18	130	1000 ppm In air	2013[31]
6.	Pd@MWCNT	Self-assembly	PET	300	510	1% H_2 in air	2010[37]

7.	Pd@Pt NW	Lithographically patterned NW Electro	Glass	35	50	4% H_2 in air	2015[67]
8.	Pd nanotubes	Chemical reduction around hydrothermally grown ZnO nanorods followed by ZnO etching	PI	78 s, 210 s	-	0.5 % H_2 in air, 1% H_2 in air	2012 [68]
9.	Pd NPs	Al-aided	PI	83 s, 95 s	76 s, 39 s	3.8% H_2 in N_2, 0.6% H_2 in N_2	2021 – (This work)
10.	Pd-Pt NPs	Al-aided	PI	40 s, 79 s	61 s, 76 s	3.8% H_2 in N_2, 0.6% H_2 in N_2	2021 – (This work)

6. SUMMARY AND SCOPE FOR FUTURE WORK

6.1 SUMMARY

A new method of fabricating hydrogen-sensitive nanostructures on flexible substrates was presented here. It uses a rapid and straightforward method to deposit conductive Pd and Pd-Pt nanostructures. The sensors thus prepared responded and recovered to hydrogen at room temperature. The simplicity of this procedure could provide a foundation for opportunities for scale-up.

6.1.1 Aluminum-aided deposition by immersion

These experiments provided a proof of concept, wherein it was demonstrated that the conductive Pd nanostructures could be obtained by reacting aluminum tapes with Pd salt solution. The sample prepared thus was tested at 2.4% and 3.8% H_2 in N_2. It gave an increasing resistance at the former concentration, while the gap-closure mechanism was observed at the higher concentration. However, there was a weak adhesion between the Pd deposits and the polyimide, making repetitive testing difficult. The polyimide was pretreated with KOH. The amount of Pd deposited was decreased by significantly decreasing the Pd salt concentration and the size of the aluminum foil.

6.1.2 Aluminum-aided deposition by drop-casting

6.1.2.1 Pd-based sensors

Drop casting the Pd salt solution proved to be an effective way to decrease the amount of Pd deposited. The amount could be altered by varying the Pd concentration in the salt solution. The gas sensing responses revealed an $\alpha \rightarrow \beta$ phase transition occurring in the concentration range of 1 – 2% H_2, which agreed with the existing literature. Samples prepared thus were also responding in air background, albeit using a different mechanism of PdO reduction. They were also tested as flexible sensors inside the pipe carrying hydrogen gas mixtures.

6.1.2.2 Pd-Pt bimetallic sensors

To further improve the speed of the sensors, the Pd-Pt bimetallic sensors were prepared by co-depositing Pd and Pt salt solutions using aluminum foil. These samples differed in their Pd: Pt contents depending on their Pd: Pt molar ratio. The samples with 5 at % Pt exhibited the fastest response and recovery times, probing further study into their behavior. It was found that such sensors exhibited a baseline drift upon repeated exposure/recovery to H_2. However, this drift could be eliminated by repeated exposure to hydrogen. The sensor responses were compared with a "control" sample with no Pt. After conducting the identical set of gas sensing tests, it was found that the Pt resulted in faster and more consistent responses at the expense of diminished sensitivity as compared to the "control" Pd sample.

6.2 SCOPE FOR FUTURE WORK

- Oxide formation – The oxide layer used to form on the Pd - Pt samples after brief periods of inactivity. Further understanding of this process is required so that the oxide formation can be eliminated
- Pt optimization – By further decreasing the Pt content, it might also improve the sensor sensitivity (thereby decreasing the drift ratio). Optimization of the Pt content of less than 5 mol% could be carried out

- Lower detection limit – Currently, the gas sensing setup can only create H_2 mixtures of up to 0.5 – 0.6%, which is still relatively high. Using a mass flow controller to decrease the hydrogen concentration up to 0.1% is necessary.
- Cross-interference – Gases such CO, H_2S, etc., interfere with catalysts such as Pd. Therefore, it will be necessary to protect them against their interference. Studies such as [69] have shown that coating zeolite networks on Pd could potentially diminish this interference and accelerate the response times. Testing in air, instead of nitrogen, would also be required
- Batch repeatability – The repeatability of this process also needs to be demonstrated via another set of experiments
- Scale-up – The potential for scale-up can be examined by automation of the process. E.g., Dropping the solution on aluminum foil instead of manually drop-casting would allow over larger areas
- Flexible sensor – The Pd sample as a flexible sensor didn't exhibit a phase transition near the pipe wall, unlike at the pipe centerline for the same hydrogen concentration. Since it was unclear whether the H_2 concentration near the wall was the same as the centerline concentration, the 95 – 5 Pd-Pt sample could be used both as a flexible and flat sensor to investigate this difference. Since this sample doesn't undergo the gap-closure mechanism, interparticle gap changing due to bending would be unlikely. A diminished sensitivity near the pipe wall would indicate that the concentration near the pipe wall would indeed be less.

7. **REFERENCES**

[1] Zhang, Y. N., Peng, H., Qian, X., Zhang, Y., An, G., & Zhao, Y. (2017). Recent advancements in optical fiber hydrogen sensors. Sensors and Actuators B: Chemical, 244, 393-416.

[2] Hadef, H., Negrou, B., Ayuso, T. G., Djebabra, M., & Ramadan, M. (2020). Preliminary hazard identification for risk assessment on a complex system for hydrogen production. International Journal of Hydrogen Energy, 45(20), 11855-11865.

[3] Hübert, T., Boon-Brett, L., & Buttner, W. (2018). Sensors for safety and process control in hydrogen technologies. CRC Press

[4] Vig, J. R., & Walls, F. L. (2000, June). A review of sensor sensitivity and stability. In Proceedings of the 2000 IEEE/EIA International Frequency Control Symposium and Exhibition (Cat. No. 00CH37052) (pp. 30-33). IEEE

[5] Hübert, T., Boon-Brett, L., Black, G., & Banach, U. (2011). Hydrogen sensors–a review. Sensors and Actuators B: Chemical, 157(2), 329-352.

[6] Darmadi, I., Nugroho, F. A. A., & Langhammer, C. (2020). High-Performance Nanostructured Palladium-Based Hydrogen Sensors—Current Limitations and Strategies for Their Mitigation. ACS sensors, 5(11), 3306-3327

[7] Fioravanti, A., & Carotta, M. C. (2020). Year 2020: A snapshot of the last progress in flexible printed gas sensors. Applied Sciences, 10(5), 1741

[8] http://i.imgur.com/haVHNA0.jpg Accessed on 12/1/2017

[9] Roberson, Luke, et al. "Chemochromic Hydrogen Leak Detectors." (2009).

[10] https://www.nasa.gov/offices/oct/feature/nasa-makes-leaks-easy-to-spot-on-tape

[11] Koo, W. T., Cho, H. J., Kim, D. H., Kim, Y. H., Shin, H., Penner, R. M., & Kim, I. D. (2020). Chemiresistive hydrogen sensors: fundamentals, recent advances, and challenges. ACS nano, 14(11), 14284-14322

[12] Adams, B. D., & Chen, A. (2011). The role of palladium in a hydrogen economy. Materials today, 14(6), 282-289.

[13] Ndaya, C. C., Javahiraly, N., & Brioude, A. (2019). Recent advances in palladium nanoparticles-based hydrogen sensors for leak detection. Sensors, 19(20), 4478

[14] Mirzaei, A., Yousefi, H. R., Falsafi, F., Bonyani, M., Lee, J. H., Kim, J. H., ... & Kim, S. S. (2019). An overview on how Pd on resistive-based nanomaterial gas sensors can enhance response toward hydrogen gas. International Journal of Hydrogen Energy, 44(36), 20552-20571.

[15] Maeland, A., & Flanagan, T. B. (1966). The hydrogen-palladium system. Platinum Metals Review, 10(1), 20-24

[16] Noh, Jin-Seo, Jun Min Lee, and Wooyoung Lee. "Low-dimensional palladium nanostructures for fast and reliable hydrogen gas detection." Sensors 11.1 (2011): 825-851.

[17] Ramanathan, M., Skudlarek, G., Wang, H. H., & Darling, S. B. (2010). Crossover behavior in the hydrogen sensing mechanism for palladium ultrathin films. Nanotechnology, 21(12), 125501.

[18] Xie, B., Liu, L., Peng, X., Zhang, Y., Xu, Q., Zheng, M., ... & Han, M. (2011). Optimizing hydrogen sensing behavior by controlling the coverage in Pd nanoparticle films. The journal of Physical chemistry C, 115(32), 16161-16166

[19] Lee, J., Shim, W., Lee, E., Noh, J. S., & Lee, W. (2011). Highly mobile palladium thin films on an elastomeric substrate: Nanogap-based hydrogen gas sensors. Angewandte Chemie International Edition, 50(23), 5301-5305.

[20] Hatakeyama, Y., Umetsu, M., Ohara, S., Kawadai, F., Takami, S., Naka, T., & Adschiri, T. (2008). Homogenous Spherical Moss like Assembly of Pd Nanoparticles by using DNA Compaction: Application of Pd–DNA Hybrid Materials to Volume-Expansion Hydrogen Switches. Advanced Materials, 20(6), 1122-1128.

[21] Atashbar, M. Z., Banerji, D., & Singamaneni, S. (2005). Room-temperature hydrogen sensor based on palladium nanowires. IEEE Sensors Journal, 5(5), 792-797.

[22] Lee, J. M., Park, J. E., Kim, S., Kim, S., Lee, E., Kim, S. J., & Lee, W. (2010). Ultra-sensitive hydrogen gas sensors based on Pd-decorated tin dioxide nanostructures: Room temperature operating sensors. international journal of hydrogen energy, 35(22), 12568-12573.

[23] Mao, S., Cui, S., Yu, K., Wen, Z., Lu, G., & Chen, J. (2012). Ultrafast hydrogen sensing through hybrids of semiconducting single-walled carbon nanotubes and tin oxide nanocrystals. Nanoscale, 4(4), 1275-1279.

[24] Hsu, C. H., Chang, C. C., Tseng, C. M., Chan, C. C., Chao, W. H., Wu, Y. R., ... & Wu, M. K. (2013). An ultra-fast response gasochromic device for hydrogen gas detection. Sensors and Actuators B: Chemical, 186, 193-198

[25] Algadri, N. A., Hassan, Z., Ibrahim, K., & Al-Diabat, A. M. (2018). A high-sensitivity hydrogen gas sensor based on carbon nanotubes fabricated on glass substrate. Journal of Electronic Materials, 47(11), 6671-6680.

[26] Kim, K. S., & Chung, G. S. (2011). Fast response hydrogen sensors based on palladium and platinum/porous 3C-SiC Schottky diodes. Sensors and Actuators B: Chemical, 160(1), 1232-1236.

[27] Martin, L. P., Pham, A. Q., & Glass, R. S. (2004). Electrochemical hydrogen sensor for safety monitoring. Solid State Ionics, 175(1-4), 527-530.

[28] Alrammouz, R., Podlecki, J., Abboud, P., Sorli, B., & Habchi, R. (2018). A review on flexible gas sensors: From materials to devices. Sensors and Actuators A: Physical, 284, 209-231

[29] Wasa, K., Kanno, I., & Kotera, H. (Eds.). (2012). Handbook of sputter technology: fundamentals and applications for functional thin films, nano-materials and MEMS. William Andrew

[30] Öztürk, S., & Kılınç, N. (2016). Pd thin films on flexible substrate for hydrogen sensor. Journal of Alloys and Compounds, 674, 179-184

[31] Rashid, T. R., Phan, D. T., & Chung, G. S. (2013). A flexible hydrogen sensor based on Pd nanoparticles decorated ZnO nanorods grown on tape. Sensors and Actuators B: Chemical, 185, 777-784

[32] Chang, T., Jung, H., Jang, B., Lee, J., Noh, J. S., & Lee, W. (2013). Nanogaps controlled by liquid nitrogen freezing and the effects on hydrogen gas sensor performance. Sensors and Actuators A: Physical, 192, 140-144

[33] Awan, T. I., Bashir, A., & Tehseen, A. (2020). Chemistry of Nanomaterials: Fundamentals and Applications. Elsevier

[34] Kim, S. M., Kim, H. J., Jung, H. J., Park, J. Y., Seok, T. J., Choa, Y. H., ... & Lee, S. W. (2019). High-performance, transparent thin film hydrogen gas sensor using 2D electron gas at interface of oxide thin film heterostructure grown by atomic layer . Advanced Functional Materials, 29(7), 1807760.

[35] Sun, Y., & Wang, H. H. (2007). High-performance, flexible hydrogen sensors that use carbon nanotubes decorated with palladium nanoparticles. Advanced Materials, 19(19), 2818-2823

[36] Richardson, J. J., Björnmalm, M., & Caruso, F. (2015). Technology-driven layer-by-layer assembly of nanofilms. Science, 348(6233), aaa2491.

[37] Su, P. G., & Chuang, Y. S. (2010). Flexible H_2 sensors fabricated by layer-by-layer self-assembly thin film of multi-walled carbon nanotubes and modified in situ with Pd nanoparticles. Sensors and Actuators B: Chemical, 145(1), 521-526

[38] Haus, J. W. (Ed.). (2016). Fundamentals and applications of nanophotonics. Woodhead Publishing

[39] Jang, B., Cho, S., Park, C., Lee, H., Song, M. J., & Lee, W. (2015). Palladium nanogap-based H_2 sensors on a patterned elastomeric substrate using nanoimprint lithography. Sensors and Actuators B: Chemical, 221, 593-598

[40] S.H. Lim, B. Radha, J.Y. Chan, M.S.M. Saifullah, G.U. Kulkarni, G.W. Ho, Flexible palladium-based H_2 sensor with fast response and low leakage detection by nanoimprint lithography, ACS Appl. Mater. Interfaces 5 (no. 15)(2013) 7274–7281

[41] da Silva, A. G., Rodrigues, T. S., Haigh, S. J., & Camargo, P. H. (2017). Galvanic replacement reaction: recent developments for engineering metal nanostructures towards catalytic applications. Chemical Communications, 53(53), 7135-7148.

[42] Vanysek, P. (2000). Electrochemical series. CRC handbook of chemistry and physics, 8.

[43] Choi, S., Jeon, S., Park, I., Ito, M., & Hiroyoshi, N. (2021). Enhanced cementation of Co2+ and Ni2+ from sulfate and chloride solutions using aluminum as an electron donor and conductive particles as an electron pathway. Metals, 11(2), 248

[44] Li, W., Cochell, T., & Manthiram, A. (2013). Activation of aluminum as an effective reducing agent by pitting corrosion for wet-chemical synthesis. Scientific reports, 3(1), 1-7

[45] Lechler, PJ. The solubility of palladium in chloride solutions and the distribution of platinum, palladium, and related elements in hydrothermal mineralization, Ph.D. Dissertation, Univ. of Nevada, Reno, 1995

[46] Wu, P. Y., Lin, C. H., & Chen, C. M. (2017). Study of surface metallization of film and interfacial characterization. Metals, 7(6), 189

[47] Zheng, G., & Altman, E. I. (2000). The oxidation of Pd (111). Surface Science, 462(1-3), 151-168

[48] Guo, X., Hoffman, A., & Yates Jr, J. T. (1989). Adsorption kinetics and isotopic equilibration of oxygen adsorbed on the Pd (111) surface. The Journal of chemical physics, 90(10), 5787-5792

[49] Lee, Young Tack, et al. "Hydrogen gas sensing properties of PdO thin films with nano-sized cracks." Nanotechnology 21.16 (2010): 165503

[50] Lee, J., Shim, W., Noh, J. S., & Lee, W. (2012). Design rules for nanogap-based hydrogen gas sensors. ChemPhysChem, 13(6), 1395-1403

[51] Bhardwaj, P., Barman, P. B., & Hazra, S. K. (2021). Hydrogen response of palladium nanoparticles washed with different solvents. Bulletin of Materials Science, 44(1), 1-7

[52] Khanuja, M., Shrestha, S., Mehta, B. R., Kala, S., & Kruis, F. E. (2011). Magnitude and time response of electronic and topographical changes during hydrogen sensing in size selected palladium nanoparticles. Journal of Applied Physics, 110(1), 014318.

[53] Khanuja, M., Kala, S., Mehta, B. R., & Kruis, F. E. (2008). Concentration-specific hydrogen sensing behavior in monosized Pd nanoparticle layers. Nanotechnology, 20(1), 015502.

[54] Xu, T., Zach, M. P., Xiao, Z. L., Rosenmann, D., Welp, U., Kwok, W. K., & Crabtree, G. W. (2005). Self-assembled monolayer-enhanced hydrogen sensing with ultrathin palladium films. Applied Physics Letters, 86(20), 203104.

[55] Yang, F., Kung, S. C., Cheng, M., Hemminger, J. C., & Penner, R. M. (2010). Smaller is faster and more sensitive: the effect of wire size on the detection of hydrogen by single palladium nanowires. ACS Nano, 4(9), 5233-5244.

[56] Ren, S., Wang, Q., Wang, Y., & Qu, S. (2012). Three distinct hydrogen sensing responses of palladium line patterns generated by femtosecond laser direct writing. Journal of Physics D: Applied Physics, 45(28), 285303

[57] Gupta, D., Dutta, D., Kumar, M., Barman, P. B., Sarkar, C. K., Basu, S., & Hazra, S. K. (2014). A low temperature hydrogen sensor based on palladium nanoparticles. Sensors and Actuators B: Chemical, 196, 215-222

[58] Noh, H. J., Kim, H. J., Park, Y. M., Park, J. S., & Lee, H. N. (2019). Complex behavior of hydrogen sensor using nanoporous palladium film prepared by evaporation. Applied Surface Science, 480, 52-56.

[59] Penner, R. M. (2017). A nose for hydrogen gas: fast, sensitive H_2 sensors using electrodeposited nanomaterials. Accounts of Chemical Research, 50(8), 1902-1910.

[60] Lewis, R., & Gomer, R. (1968). Adsorption of oxygen on platinum. Surface Science, 12(2), 157-176

[61] Yoo, Hae-Wook, et al. "Well-defined and high resolution Pt nanowire arrays for a high performance hydrogen sensor by a surface scattering phenomenon." Analytical chemistry 87.3 (2015): 1480-1484

[62] Yang, F., Donavan, K. C., Kung, S. C., & Penner, R. M. (2012). The surface scattering-based detection of hydrogen in air using a platinum nanowire. Nano letters, 12(6), 2924-2930

[63] Kobayashi, H., Yamauchi, M., Kitagawa, H., Kubota, Y., Kato, K., & Takata, M. (2010). Atomic-level Pd− Pt alloying and largely enhanced hydrogen-storage capacity in bimetallic nanoparticles reconstructed from core/shell structure by a process of hydrogen absorption/desorption. Journal of the American Chemical Society, 132(16), 5576-5577

[64] Hao, L., Liu, H., Xu, H., Dong, S., Du, Y., Wu, Y., ... & Liu, Y. (2019). Flexible Pd-WS2/Si heterojunction sensors for highly sensitive detection of hydrogen at room temperature. Sensors and Actuators B: Chemical, 283, 740-748.

[65] Cho, M., Yun, J., Kwon, D., Kim, K., & Park, I. (2018). High-sensitivity and low-power flexible Schottky hydrogen sensor based on silicon nanomembrane. ACS applied materials & interfaces, 10(15), 12870-12877

[66] Menumerov, E., Marks, B. A., Dikin, D. A., Lee, F. X., Winslow, R. D., Guru, S., ... & Neretina, S. (2016). Sensing hydrogen gas from atmospheric pressure to a hundred parts per million with nanogaps fabricated using a single-step bending deformation. ACS Sensors, 1(1), 73-80

[67] Li, X., Liu, Y., Hemminger, J. C., & Penner, R. M. (2015). Catalytically activated palladium@ platinum nanowires for accelerated hydrogen gas detection. ACS nano, 9(3), 3215-3225

[68] Lim, M. A., Kim, D. H., Park, C. O., Lee, Y. W., Han, S. W., Li, Z., ... & Park, I. (2012). A new route toward ultrasensitive, flexible chemical sensors: metal nanotubes by wet-chemical synthesis along sacrificial nanowire templates. ACS Nano, 6(1), 598-608

[69] Koo, Won-Tae, et al. "Accelerating palladium nanowire H_2 sensors using engineered nanofiltration." *ACS nano* 11.9 (2017): 9276-9285.)

[70]: Joshi, P., & Santhanam, V. (2016). Paper-based SERS active substrates on demand. RSC advances, 6(72), 68545-68552

[71]: Hydrogen Detector: ISO/TC 197, WG 13 DIS 26142

[72]: Naoya SAWAGUCHI, Maiko NISHIBORI, Kazuki TAJIMA, Woosuck SHIN, Noriya IZU, N. M. and I. M. Practical Test Methods for Hydrogen Gas Sensor Response Characterization. Electrochemistry 2006, 74 (4), 315–320. https://doi.org/10.5796/electrochemistry.74.315

[73]: Keithley 6220/6221 AC and DC Current Source User's Manual. 2005

[74]: Keithley. Model 2182A Nanovoltmeter Datasheet. Keithley Instruments, Inc

[75]: Nadagouda, M. N.; Varma, R. S. Green Synthesis of Silver and Palladium Nanoparticles at Room Temperature Using Coffee and Tea Extract. Green Chem. 2008, 10 (8), 859. https://doi.org/10.1039/b804703k

[76]: Wang, Z.; Yan, J.; Wang, H.; Ping, Y.; Jiang, Q. Pd / C Synthesized with Citric Acid : An Efficient Catalyst for Hydrogen Generation from Formic Acid / Sodium Formate — Supplementary Information (B). 1–10, Sci Rep - UK 2, 2012

[77]: Xiong, Y.; McLellan, J. M.; Yin, Y.; Xia, Y. Synthesis of Palladium Icosahedra with Twinned Structure by Blocking Oxidative Etching with Citric Acid or Citrate Ions. Angew. Chemie - Int. Ed. 2007, 46 (5), 790–794. https://doi.org/10.1002/anie.200604032

[78]: Canlier, A.; Volkan, U. Development of Highly Transparent Pd- Coated Ag Nanowire Electrode via Controlled Galvanic Displacement Reaction. 2014, 475– 487. https://doi.org/10.1016/j.apsusc.2015.04.017

[79]: Kumar, G.; Blackburn, J. R.; Albridge, R. G.; Moddeman, W. E.; Jones, M. M. Photoelectron Spectroscopy of Coordination Compounds. II. Palladium Complexes. Inorg. Chem. 1972, 11 (2), 296–300. https://doi.org/10.1021/ic50108a020

[80]: Militello, M. C.; Simko, S. J. Elemental Palladium by XPS. Surf. Sci. Spectra 1994, 3 (4), 387–394. https://doi.org/10.1116/1.1247783

[81]: Kaushik, V. K. Xps Core Level Spectra And Auger Parameters For Some Silver Compounds. J. Electron Spectros. Relat. Phenomena 1991, No. 56, 273–277. https://doi.org/10.1016/0368-2048(91)85008-H

Appendix A – Increasing resistance of the 95-5 sample

A different 95-5 sample was exposed to various hydrogen concentrations ranging from 0.6% to 3.2%. The first exposure (3.2% H_2) showed the usual oxide reduction phenomenon. The subsequent tests showed unidirectional responses at all concentrations. These responses were recorded on the first day of the gas sensing, as seen by the considerable drift in the baseline resistance. The drift between consecutive cycles was decreasing here as well.

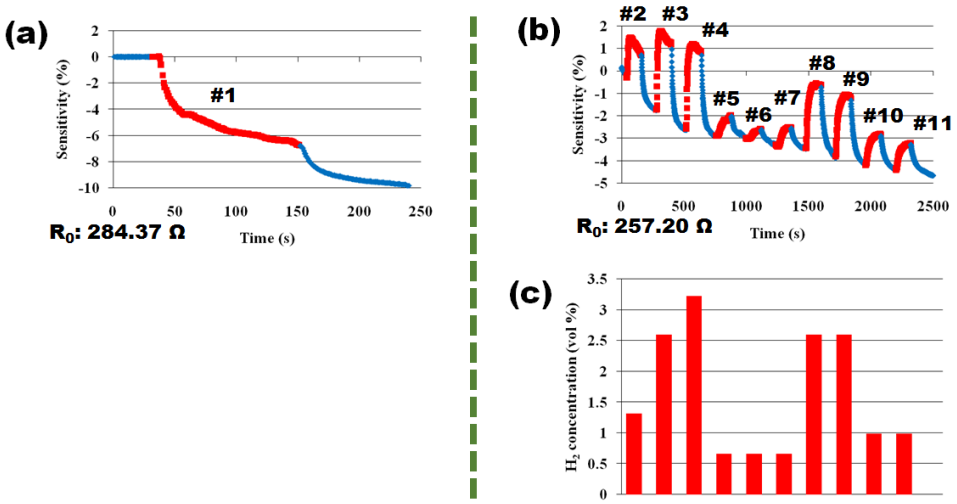

Figure 105: (a)First exposure of a replicate "95 – 5" sample to 3.6% H_2 (b) subsequent exposure to different concentrations

Thus, unlike the Pd sample, the 95-5 sample shows no signs of phase transition in the same hydrogen concentration range. This change was brought about by adding 5 mol% Pt, as confirmed by the "control" Pd experiment.

Appendix B – Flow fluctuations

For the 95-5 sample, the sensitivity change appeared to be 1:1 with the hydrogen flow rate. Could it have been possible that the changing resistance was brought about by the changing flow rate, not hydrogen?

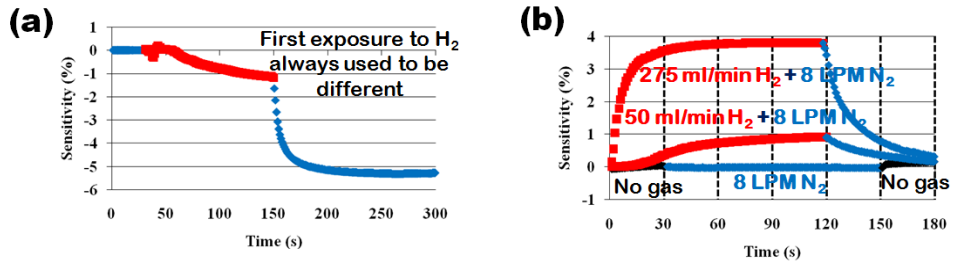

Figure 106: (a) Oxide species reduction for first exposures (b)Superimposed responses of the same "95 – 5" sample to flow rate changes

This proposition would have to be untrue for two reasons. The first hydrogen exposure always yielded a different type of response than the subsequent responses. If the response were related to the flow change and not the hydrogen specifically, then the first exposure would have to be the same as the subsequent ones. Also, an experiment was conducted where the flow rate in the test pipe was changed from 0 LPM N_2 to 8 LPM N_2 instantly. The change in sensitivity has been superimposed against two responses at 3.6% H_2 and 0.6% H_2. It is visible that even a 50 ml/min flow rate change of H_2 was enough to generate an observable signal, which 8 LPM of N_2 couldn't. Therefore, the sensor in all the tests shown in this report responded to H_2.

Appendix C – Communication with the 6221-2182A for pulsed testing

This is an example of the program entered in the Keithley communicator to send command to the combined 6221-2182A instrument to start the pulsed test. The program is based on the SCPI code generated by the KI6220 example software.

```
:sour:swe:abort WAIT3000

*rst

:SYST:COMM:SERIal:SEND "SYST:FFIL ON"

:OUTP:ISH OLOW

:outp:lte OFF WAIT500

:sour:del 0.094

:form:elem READ

:sour:pdel:high 0.004

:sour:pdel:low 0

:sour:pdel:count 30

:sour:pdel:rang best

:sour:swe:rang best

:sour:pdel:width 0.001

:sour:pdel:sdel 0.0001

:sour:pdel:swe off

:sour:pdel:lme 1

:sour:pdel:int 50

:sour:curr:comp 10

:sour:curr:start 0

:sour:curr:stop 0.01

:sour:curr:step 0.01

:SYST:COMM:SERIal:SEND ":sens:volt:rang 10"

:sens:aver:wind 0

:sens:aver:stat off

:sour:pdel:arm WAIT3000

:init:imm
```

After test completion, use the “trace:data?” command to retrieve the voltage readings.